TRAJECTORY-BASED COMBUSTION CONTROL ENABLED BY FREE PISTON ENGINE

A DISSERTATION
SUBMITTED TO THE FACULTY OF
UNIVERSITY OF MINNESOTA
BY

Chen Zhang

IN PARTIAL FULFILLMENT OF THE REQUIREMENTS
FOR THE DEGREE OF
DOCTOR OF PHILOSOPHY

Professor Zongxuan Sun, Advisor

August 2017

Acknowledgements

I owe my gratitude to all the people who offer valuable guidance and instrumental support during my doctoral education. I know for certain that this dissertation would not be possible without all of your kindly favor.

Foremost, I would like to express my special thanks to my advisor, Professor Zongxuan Sun, for his insightful vision of the project, his consistent instrumental advice on the research and his meticulous care to me and my family. I consider myself extremely lucky to be one of Professor Sun's students. His execution, passion, and dedication always inspire me a lot in these years, and his instructions, both technical and non-technical, will become the priceless treasure through the rest of my life.

In addition, I would like to thank the rest of my committee members: Professor Kim Stelson, Professor William Northrop, and Professor Peter Seiler for their helpful comments and valuable feedback to my thesis and their instrumental teachings and supports at the University of Minnesota.

Besides, I would like to acknowledge Ford Motor Company for donating the hydraulic free piston engine and appreciate the financial and hardware supports from the Center for Compact and Efficient Fluid Power (CCEFP). Especially, I would like to thank Mr. Michael Gust, Mr. Brad Bohlmann, Mr. Donald Haney and Mrs. Alyssa Burger for their technical guidance on my research and administrative support for my project.

Also, I would like to thank all of the colleagues and group members in the Automotive Propulsion Control Laboratory, especially for Ke Li, Abhinav Tripathi, and

Keyan Liu. As a group of motivated and talented individuals, you guys offer me an endless source of technical wisdom and fun.

Finally, I would like to thank all the members of my family. As my foundation, my parents, Jiujiu Zhang and Guihua Chen, offer me infinite support and encouragement since I was a child. Their love and patience make me feel grateful and fortunate as their son. I would also like to thank my parents-in-law, Zhuan Zhu and Hanzhen Xiong, who provide a huge life support to me and my family during my doctoral life. To my wife, Sinan Zhu, I would like to express my highest gratitude for your love, support, and understanding which made the last few years among the best ever. At last, I will also thank my little one, Olivia Zhang, who offers me endless happiness and motivation in my life.

To my family

Abstract

The free piston engine (FPE), considered as a promising alternative to the conventional internal combustion engine, has received more and more attention due to its great potential for efficiency improvement and emission reduction. Such a potential arises from its unique characteristic that the piston motion of the FPE is ultimately free due to the absence of the mechanical crankshaft. With the capability of employing variable piston trajectories, the FPE enables real-time control of the combustion chamber volume and therefore can adjust the in-cylinder gas pressure-temperature history and species concentration prior, during and after the combustion event. Enlightened by this capability, a new control method, namely piston trajectory-based combustion control, is proposed. The objective of this research is to investigate the feasibility and advantages of this advanced control method and realize the fuel-engine co-optimization in real-time. In order to achieve this objective, the entire research is separated into three phases.

The first phase of the research focuses on the modeling and analysis of the trajectory-based combustion control in the FPE. A comprehensive model, representing the HCCI combustion process in the FPE along various piston trajectories, is developed, which includes the geometric structure of the FPE, the physics-based model of the FPE operation, and the detailed chemical kinetics of the utilized fuel. Extensive simulation results and the corresponding analysis clearly show that the FPE is able to adjust the entire combustion process by varying the volume of the combustion chamber and therefore altering the in-cylinder gas temperature and pressure traces to increase the indicated output work. In addition, the trajectory-based combustion control can also

influence the chemical kinetics of the combustion via manipulating the in-cylinder temperature-pressure history. Specifically, unique asymmetric trajectories are designed that decreases the amount of NOx emission and increases the engine thermal efficiency simultaneously. At last, the analysis of the trajectory-based combustion control is also extended to multiple renewable fuels, e.g. hydrogen, biogas, syngas, ethanol, DME (dimethyl ether), biodiesel, and F-T (Fisher-Tropsch) fuels. It shows that an optimal asymmetric piston trajectory can be designed for each specific renewable fuel, which enables a significant reduction in the NOx emission and an improvement in the thermal efficiency simultaneously. In this way, the trajectory-based combustion control realizes the co-optimization of fuels and engine operation.

The second phase of the research is aimed to develop a novel control-oriented model to realize the trajectory-based HCCI combustion control in practice. Intuitively, the comprehensive model from the first phase is not suitable for the control purpose, since the detailed reaction mechanisms usually generate heavy computational burdens. In order to reduce the computational burden and keep sufficient chemical kinetics information for HCCI combustion simulation, in the new control-oriented model, the engine cycle is separated into multiple phases and in each phase, a specific reaction mechanism with the minimal size is applied. With this unique phase separation method, the proposed control-oriented model not only shows a good agreement with the detailed physics-based model but also reduces the computational time significantly. In addition, such a good agreement is sustained at various working conditions, including different CRs, multiple AFRs and various piston motion patterns Ω.

The last phase of this dissertation discusses systematic approaches to optimize piston trajectory for the trajectory-based HCCI combustion control. As claimed by the concept of trajectory-based combustion control, the derived optimal piston trajectory is considered as the optimal control signal to the FPE, which provides ultimate engine performance, in terms of maximal engine thermal efficiency and minimal emissions production. In this part, both offline and online optimizations are investigated. For the offline optimization, two approaches are proposed and implemented into the proposed control-oriented model: The first approach represents the piston trajectory as a function of parameter Ω and converts the original problem to a parameters optimization problem. Both optimal symmetric trajectories and asymmetric trajectories are derived at given CR. The advantages of this optimization approach lie on its much lighter computational burden; the second method transforms the trajectory optimization problem into a constrained nonlinear programming and then solves it via the SQP algorithm. By removing the constraints placed by piston motion patterns, this approach enlarges the candidate pool of various piston trajectories. Hence, the derived optimal trajectory further increases the engine output work and sustains the NOx emissions at the same level. For the online optimization, a searching process aimed to determine the optimal piston motion pattern Ω according to variable working conditions is developed. By using the proposed control-oriented model, the designed piston trajectory can be achieved within 0.4s under different working conditions, which enables real time optimal control of HCCI combustion phasing.

Table of Contents

List of Tables

List of Figures

Chapter 1

Introduction

1.1 Motivation

Currently, transportation sector alone consumes about 30% of the total energy in the USA [1]. Almost 95% of this energy comes from petroleum-based fuels [1], [2]. This situation raises two concerns: the risk of energy sources depletion and environmental impact caused by emissions. As projected, the worldwide oil reserves can only sustain 40~50 years at current consumption rate. Meanwhile, almost 14% of global greenhouse gas (GHG), as well as other engine emissions, are produced by the combustion of fossil fuels in the transportation sector [3]. Such concerns will be even more exacerbated due to the rapid growth of energy demands for transportation in the future [4].

1.1.1 Energy Sources Depletion

Extensive studies have been conducted to deal with the concern on the energy sources depletion for transportation. Those studies can be roughly separated into two directions. The first direction is to continuously increase vehicles' fuel economy. However, the current vehicle propulsion systems are still dominated by conventional internal combustion engines (ICEs), a relatively mature technology invented more than a century ago. Although significant progress has been made, the overall efficiency of the conventional ICE is still relatively low and the room for further improvement is limited.

Another direction is to adopt renewable fuels into the current ICEs. Such an adoption certainly increases the diversity of energy sources. In addition, based on the life cycle assessment (LCA) of renewable fuels, the GHG emission is also reduced significantly since their feedstock production are mainly via the photosynthesis process, which absorbs a large amount of CO_2 from the atmosphere. [2], [5]-[11].

However, broad implementation of renewable fuels in automobiles still remains elusive to date, mainly caused by its high cost. Such a high cost comes from two aspects: One is the feedstock price and the other is the processing expenditure, which is spent to convert the feedstock to available fuels for conventional ICE. Currently, mature technologies producing renewable fuels, e.g. ethanol and biodiesel, require valuable crops or animal fats as the feedstock, which raises public concerns due to the shortage of food for increasing global population [12]. As a result, low-cost feedstock, such as lignocellulose, algae, waste vegetable oil, and municipal solid waste are then proposed. However, these feedstocks inevitably increase the processing expenditure, since they require complicated pretreatments and purification processes.

1.1.2 Environmental Impact

It is clear that the engine emissions will affect the environment significantly. Typically, the term “engine emissions” refers to several components in the engine exhaust, including carbon monoxide (CO), various oxides of nitrogen (NOx), unburnt hydrocarbons (HC), and particulate matter (PM). It is widely-known that unlimited release of these pollutants would cause formidable damages to both human health and

environment [13], [14]. As a result, more and more countries and regions have provided or followed increasingly stringent emissions regulations [15], [16].

Technologies to reduce emissions are mainly separated into two categories. One is aimed to optimize the combustion processes inside the ICE and reduces so-called "engine-out" emissions directly. Extensive researches have been conducted on this approach and several technologies, including retarding the ignition time [17]-[19], exhaust gas recirculation (EGR) [20]-[23] and advanced fuel injection strategy [24]-[27], have been widely adopted in real world applications. However, the reductions in emissions achieved by these methods are limited, especially if higher engine efficiency and fuel economy are required. For instance, it was reported that between 5% and 10% EGR in the spark–ignition (SI) engine could reduce almost half NOx emission in specific working conditions [28]. Nonetheless, this NOx reduction is achieved by adding large amounts of inert gases into the intake air-fuel mixture and therefore reducing the combustion rate and peak temperature. As a result, the EGR method decreases the maximal achievable power in high load, increases the fuel consumption in elevated load and causes unstable combustion or even misfire in low load or idle condition.

The other approach is to reduce the engine emissions through advanced after-treatment systems. Such method receives great success in vehicles powered by SI engines since its air-fuel mixture remains at stoichiometric ratio for the majority of loading conditions [29]. This feature ensures the effectiveness of the three-way catalyst converter which decreases the tail-out production of CO, HC, and NOx simultaneously. Unfortunately, this system possesses a severe cold-start problem [30]-[32] and also fails

to regulate the emissions performance while the engine is in transient (e.g. acceleration) conditions [33], [34]. On the other hand, comprehensive after-treatment system for compression-ignition (CI) engine is still an open question which asks for further research. The existing three-way catalyst converter cannot be adopted in diesel engines directly due to the following two reasons: first, diesel engines usually operate in fuel-lean condition; second, the exhaust from the diesel engine contains large amounts of PM and other organic compounds which poison the catalyst easily. Other methods, such as diesel oxidation catalyst [35], [36], diesel particulate filter [37], [38] and selective catalytic reduction [39] are also proposed, but those systems are quite complicated due to their strong temperature dependence while the corresponding manufacture costs also increase significantly.

1.1.3 Overcome the Challenges in a New Way

From the aforementioned discussion, it is clear that the existing technologies in conventional ICE may not be able to optimize the engine efficiency and reduce the pollutants under the entire engine operation domain. In addition, the fixed mechanical structure of the conventional ICE also limits the applications of various renewable fuels. As a consequence, revolutionary technical innovation is required to transform the conventional ICE into a more efficient, environment-friendly and flexible energy conversion device.

A technical solution is proposed in this dissertation, mainly based on a new architecture of ICE, Free Piston Engine (FPE). Due to the absence of the mechanical crankshaft, the piston motion in the FPE is not constrained and therefore variable

compression ratio (CR) control, as well as real-time piston motion pattern control, can be achieved. Attributed to the ultimate freedom of the piston motion, the homogeneous charge compression ignition (HCCI) combustion mode can be realized in the FPE, which is a promising method for improving both the engine efficiency and emissions performance. Furthermore, by removing the traditional constraints on gas pressure-temperature history imposed by the mechanical crankshaft, the dynamics of the HCCI combustion can be even further optimized. Certainly, such an optimization can be extended to various renewable fuels and thus increase the diversity of the energy sources for the FPE.

1.2 Background

1.2.1 HCCI Combustion

HCCI, originally conceived in 1979 [40], has gained a lot of attention due to its ability to combine the advantages of two types of traditional ICEs. Comparing to spark ignition (SI) engines, HCCI engines are more efficient due to the elimination of throttling losses, the use of higher compression ratios and a relatively shorter combustion duration (since it is not necessary for a flame to propagate across the cylinder). By employing HCCI strategy to an SI engine, Zhao et al [41] claimed that 15-20% efficiency improvement was achieved under specific working load attributed to its rapid combustion of a homogeneous mixture of reactants. Relative to compression ignition (CI) engines, HCCI engines have substantially lower emissions of particulate matters (PM). These low emissions are a result of the dilute homogeneous air/fuel mixture in addition to low combustion temperatures. The charge in an HCCI engine may be made dilute by using

exhaust gas recirculation (EGR) or by charge stratification and such dilution levels can be much higher than the levels tolerated by either SI or CI engines since flame propagation is not required. Therefore the generation of PM emission is certainly reduced. On the other hand, HCCI combustion is induced throughout the chamber volume by compression heating due to the piston motion, and it will ignite the gas mixture once the in-cylinder temperature reaches 800K to 1100 K [42]. In contrast, the flame temperatures are almost 2000 K [43] in a CI engine, which is high enough to make unacceptable levels of NOx emission. Additionally, the combustion duration in HCCI engines is much shorter than in CI engines since it is not limited by the rate of fuel/air mixing. This shorter combustion duration offers the HCCI engine an efficiency advantage too.

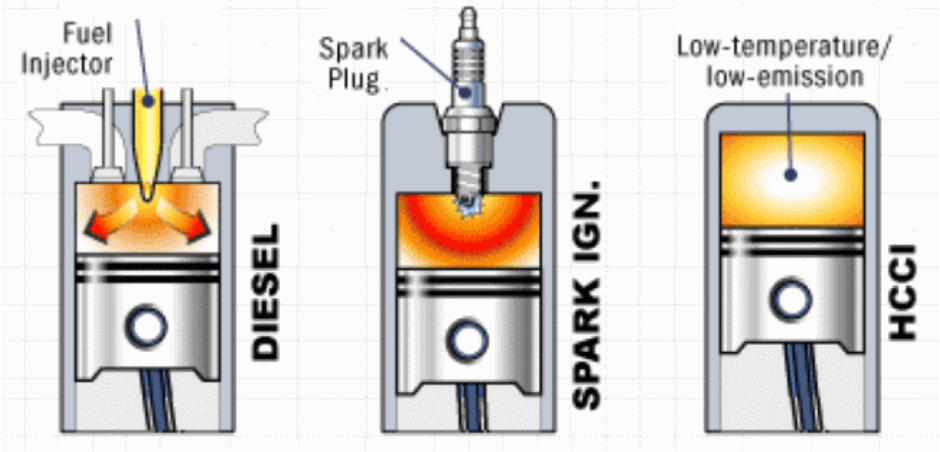

Figure 1.1 Comparison of compression ignition engine, spark ignition engine and HCCI engine

However, despite the fact that HCCI combustion has so many significant advantages, it has not been widely applied to the automobile engine so far. One of the biggest challenges is how to control HCCI timing adequately under the current framework of ICE. The ignition of the in-cylinder gas is predominantly controlled by the fuel chemical kinetics, which implies that the gas temperature-pressure history influences the

combustion process strongly. Consequently, unlike the spark in SI engines or the fuel injection in diesel engines, the ignition cannot be controlled directly in HCCI engines (Figure 1.1).

Existing combustion timing control methods mainly focus on the strategies that change the air-fuel mixture at the initial stage of engine operation via regulating EGR [44]-[46], variable valve time [47] or stratifying charge [48], [49]. Zhao et al [44], following the work of Ladommatos et al. [45] for diesel engines, examined the effects of recycled burned gases through EGR on controlling HCCI combustion timing in 4-cycle SI engines and claimed that the dilution and heat capacity effects are responsible for reducing the heat-release rates and extending the combustion duration, which, substantially is in agreement with computational results obtained by Dec [46]. Additionally, a comprehensive study performed by Caton et al. [47] in a single-cylinder engine with flexible valve actuation mechanism showed significantly lower fuel consumption and NO emissions over a relatively wide load range. Besides, Marriott and Reitz [48], using a high-compression ratio (16.1:1) diesel engine converted to gasoline DI engine, concluded that fuel stratification may be used to control CI combustion over a wide speed/load range of the engine. Sjoberg et al. [49] using a similar facility, claimed that fuel stratification could cause a trade-off between combustion efficiency and NO emissions. Unfortunately, although lots of researches have been conducted so far, none of these aforementioned control schemes are able to actually moderate HCCI combustion over the full range of operation demanded by vehicle applications and simultaneously maintain fuel efficiency and regulated emissions targets in the current ICE architecture.

1.2.2 Free Piston Engine

The original FPE patent was published by Pescara in 1928 [50]. Pescara started his work on FPEs in 1922 and developed prototypes for both SI and CI combustion. This work then led to the patent which describes a single piston spark ignited air compressor. After that, more related work on FPEs has been reported. During the 40s and 60s, many research works had been done on the development of free piston gas generators, but the results are not as good as expected. For example, both Ford and General Motors developed prototype vehicles with small scale free-piston gas generators, but none of these made it fully commercialized. In addition, FPEs are also used as air compressors, which have been considered by many as the only real success [51]. A free-piston air compressor aims to launch torpedoes was proposed by the German company Junkers during WWII. This engine was introduced with a mechanical synchronization mechanism which provided precise control on the two opposite pistons. With such mechanism, the compression ratio of the engine could even reach to 40:1 [52]. Nowadays, the modern FPEs are usually hydraulic engines: Hibi and Ito developed an opposed piston hydraulic FPE whose pistons were synchronized by the combination of an electronically controlled hydraulic rebound and a mechanical spring system [53]; The Dutch company Innas claimed that their hydraulic FPE product has power output of 17 kW with nearly 50% efficiencies [54]; Tikkanen and Vilenius also reported a hydraulic FPE operated with PID and feed forward control [55]. Attracted by its high efficiency and flexibility, free piston linear alternator has also been investigated worldwide. Sandia national laboratory reported a 15kW FPE with linear alternator runs at high compression ratio range (20 –

40) in 1999 [56]. The engine features opposed piston design and oscillates around 24 Hz. Multi-fuel operations on free piston engine have also been examined by Flynn [57] and others [58]. Besides, researchers from Toyota Central R&D Laboratory have also developed a 10 kW two-stroke FPE linear generator [59], [60]. In addition, an opposed-piston free piston linear generator (FPLG) has been developed at the German Aerospace Center as well [61].

As an alternative to the conventional ICE, the free piston engine (FPE) has great potential for efficiency improvement and emissions reduction. The FPE removes the crankshaft that constrains the movement of the piston, therefore it features linear piston motion that is determined by the combustion force and load in real time. The advantages of the FPE design are:

- **Variable compression ratio**: Engine efficiency is found to be closely related to the engine compression ratio [29]. By applying proper compression ratios to different loading conditions, the overall efficiency of the ICE can be significantly improved. The ability to vary compression ratio allows the engine to operate on various fuels as well. Different variable compression ratio mechanisms have been proposed. Most of them suggest a modification of the crank/connecting rod mechanism with mechanical linkages and an actuation system [62]-[64]. Even though the designs offer some flexibility of variable compression ratio control, the improvement of engine performance is limited by the operating range of the mechanism. The large inertia limits the response time of the mechanism, which leads to undesired engine transient behavior, thus degrades the engine performance. What's more, modification of current

engine parts and addition of extra components increase the system cost and complexity. The FPE, on the other hand, offers the ultimate flexibility for variable compression ratio control by eliminating the crankshaft, therefore enables advanced combustions such as low-temperature combustion, which provides better fuel economy and less NOx emission. Initial testing of an FPE, conducted by Sandia National Laboratory, has demonstrated an indicated thermal efficiency of 56% with near zero NOx emissions in a single-cycle experiment [65].

- **Reduced friction loss**: By removing the crankshaft, the crankshaft bearing friction and piston side friction are eliminated as well.
- **Simpler design**: Compared to its crankshaft-based counterpart, FPE carries a simpler design with fewer moving parts, resulting in a compact engine with low production and maintenance costs.
- **Modularity**: For mobile applications including both highway vehicles and mobile heavy equipment, fluid power is currently generated on board using a crankshaft-based ICE (either gasoline or diesel) with a rotational hydraulic pump (Figure 1.2). The main drawbacks of this configuration are its relatively low efficiency and complex design of both the ICE and the hydraulic pumping system due to the dynamic operating requirements. The FPE does not connect to load mechanically, which results in a modular design with high flexibility. For a particular application, several FPE units can be combined to provide the power required. However, unlike conventional ICEs, these units can be placed at different locations because they are not interconnected by mechanical linkages. More importantly, they can be turned on

and off individually with respect to the loading conditions to ensure optimal efficiency.

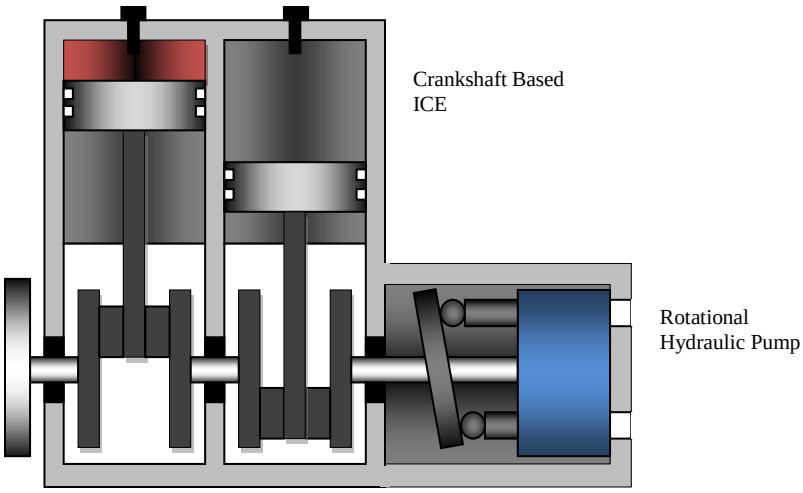

Figure 1.2 Crankshaft-based ICE with rotational hydraulic pump

Free-piston engine driven hydraulic pump can be designed with three different architectures: single piston, opposed piston, and opposed chamber arrangement: Single-piston architecture is the most widely-used one for research due to its simplest structure; Opposed-piston architecture produces no vibration due to its self-balanced structure; Opposed chamber arrangement offers higher power density and scavenge efficiency. The free-piston engine we are investigating right now is an opposed-piston opposed-cylinder (OPOC), two-stroke combustion engine [66], whose schematic diagram and picture are shown in Figure 1.3. This configuration offers the ultimate power density and energy density (order of magnitude higher than electrical systems) and therefore become extremely attractive for mobile applications.

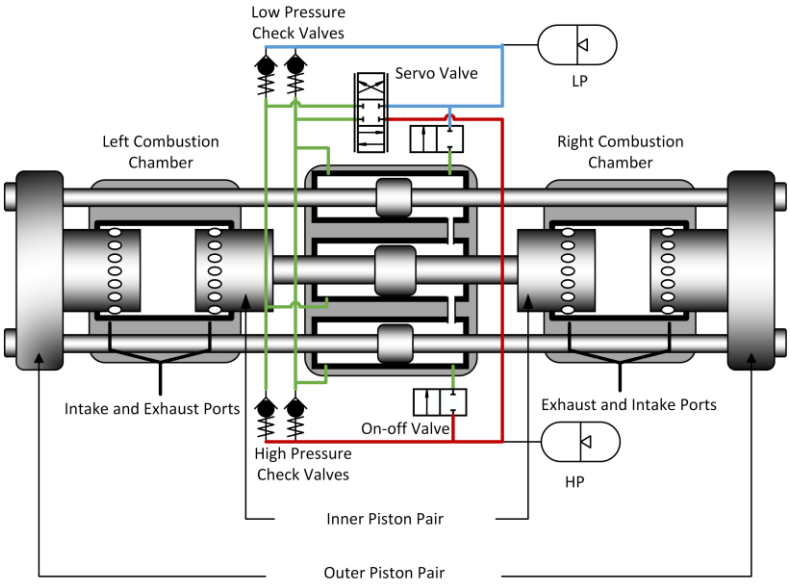

(a)

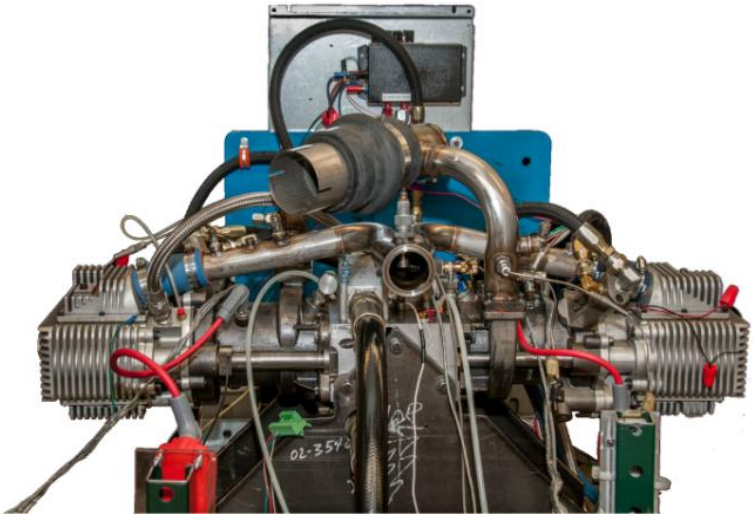

(b)

Figure 1.3 (a) Schematics of the OPOC free-piston engine (b) Picture of the FPE

As shown in Figure 1.3 (a), the left chamber of the engine starts at its bottom dead center (BDC), where the distance between the left ends of two piston pairs are at the furthest. Then the pistons move toward each other while the in-cylinder gas is compressed until the top dead center (TDC), where the in-cylinder gas is ignited. Force generated by the subsequent combustion process would then push the pistons away from

each other while the gas inside the right chamber is being compressed to auto-ignition similar to the above process in the left. Afterward, two chambers fire alternately to keep the piston pair moving linearly. The engine specifications are summarized in [66] as well.

Table 1.1 Hydraulic free piston engine specifications [66]

Item	Specification
Engine	
Bore	79.5 mm
Stroke	120 mm
Displacement/Cylinder	0.6 L
Hydraulic system	
Inner plunger diameter	13.4 mm
Outer plunger diameter	9.48 mm
Piston Mass	9 kg

1.2.3 Virtual Crankshaft Mechanism

The key enabler for the FPE technology is the piston motion control since its piston motion is completely determined by the forces acting on the piston in real time. Several FPE motion control strategies have been published in the literature. Among them is the Pulse Pause Modulation (PPM) control which has been implemented by a number of researchers on single-piston and opposed-piston FPEs [53], [54] and [67]. The main idea is to utilize hydraulic circuits as a bounce chamber which holds the piston at its BDC to achieve identical piston motion of each engine cycle. A flow control valve is used to adjust the waiting period between the consecutive cycles. Therefore, the output flow rate of the engine can be changed in real time by adjusting the timing of the flow control valve. Researchers from Beijing Institute of Technology have developed a single-

chamber hydraulic FPE with 15 kW maximum power output [68]. The engine utilizes its hydraulic circuits and the pulse pause modulation technique [69] to control the operating frequency and adapts the pause width to the BDC position to minimize cycle-to-cycle variation. The hydraulic FPE is able to achieve stable engine operation with an indicated thermal efficiency of 41%. Due to the identical engine cycles, the PPM control produces nearly constant efficiencies across the engine power output range. However, this approach is only applicable to the single-chamber FPE architectures where continuous operation is not required. Johansen et al. [70] developed a control system for an FPE powered turbine with air bounce chamber. The control system utilizes PID controllers to regulate the location of the TDC by adjusting the air mass in the bounce chamber, while the location of the BDC is controlled by adjusting the fuel injection quantity. Stable engine operation was achieved at a specific operating condition with the proposed control. Mikalsen and Roskilly [71] investigated the motion control of an FPE linear generator with air bounce chamber. A pseudo-derivative feedback (PDF) control maintains the TDC and BDC at the reference by adjusting the fuel injection quantity and air mass of the bounce chamber. In addition, a feedforward control modifies the fuel quantity and air mass according to the load. Simulation results show that the PDF plus feedforward control have a better transient performance than PID control when handling load change. Researchers from Nanjing University of Science and Technology reported the prototype testing results of a single-chamber four-stroke FPE linear generator [72]. A PID control scheme is employed for TDC and BDC location control by adjusting the current and fuel injection quantity. The engine is able to realize Atkinson cycle with a

generating efficiency of 32% at 2.2 kW. Researchers from Toyota Central R&D Laboratory [59], [60] have developed a piston motion control for an FPE linear generator. The motion control consists of a PID control and a gain scheduling map to alter the loading force to regulate the piston motion. The experimental results demonstrate stable engine operation at a specific operating point with the control scheme. An energy-balance based feedback control strategy, which adjusts the fuel injection quantity each cycle by calculating the energy flows in and out from the combustion chamber, was proposed by Tikkanen and Vilenius [55] for a dual-chamber FPE. Simulation results showed that the control strategy was able to produce stable energy operation at various operation points, but it does not address the engine stall issue of the FPE in the case of a misfire. Researchers from the German Aerospace Center have been developing a free piston linear generator (FPLG). A hydraulic test stand is utilized initially to test the components of the FPLG. With a flatness-based feedforward plus PID and PD repetitive feedback control structure, the hydraulic actuator is able to track high frequency and high amplitude trajectory without the presence of combustion chambers [73]. A demonstrator system (with a linear generator and two opposed air chamber) was then built along with the development of a piston motion control strategy, which is also energy-based but derives the required instantaneous linear generator force to reach the TDC and BDC target [61].

Besides the limitation of being applicable to only a specific FPE architecture, many of the existing control strategies rely on calibration to be effective. However, the complex interactions between the gas dynamics and the load in real time make the calibration a

tedious task, and the resulting controllers are sensitive to the variation of the operating conditions and disturbances. It imposes a huge challenge on the engine operation control and systematic active control that can precisely regulate the piston motion is required.

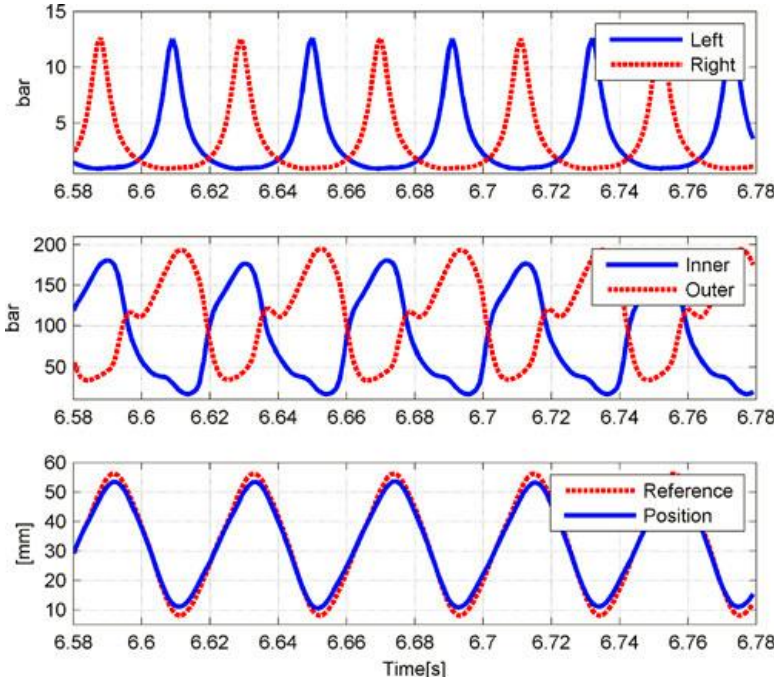

Figure 1.4 Motoring data (from top to bottom): combustion chamber pressure, hydraulic chamber pressure, tracking performance [66]

One of the main milestones achieved for our FPE was the successful development and implementation of an advanced piston motion control. The active controller was designed to act as a virtual crankshaft [66], which forces the piston to follow any reference trajectory using the energy from the storage elements. The controller generates actuator (Servo valve) signal which is calculated based on the feedback of the piston position. By controlling the opening of the servo valve, the controller actually controls the hydraulic forces acting on the piston pair, and therefore the piston motion. Figure 1.4 shows a set of engine motoring results where the FPE was commanded to utilize the

stored energy from the accumulator to motor the engine at 25 Hz. Obviously, from the agreement between the piston actual position and the corresponding piston trajectory reference, we have demonstrated the effectiveness of the "virtual crankshaft" mechanism.

On top of that, a feedforward control method was developed to further enhance the tracking performance of the virtual crankshaft mechanism [74] and a transient control was also developed aimed to reduce the transient period when the FPE operates from motoring to firing [75]. Attributed to the above developments, the continuous combustion operation is finally achieved, which is the first successful experimental test in the world for the FPE with the OPOC architecture (Figure 1.5).

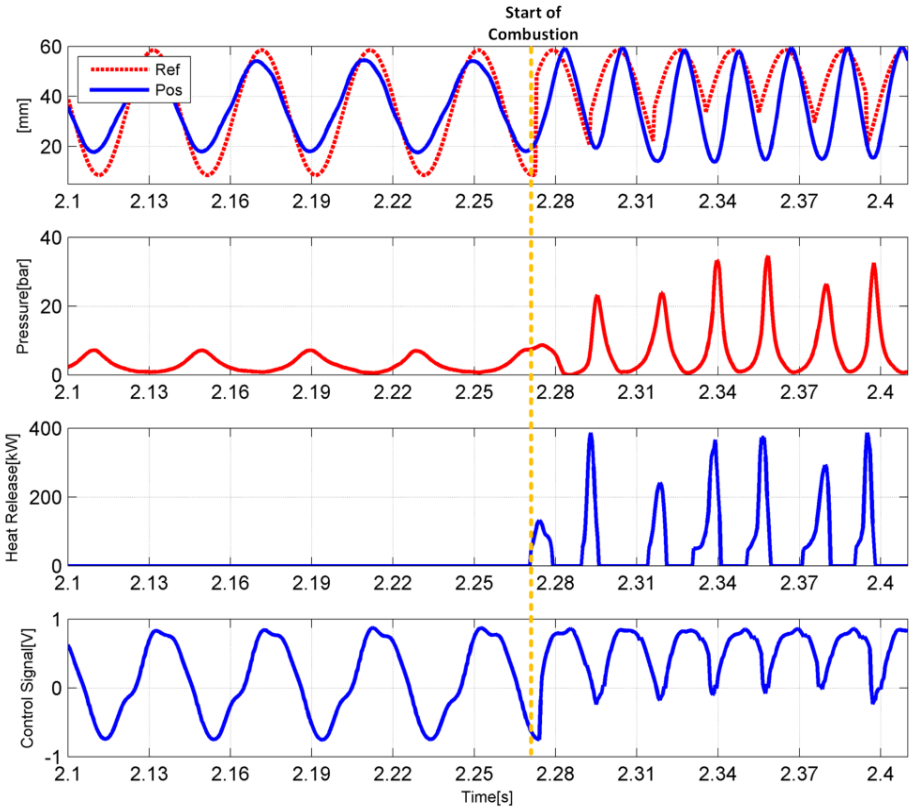

Figure 1.5 Continuous engine operation data during the transient period: first 4 cycles are motoring result and Afterward continuous firing operation (from top to bottom: piston motion

with the corresponding reference trajectory, in-cylinder pressure, heat release rate in combustion, and control signals) [75]

Furthermore, not only can the active control guarantee a stable operation, it could also regulate the engine to run at maximum efficiency and operate optimal emission performance. With a mechanical crankshaft, the piston trajectory is fixed and is independent of variant engine speed and diverse load conditions. Thus, there are limited means for optimizing the engine performance. However, with the "virtual crankshaft", piston trajectory can be varied in real time by altering the reference to the piston motion controller. Given the periodic nature of the FPE piston motion, the advanced controller employed here is of the robust repetitive type which is capable of tracking any periodic reference signals with known period. A key feature of the repetitive control is its extremely fast convergence rate of the tracking error due to its high feedback gains at the desired frequency locations [76]-[78].

1.3 Research Objectives

Enlightened by this capability of the FPE, e.g. varying piston trajectories in real-time, an advanced combustion control, namely the "Trajectory-based Combustion control", has been proposed [79]. In this method, the controllable piston trajectory in the FPE works as an extra control means to actively regulate the combustion chamber volume in real-time, and therefore adjust the gas pressure-temperature history and species concentration prior, during, and after the combustion event within each engine cycle (as shown in Figure 1.6). Extensive simulation work has been conducted and the corresponding results demonstrate that the trajectory-based combustion control enabled by the FPE is able to increase the

engine thermal efficiency significantly and reduce the engine-out emissions simultaneously [80].

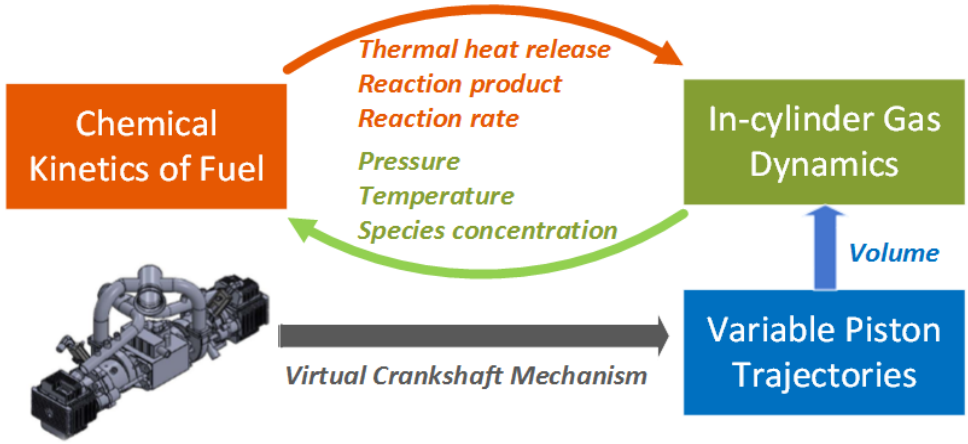

Figure 1.6 Interaction between chemical kinetics and gas dynamics

Considering the fact that the HCCI combustion is mainly driven by the chemical kinetics of the fuels, the trajectory-based combustion control is even more powerful for this combustion mode and enables optimization of its chemical reactivity and heat transfer processes by removing the traditional constraints on gas pressure-temperature history imposed by the mechanical crankshaft. Hence, an optimal trajectory can be designed and implemented to the FPE by taking the chemical kinetics of utilized fuels and associated thermodynamics processes of in-cylinder gases into account. The overall system configuration of the trajectory-based combustion control in the FPE is then shown in Figure 1.7. The inner loop is the piston motion control, which is achieved through the "Virtual Crankshaft" mechanism [66], and the outer loop is the trajectory optimization that will generate the desired optimal piston trajectory reference for the inner loop. Considering the repetitive nature of the piston trajectory in the FPE, the focus is to design the optimal piston trajectory within an engine cycle.

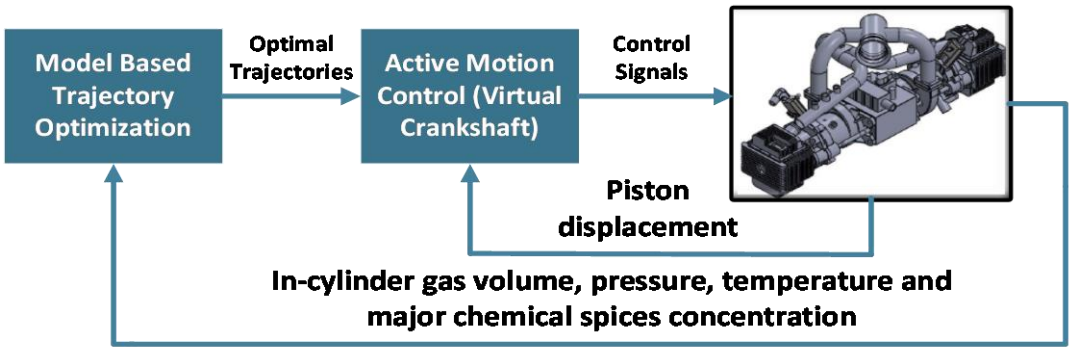

Figure 1.7 Overall system configuration

To summary, the research aims to characterize and optimize the dynamics of HCCI combustion with unconstrained gas pressure-temperature history enabled by the free piston engine. This approach essentially opens up a new framework for controlling advanced combustion. Fundamental properties of the in-cylinder processes will first be investigated to gain insights into the influence of the unconstrained gas pressure-temperature history. On this basis, the control-oriented model will be developed to achieve the maximum attainable fuel efficiency and emissions benefits by designing the optimal piston trajectory. Specific tasks include:

Task 1: Model the in-cylinder processes with chemical kinetics and thermodynamic states to explore sensitivities of species production and destruction rates as a function of piston trajectory. This task will reveal how the piston trajectory affects the combustion process through both chemical kinetics of various fuels (including alternative fuels) and the engine output parameters such as the start of combustion (SOC), heat loss, and emissions.

Task 2: Develop a control-oriented model to realize the trajectory-based HCCI combustion control in practice. Considering the fact that the HCCI combustion is mainly

driven by the chemical kinetics of the utilized fuel, such a control-oriented model needs to capture sufficient chemical kinetics information to reproduce the combustion process while the related computational burden has to be small enough.

Task 3: Based on the above models, optimal piston trajectories, in terms of the highest attainable engine efficiency and minimum emission production, will be designed by leveraging the dynamic coupling between chemical kinetics and gas dynamics. Both off-line and on-line optimization methods will be developed, which are aimed to realize the real-time optimization in FPE eventually.

1.4 Contribution Summary

1. Proposed a novel combustion control, namely the trajectory-based combustion control, enabled by the FPE. In this control method, the controllable piston trajectory of the FPE becomes an active control means to effectively influence the temperature, pressure and species concentration prior to, during and after the combustion events within an engine cycle.
2. Conducted extensive simulation to demonstrate the effects of various piston trajectories on the combustion process, in terms of the start of combustion, the location of peak temperature, output work, and NOx emission. The simulation results also show that significant improvement in engine efficiency and NOx emission can be achieved simultaneously by designing and implementing specific asymmetric piston trajectory into the FPE. In addition, such a benefit on the engine performance can be obtained for both conventional fuels and alternative fuels applications.

3. Developed a control-oriented model aims to implement the trajectory-based combustion control in practice. In the control-oriented model, a unique phase separation method has been proposed, which separates an engine cycle into four phases and employs the minimal reaction mechanism accordingly to represent the chemical kinetics of the fuel. In this way, the proposed model not only reduces significant computational burden but also keeps sufficient chemical kinetics information. On top of that, the high fidelity of the control-oriented model has been sustained at various working conditions, including different compression ratios and various air-fuel ratios.
4. Developed both offline and online optimization approaches for the trajectory-based combustion control. Both the load conditions and chemical kinetics of the utilize fuel are taken into account while designing the optimal piston trajectory for the FPE operation. By implementing the derived optimal piston trajectory into the FPE, the engine achieves the maximal engine thermal efficiency and minimal engine emissions simultaneously.

1.5 Dissertation Overview

The research achievements in the thesis will be presented in details as follows:

Chapter 2 (Development of the chemical kinetics driven model for the trajectory-based combustion control): In this chapter, a model of the FPE running HCCI combustion under various piston trajectories is presented. The various piston trajectories have the ability to change the compression ratio and accommodate different piston motion patterns between the top dead center and the bottom dead center. Six

reaction mechanisms are employed in the model in order to demonstrate the multi-fuel combustion ability of the FPE and to describe the chemical kinetics of different fuels under various piston trajectories.

Chapter 3 (Effects of the trajectory-based combustion control on combustion performance): In this chapter, the simulation results of the above chemical kinetics driven model are presented and analyzed. The corresponding results reveal the various piston trajectory effects on the combustion in terms of in-cylinder gas temperature trace, indicated output work and heat loss. In addition, such an effect is also illustrated through a chemical kinetics perspective, which shows how the different piston trajectories varying the accumulation process of the radical species and then subsequently influence the corresponding HCCI combustion process.

Chapter 4 (Effects of the trajectory-based combustion control on engine emissions): In this chapter, the effects of the trajectory-based combustion control on engine-out emissions are investigated. First, the aforementioned chemical kinetics driven model is further expanded to include a mechanism producing asymmetric piston trajectories in the FPE. Afterward, the chemical kinetics of CO and NOx emissions in a reduced n-heptane mechanism are described in details that reveal the feasibility of reducing engine-out emissions by employing novel piston trajectories. At last, analyses of the corresponding simulation results and comparisons of emissions and thermal efficiencies between the FPE and conventional ICEs are presented, which further shows the advantages of the trajectory-based combustion control.

Chapter 5 (Effects of the trajectory-based combustion control on renewable fuels): In this chapter, the utilization of the trajectory-based combustion control is extended to renewable fuels applications. Seven renewable fuels are considered including hydrogen, biogas, syngas, ethanol, dimethyl ether (DME), biodiesel, and Fischer-Tropsch fuel. The influences of both CR and piston motion pattern between the two dead centers on the combustion process are considered in the study, which demonstrates the ultimate fuel flexibility and large tolerance of fuel impurity possessed by the FPE. In addition, the simulation results show that at a fixed CR, the thermal efficiency of the FPE can still be enhanced (5% in DME case) by varying the piston motion patterns alone. Furthermore, specific asymmetric piston trajectories are synthesized to further improve the engine thermal efficiency (8% in hydrogen case) and reduce the NOx emission simultaneously (around 70% reduction in hydrogen case). In other words, due to its ultimate fuel flexibility, large tolerance of fuel impurity, and controllable piston trajectory, the FPE, with the trajectory-based combustion control, enables a co-optimization of renewable fuels and engine operation.

Chapter 6 (Development of the control-oriented model for the trajectory-based combustion control): In this chapter, a control-oriented model is proposed and its performances, in terms of computational speed and model fidelity, are compared to two existing models: a simplified model using a one-step global reaction and a complex physics-based model including detailed chemical reaction mechanisms. A unique phase separation method is employed in the proposed model to significantly reduce the computational time and guarantee the prediction accuracy simultaneously. In addition,

extensive simulation results also show that the high fidelity of the proposed model is sustained at multiple working conditions, including different air-fuel ratios, various compression ratios and distinct piston motion patterns between the two end positions.

Chapter 7 (Optimization of the trajectory-based combustion control): In this chapter, the study of the optimization of the trajectory-based combustion control, based on the control-oriented model, is presented. Both offline and online optimizations are investigated. For the offline optimization, two optimization methods are proposed in this chapter: one is converting the original problem to parameters optimization; the other is transforming it to a constrained nonlinear programming and solving it via the sequential quadratic programming (SQP) method. The corresponding optimization results and detailed discussions are followed, which clearly demonstrate the advantage of the trajectory-based HCCI combustion with regard to FPE output work and NOx emission. In addition, an example is presented in the end of the chapter showing how the proposed control-oriented model enables online optimization of the HCCI combustion phasing by varying the trajectories shapes. The simulation results show that the combustion phasing can be adjusted quickly as desired, which further demonstrates the effectiveness of the piston trajectory-based combustion control.

Chapter 8 (Conclusions and Future Work): This chapter concludes the thesis with a summary of the research achievements and future work.

Chapter 2

Development of the Chemical Kinetics Driven Model for the Trajectory-based Combustion Control

The chemical kinetics driven model is developed by assigning the FPE combustion chamber as a homogeneous variable-volume batch reactor, and the scavenging process is neglected during this simulation. In this section, the geometric structure of the FPE and the formation of variant piston trajectories are presented at first. Secondly, a physics-based model is constructed with thermodynamics and heat transfer. Then, individual chemical reaction mechanisms are employed to represent the combustion processes of different fuels. Finally, the modeling tools used to integrate the above subsystems into a complete model and analyze the model dynamics are introduced.

2.1 Geometric Structure

Composed of three main components, namely two combustion chamber at both ends and a center hydraulic unit, the FPE is built in a symmetric configuration, as shown in Figure 1.3. At the specific time instant shown in Figure 1.3 (b), the right combustion chamber is at its TDC point and the left combustion chamber is at its BDC point. Combustion in the right chamber will push the two piston heads away from each other and generate fluid power in the hydraulic unit. Meanwhile, the gas inside the left chamber is compressed to trigger the auto-ignition therein. Consequently, these two chambers fire alternately and examining the dynamics of a single chamber is sufficient to

understand the influence of the piston trajectory. Besides, the hydraulic unit not only enables the two piston pairs to track the prescribed reference but also synchronizes them with the same speed but opposite direction [66]. Therefore, the two piston heads move in mirror symmetry with respect to the center of the combustion chamber and the corresponding chamber volume profile can be derived by the distance between the piston head to the center line.

Unlike the conventional ICE, the piston motion in FPE is not constrained by the slider-crank mechanism. With the ultimate freedom of piston motion, FPE enables the continuously variable CR as well as variable piston motion patterns between the BDC and TDC. Therefore, a new method describing such piston motion is presented.

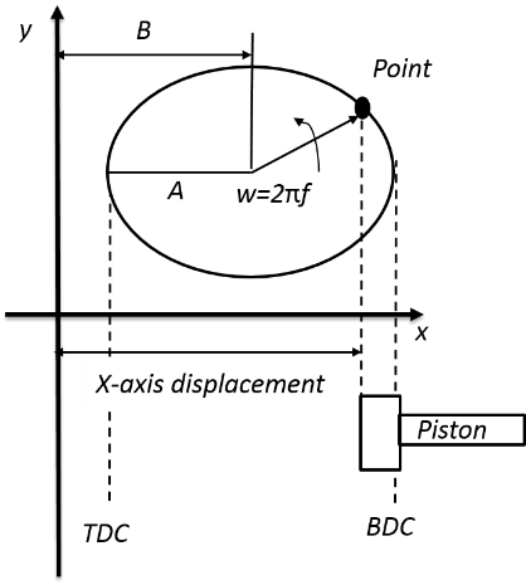

Figure 2.1 Description of FPE piston motions

As shown in Figure 2.1, the FPE piston motion is represented as the x-axis displacement of a point moving around an ellipse in the Cartesian coordinate. Four parameters are then used to reflect the piston motion:

(1) Amplitude *A* represents the major axis of the ellipse;

(2) Bias *B* indicates the location of the ellipse center;

(3) Frequency *f* reflects the angular velocity of the mass point;

(4) Ellipse ratio Ω (= minor axis / major axis), describes the shape of the ellipse.

As a result, the piston trajectory can be derived as follow:

$$X = \frac{A \cdot \Omega \cdot \cos(2\pi f \cdot t)}{\sqrt{\Omega^2 \cdot \cos(2\pi f \cdot t)^2 + \sin(2\pi f \cdot t)^2}} + B \tag{2.1}$$

While *A* and *B* identify the locations of the TDC and the BDC and therefore the compression ratio. *f* and Ω indicate the frequency of the piston movement and its motion pattern between the TDC and the BDC respectively. *t* stands for time.

Figure 2.2 shows piston trajectories with different CR and Ω. It is clear that piston trajectory with higher CR compresses the in-cylinder gas more aggressively, and higher Ω indicates the longer duration of the piston staying around the TDC.

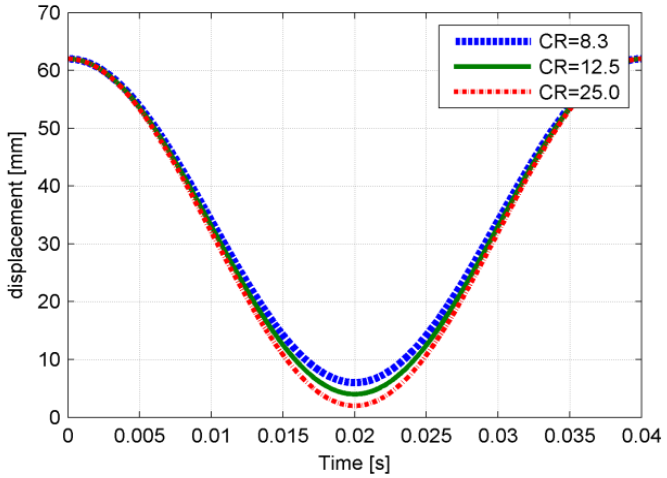

(a)

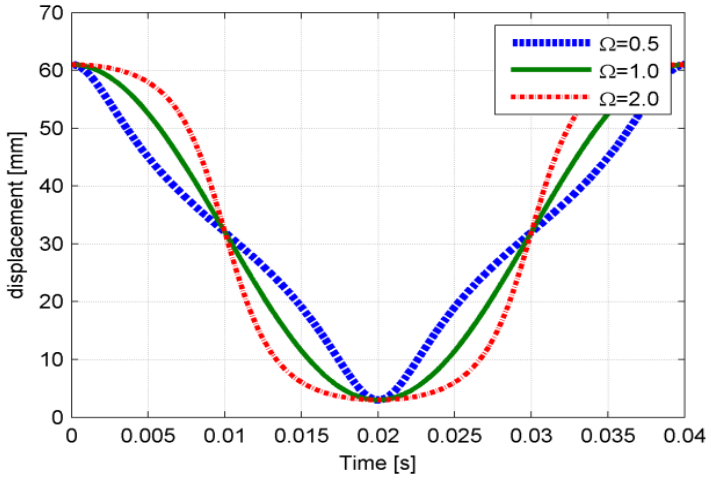

(b)

Figure 2.2 Piston trajectories with different (a) CR and (b) Ω

2.2 Physics-based Model

Since the scavenging process is neglected, the combustion chamber is modeled as a closed thermodynamic system by energy and species mass conservation equations [81]:

$$\frac{dU}{dt} = -P\frac{dV}{dt} - \dot{Q}_{HT} + \dot{Q}_{Chem} \tag{2.2}$$

$$m\frac{d\omega_i}{dt} = \dot{m}_{i,chem} \qquad i=1, 2\ldots N_s \tag{2.3}$$

In (2.2), the left term, *dU/dt* reflects the change rate of the internal energy of the charge mixture in the combustion chamber. The three terms on the right of (2.2) represent the volumetric work, heat loss through the engine wall and the heat release from the chemical reaction respectively. One should be noted that the *dV/dt* term is determined by various piston trajectories, as shown in Figure 2.2.

In (2.3), m is the total mass in the combustion chamber which is a constant determined by the initial conditions such as the mass of fuel and the air-fuel equivalence ratio λ, N_s is the total number of species in the mechanism, ω_i represents the mass fraction of species i. The right term in (2.3) reflects the net mass production rate of species i due to the chemical reactions.

To be more specific, dU/dt can be yielded:

$$\frac{dU}{dt} = \sum_{i=1}^{N_S} C_{v,i} \cdot m \cdot \omega_i \frac{dT}{dt} + \sum_{i=1}^{N_S} C_{v,i} \cdot m \cdot T \cdot \frac{d\omega_i}{dt} \tag{2.4}$$

where $C_{v,i}$ is the constant volume heat capacity of species i and T is the in-cylinder gas temperature.

The heat loss term is described via the convection model:

$$\dot{Q}_{HT} = h \cdot A_{wall} (T - T_{wall}) \tag{2.5}$$

where A_{wall} is the variable surface area of the chamber, T_{wall} is the wall temperature and h is the heat transfer coefficient.

For the sake of convenience, T_{wall} is assumed as 500K during the simulation, which is the typical average temperature of the inner engine wall [82], [83]. The coefficient of heat transfer h is determined via modified Woschni correlation [29]:

$$h = 3.26 \cdot b^{-0.2} P^{0.8} T^{-0.55} w^{0.8} \tag{2.6}$$

where b is the bore of the engine, which is 79.5 mm, P and T are the pressure and temperature of the in-cylinder gas respectively, and w is the average in-cylinder gas velocity, which is set as 8 m/s based on the operation of the FPE [29]. The feasibility of the modified Woschini correlation is demonstrated experimentally in [84].

Moreover, the in-cylinder pressure P and temperature T are coupled with each other through the ideal gas law:

$$P \cdot V = m \cdot R_{mass} \cdot T \tag{2.7}$$

where V represents the volume of chamber and R_{mass} is the gas constant of the intake charge in mass base,

$$R_{mass} = \sum_{i=1}^{N_S} R_i \cdot \omega_i = \sum_{i=1}^{N_S} \frac{R}{M_i} \omega_i \tag{2.8}$$

where R_i and M_i indicate the gas constant and the molar weight of each species i, and R is the universal gas constant.

2.3 Chemical Reaction Mechanisms

In order to solve (2.2) to (2.4), a proper reaction mechanism is needed to acquire thermal data of each species and calculate the corresponding chemical states:

$$\dot{Q}_{Chem} = -V \cdot \sum_{i=1}^{N_S} v_i \cdot h_{i,m} \tag{2.9}$$

$$m \frac{d\omega_i}{dt} = \dot{m}_{i,chem} = V \cdot M_i \cdot v_i \tag{2.10}$$

where v_i and $h_{i,m}$ denote the net production rate and the molar enthalpy of species i respectively.

A complete reaction mechanism usually includes two parts, namely the thermal data part and the chemical reactions part. In the first part, thermodynamic properties of each species are represented via the NASA polynomial parameterization [85]:

$$\frac{C_{v,i}(T)}{R} = a_0 + a_1 T + a_2 T^2 + a_3 T^3 + a_4 T^4 - 1 \tag{2.11}$$

$$\frac{h_{i,m}(T)}{RT} = a_0 + \frac{a_1}{2}T + \frac{a_2}{3}T^2 + \frac{a_3}{4}T^3 + \frac{a_4}{5}T^4 + a_5 \tag{2.12}$$

$$\frac{S_{i,m}(T)}{R} = a_0 \ln T + a_1 T + \frac{a_2}{2}T^2 + \frac{a_3}{3}T^3 + \frac{a_4}{4}T^4 + a_6 \tag{2.13}$$

where a_0 to a_6 are seven parameters in the NASA polynomial parametrization. Thus, these thermodynamic properties, $C_{v,i}$, $h_{i,m}$ and the species molar entropy $S_{i,m}$, can be obtained if the in-cylinder temperature T is given.

The net production rate of specific species i, namely v_i in (2.9) and (2.10), is calculated using the chemical reaction part of the mechanism and as follows. One should be noted that within this approach, the volume of the combustion chamber is assumed to be constant at each time step.

For a standard reaction:

$$n_a A + n_b B \Leftrightarrow n_c C + n_d D \tag{2.14}$$

the stoichiometric parameters, n_a, n_b, n_c, n_d, are readily specified in the mechanism. As a result, the net rate of production of species A can be yield as [81]:

$$\frac{d[A]}{dt} = n_a \cdot (-k_f [A]^{n_a} [B]^{n_b} + k_b [C]^{n_c} [D]^{n_d}) \tag{2.15}$$

where [A] represents the molar concentration of A:

$$[A] = \frac{m \cdot \omega_A}{M_A \cdot V} \tag{2.16}$$

where ω_A and M_A denote the mass fraction and the molar weight of species A respectively. Other species molar concentration can be obtained similarly.

k_f is the forward reaction rate coefficient, determined by a standard Arrhenius equation.

$$k_f = A \cdot T^n \cdot \exp^{(-\frac{E_a}{RT})} \tag{2.17}$$

where A is the pre-exponential factor, n is the temperature dependence and E_a indicates the reaction active energy. It should be noted that special treatments need to be employed if the reaction is pressure-dependent or includes a third body collision.

The reverse rate coefficient k_b can then be computed with the equilibrium coefficient K_e, which is a function of Gibbs free energies of the species in (2.14)

$$\frac{k_f}{k_b} = K_e = \exp^{(-\frac{\Delta G^o}{RT})} \tag{2.18}$$

$$\Delta G^o = \sum_{i=c,d} n_i \cdot (h_{i,m} - TS_{i,m}) - \sum_{i=a,b} n_i \cdot (h_{i,m} - TS_{i,m}) \tag{2.19}$$

where ΔG^o is the difference of the gross Gibbs free energies between the reactants and the products in (2.14).

Of course, there are other reactions relative to species A in the mechanism as well and therefore the gross net production of A is the sum of such reaction rates:

$$\nu_A = \sum_{1}^{N_{rxn}} \frac{d[A]}{dt} \tag{2.20}$$

where N_{rxn} represents the total number of the reactions related to species A. Similarly, the net production rate of other species can be obtained as well.

In order to reflect the relationship among the aforementioned equations more clearly, the logical flow of the dynamic model is shown in Figure 2.3. Typically, the piston trajectory provides volume V, volume change rate dV/dt and variable chamber surface

area A_{wall} to the other two models. Meanwhile, the chemical reaction mechanism sends the thermal properties of each species and the calculated chemical states into the physical-based model, while the physical-based model offers temperature T, pressure P and mass fraction of each species w_i in return. Inside the physics-based model, the heat loss submodel provides the heat loss term to the thermal dynamics submodel after receiving T and P.

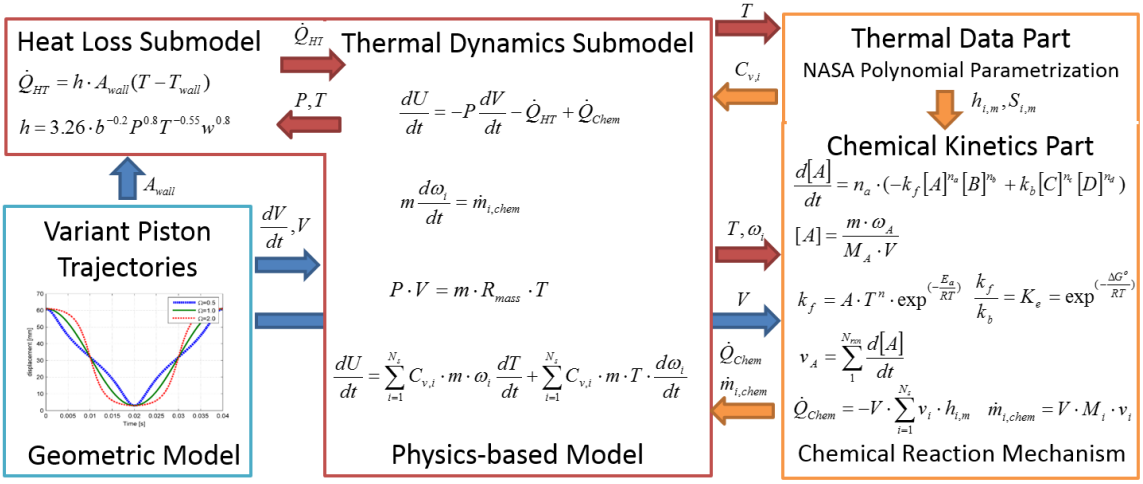

Figure 2.3 Diagram of the presented modeling approach

The utilization of a detailed reaction mechanism in the model enables the investigation of the complex interaction between the gas dynamics and the fuel chemical kinetics. Such investigation cannot be obtained by existing control-oriented models, which oversimplifies the chemical kinetics by utilizing the integration of Arrhenius equation to predict the SOC and assuming chemical heat release is instantaneous [86]-[88].

However, selecting the proper mechanism is a nontrivial task. First of all, the chosen mechanism has to be sufficiently accurate to predict the combustion process precisely. To

fulfill this requirement, a number of element reactions need to be included in the mechanism which increases the number of species N_s and extends the calculation time. The large size of the reaction mechanism implies higher dimensions of the dynamic system, which increases the difficulty to achieve the convergence of the numerical results. Therefore, the selected reaction mechanism should make a good balance between the precise prediction of the combustion and the computational burden. For example, the UC San Diego (UCSD) mechanism [89] is selected to represent the chemical kinetics of propane in this study among out of tremendous propane reaction mechanisms proposed in combustion community. It was derived with simple chemical kinetics at the beginning and then augmented gradually to form more complex systems. In this approach, the numbers of species (50) and reactions (244) are kept to the minimum needed to describe the combustion process accurately. Other fuels mechanisms are selected based on this requirement as well. The selected reaction mechanisms are listed in Table 2.1, which shows up the corresponding numbers of species and reactions.

Table 2.1 Selected reaction mechanisms

Fuel	Number of species	Number of reactions	Resource
Methane	53	325	GRI-30 [a]
Propane	50	244	UC Santiago
Ethanol	57	383	LLNL [b]
DME	79	683	LLNL
Ammonia	23	98	Cal-tech
n-Heptane	160	1540	LLNL

a: GRI-30 mechanism is mainly proposed by UC

b: LLNL stands for Lawrence Livermore National Laboratory

2.4 Modeling Tool—Cantera and Mixmaster

Cantera is an open-sourced software package which is capable of executing the chemical, thermodynamic and kinetics calculation [85]. In this research, it is used to implement the reaction mechanisms into the physics-based model and simulate the combustion under variant piston trajectories within the Python environment. Additionally, the combustion process can be illustrated from a chemical kinetic perspective via the MixMaster, which is a post-processing application of Cantera that allows users to gain more information on the reaction process via the reaction paths diagrams at a different time instant.

Chapter 3

Effects of the Trajectory-based Combustion Control on Combustion Performance

As shown in Figure 2.2, piston trajectories are characterized by different CRs and motion patterns between the TDC and the BDC (represented by Ω). It is widely known that variable CR has a significant influence on engine efficiency [29] and able to provide ultimate fuel flexibility [42], [57] and [90]. However, the parameter Ω can also affect the combustion process in terms of SOC (start of combustion), indicated output work, heat loss, and radical species accumulation process. The corresponding results are shown in this chapter.

3.1 In-cylinder Temperature Traces

Six fuels, namely methane, propane, ethanol, DME, n-heptane and ammonia, and four CRs are investigated at first to reveal how CR of piston trajectory influences the combustion process (Figure 3.1). Noting that at 20ms, the piston is located at the TDC point since the frequency of the engine operation is fixed at 25 Hz. As can be seen in Figure 3.1, when CR is 20.3, only n-heptane and DME are able to be ignited by compression. If CR is increased to 24.6, propane and ethanol are able to combust as well. Further increasing CR over 30, even methane, which is the most stable hydrocarbon fuel, can react and completely combust. Finally, when CR reaches 48.2, all six fuels, including

ammonia, have abrupt temperature rise which indicates the combustion occurrence. Therefore, varying CR solely enables multiple fuel combustion in FPE

Furthermore, from the temperature trace of propane or other utilized fuel, it is apparent that the SOC timing is advanced as the CR increases. It is intuitive since larger CR of piston trajectory, more aggressive compression the in-cylinder gas is subject to.

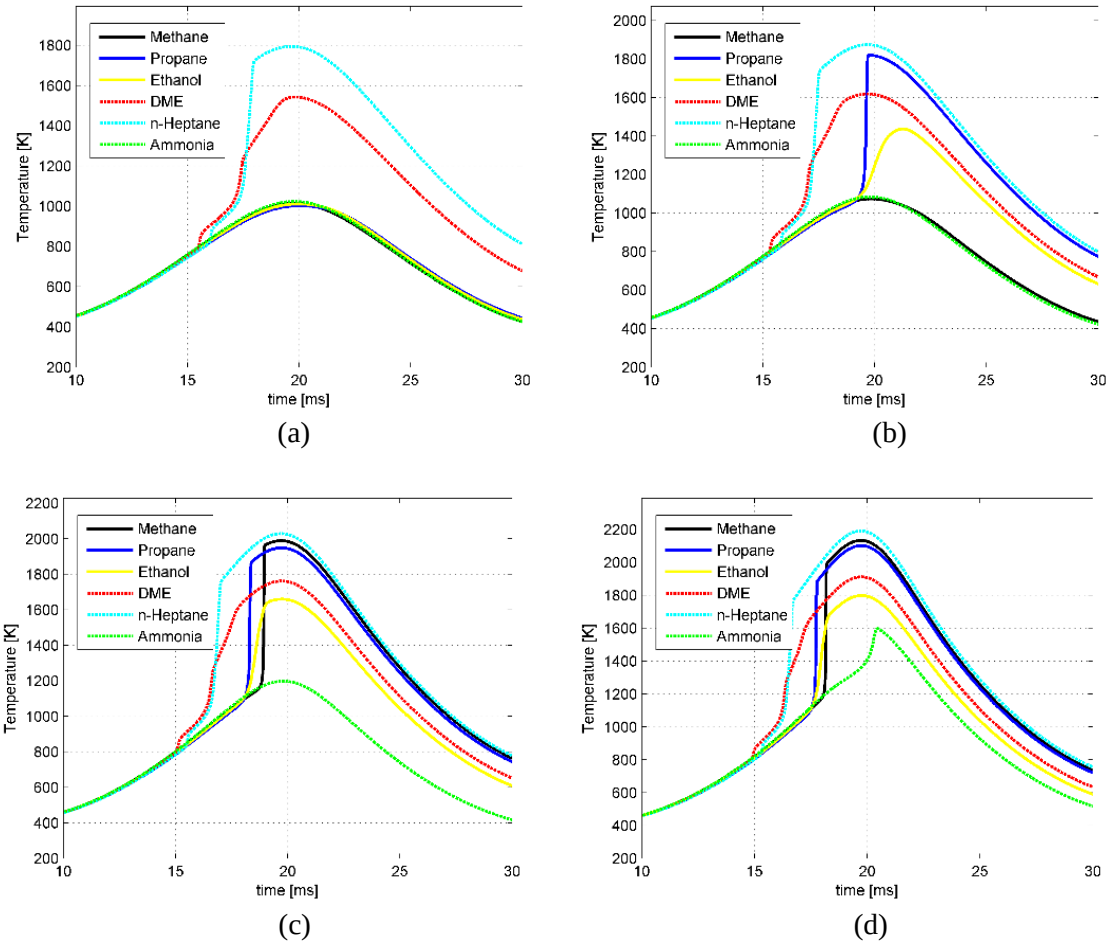

Figure 3.1 Temperature traces of different fuels along piston trajectories with identical Ω = 1.5, but varied CR ((a) CR = 20.3 (b) CR = 24.6 (c) CR = 34.6 (d) CR = 48.2)

In order to explore the influence of piston trajectory with varying Ω alone, the combustion processes of five fuels are further simulated along three piston trajectories

whose Ω are 0.5, 1.0 and 1.5 respectively and CR is fixed at 31.0. As shown in Figure 3.2, all five fuels combust under these piston trajectories. Similar to CR, Ω can also adjust the SOC timing with the similar trend: Larger Ω, more advanced SOC timing.

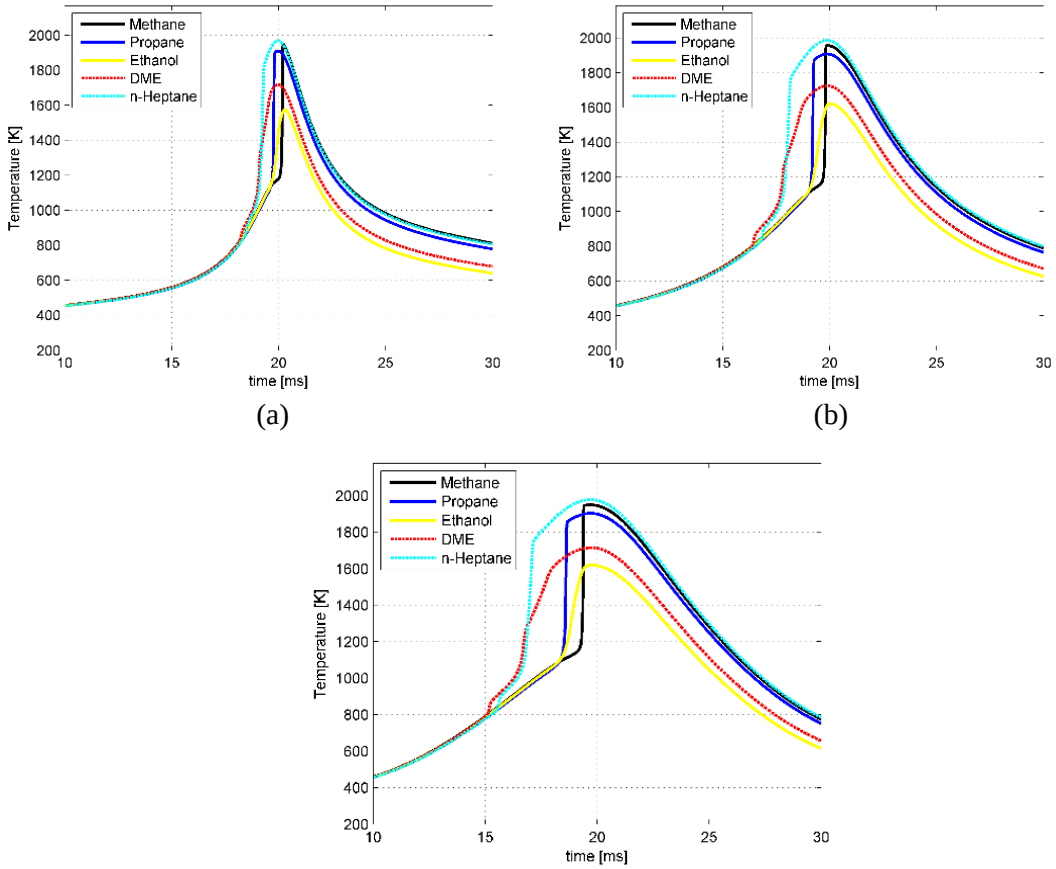

Figure 3.2 Temperature traces of different fuels along piston trajectories with identical CR = 31, but varied Ω ((a) Ω = 0.5 (b) Ω = 1.0 (c) Ω = 1.5)

The influence of Ω on the combustion process is more explicit if the in-cylinder temperature traces of one specific fuel is examined. The n-heptane is selected herein since it is the most widely-used gasoline surrogate in HCCI combustion research. Besides, in order to quantify the variation of SOC timing caused by different Ω, a new operating parameter T10, standing for the time instant when 10% of the chemical energy has been

released, is reported as well. As the alternative of CA10, which represents the crank angle in conventional ICE when 10% of the chemical energy has been released, T10 is more practical for FPE operation due to the elimination of the crankshaft in FPE.

Figure 3.3 shows the in-cylinder gas temperature traces of n-heptane under piston trajectories with different Ω and the corresponding T10s are listed in Table 3.1. It is obvious that no combustion occurs when Ω = 0.2. However, when Ω is increased to 0.4, there is a small temperature rise after the TDC which indicates an incomplete combustion occurrence. After Ω reaches 0.7 and higher, the in-cylinder gas experiences complete combustion and a significant temperature rise as well as the negative temperature coefficient (NTC) behavior [91], [92] is reflected explicitly. As shown in Figure 3.3 and Table 3.1, the piston trajectory with Ω = 0.7 enforces the SOC timing after the TDC while another trajectory whose Ω = 1.3 advances the SOC timing to 20.05ms (20ms as the TDC point).

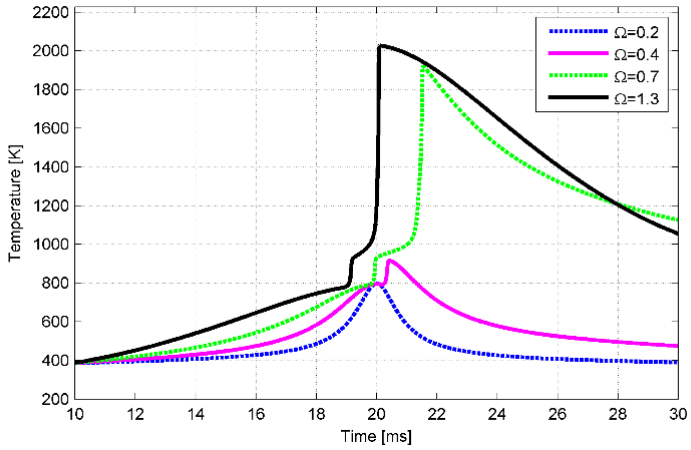

Figure 3.3 Temperature traces of n-heptane along piston trajectories with different Ω (CR = 15.0, air-fuel equivalence ratio λ =2.0 and T_{intake} = 300K)

Table 3.1 T10 parameter for each piston trajectory in Figure 3.3

Piston trajectory	T10 (ms)
Ω = 0.2	-[a]
Ω = 0.4	-[a]
Ω = 0.7	21.47
Ω = 1.3	20.05

a: the corresponding heat release has not reached to 10% of available chemical energy.

These distinct temperature traces can be further explained by inspecting Figure 2.2 (b) again. Around the TDC, higher Ω trajectory leads to a smaller volume of the combustion chamber and therefore accelerates the radical accumulation process in two ways—increasing the reactant concentration directly and raising the combustion chamber temperature. Consequently, this acceleration advances the ignition time at higher Ω trajectory. On the other hand, lower Ω trajectory retards the accumulation process and postpones or even prevents the combustion from occurring.

More importantly, such variable Ω offers us a method to adjust the combustion timing. This capability is critical for HCCI combustion since one of the most important challenges for HCCI implementation is the combustion phasing control.

Figure 3.4 shows temperature traces under different loads. Apparently, different λ causes distinct SOC timing if Ω is identical, as shown in Figure 3.4 (a). However, in FPE, the piston trajectory can be adjusted to maintain the SOC timing at the fixed time instant, e.g. the TDC point (20ms), under various loads, as shown in Figure 3.4 (b) and Table 3.2.

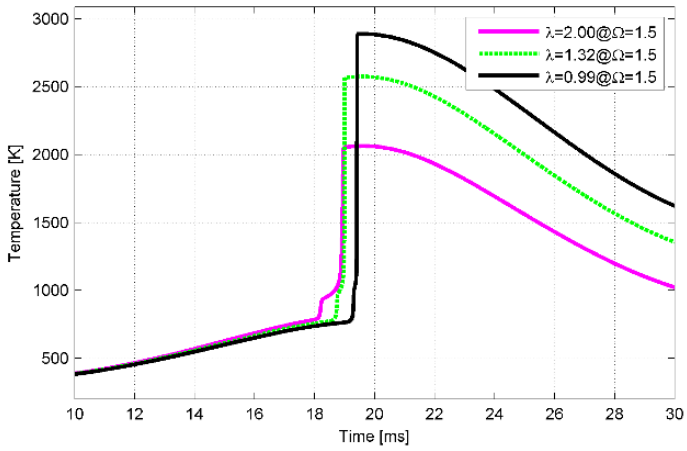

(a)

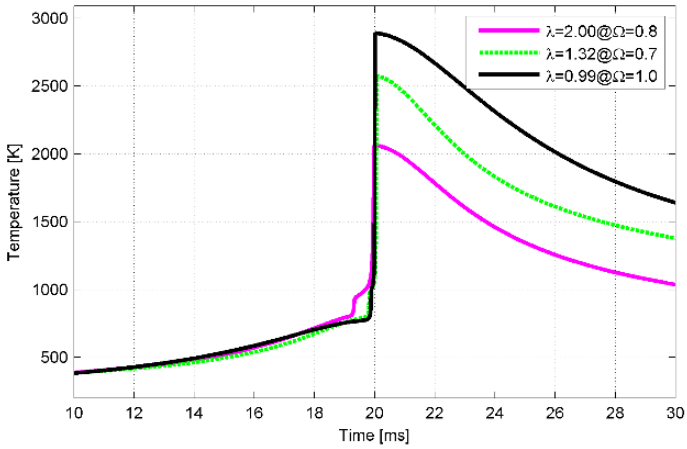

(b)

Figure 3.4 Temperature traces of n-heptane under different λ (CR=20.3 and T_{intake}=300K) (a) Piston trajectories with Ω=1.5 (b) Variant piston trajectories

Table 3.2 T10 parameter for each piston trajectory in Figure 3.4

Load	Original T10 (ms)	Adjusted Ω	Adjusted T10 (ms)
λ = 2.00	18.90	0.8	19.92
λ = 1.32	19.00	0.7	20.04
λ = 0.99	19.41	1.0	19.99

Besides, this control method can also be applied to compensate different T_{intake} as shown in Figure 3.5 and Table 3.3:

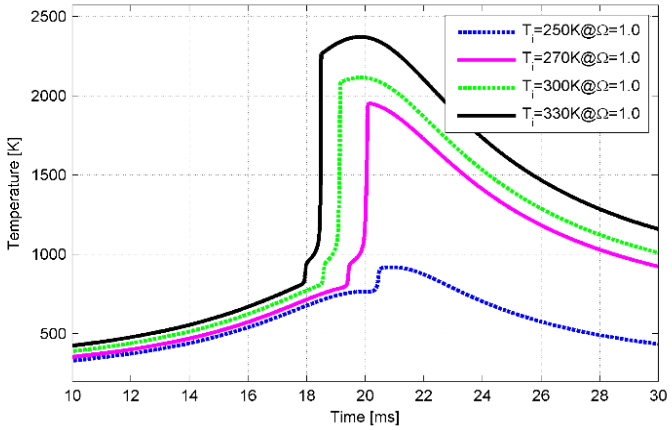

(a)

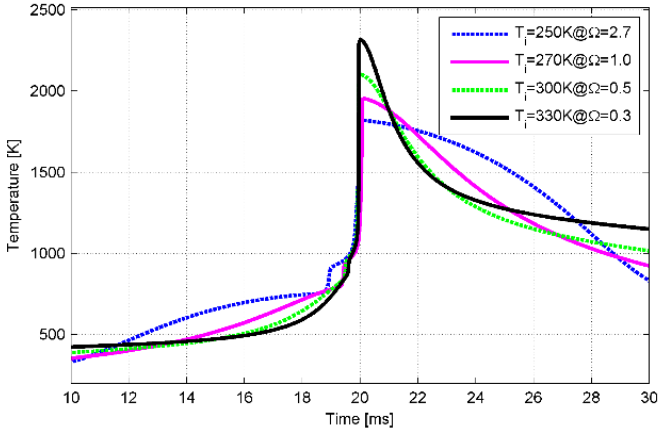

(b)

Figure 3.5 Temperature traces of n-heptane under different T_{intake} (CR=20.3 and λ=2) (a) Piston trajectories with Ω = 1. (b) Variant piston trajectories

Table 3.3 T10 parameter for each piston trajectory in Figure 3.5

Temperature	Original T10 (ms)	Adjusted Ω	Adjusted T10 (ms)
T_{intake} = 250K	-	2.7	20.00
T_{intake} = 270K	20.06	1.0	20.06
T_{intake} = 300K	19.12	0.5	19.93
T_{intake} = 330K	18.47	0.3	19.94

3.2 Indicated Output Works and Heat Losses

Both CR and Ω are able to influence indicated output work and heat loss due to their capabilities of altering the in-cylinder gas temperature traces. In order to represent such effects, 3D plots of the simulation results are shown in this subsection. In each plot, the x-y plane is the piston trajectory domain which is indicated by CR (15 to 61) and Ω (0.1 to 3.0). Consequently, each point in the x-y plane represents a specific piston trajectory, and the z-axis is the calculated indicated output work and the corresponding heat loss.

As shown in Figure 3.6, there is an incomplete combustion zone locating at the small CR or small Ω area in each plot. In other words, the in-cylinder charge cannot be ignited by the compression solely if the piston trajectory is within this area since the species accumulation process cannot achieve sufficient amount of radical species. In addition, the area of the incomplete combustion zone is also varied according to the utilized fuels.

Outside the incomplete combustion zone, the in-cylinder charge is able to convert to the completed combustion products and the peak of the indicated output work is always located in the area with the highest CR and the lowest Ω. This conclusion is intuitive since higher CR enhances the combustion intensity significantly and lower Ω ensures the SOC timing locating around the TDC, achieving the ideal Otto cycle [29].

Additionally, no matter which fuel is used, the greatest heat loss is always produced by the piston trajectory with the largest CR and Ω as shown in Figure 3.7. This conclusion is intuitive as well since enlarging CR and Ω advance the SOC timing and increase both in-cylinder gas temperature and the high-temperature duration. In other

words, advanced combustion SOC timing extends the duration while the in-cylinder gas temperature is high and therefore increases the amount of thermal dissipation energy.

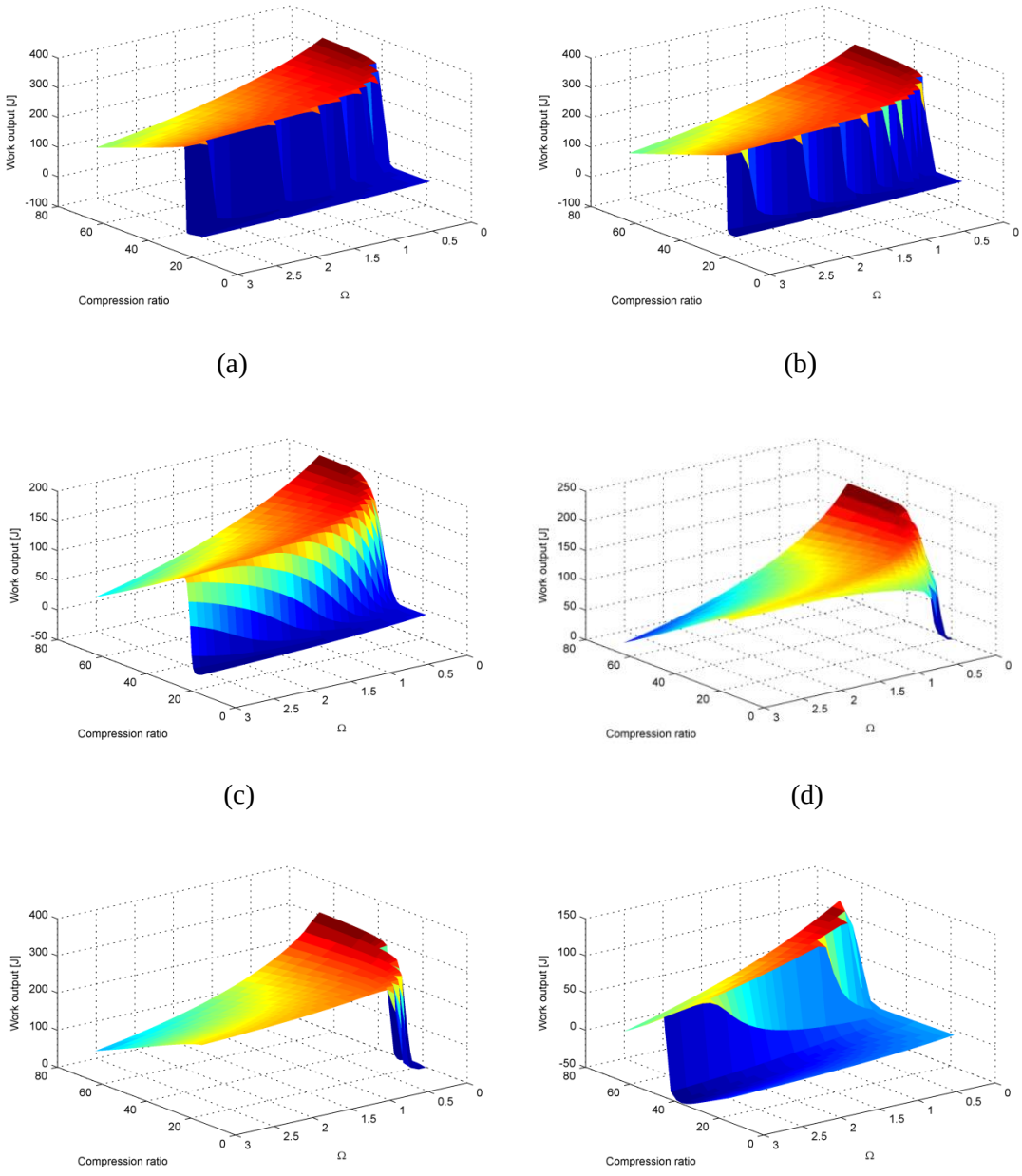

Figure 3.6 The amount of output work against different piston trajectories with diverse fuels ((a) Methane (b) Propane (c) Ethanol (d) DME (e) n-heptane (f) Ammonia)

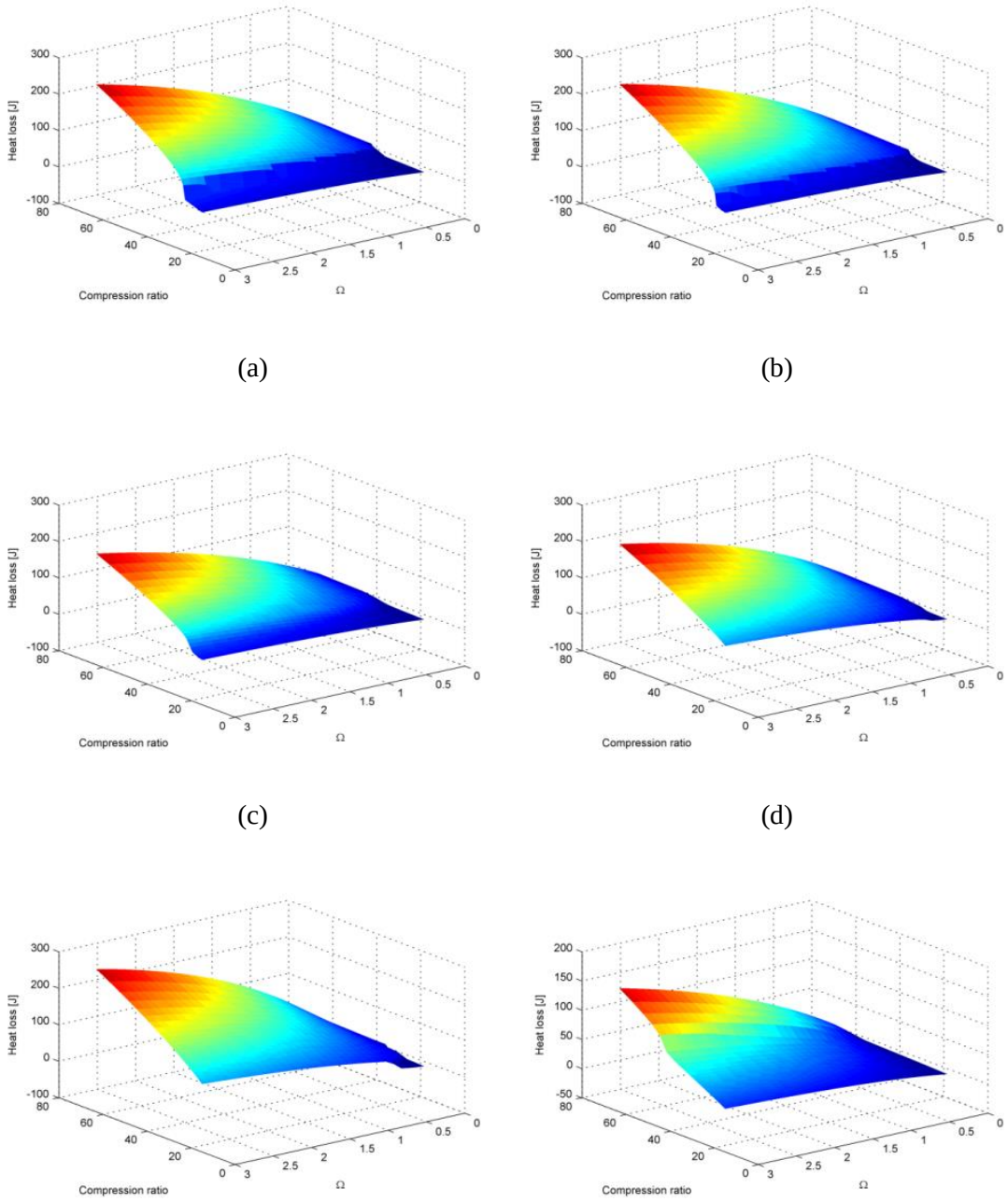

Figure 3.7 The amount of heat loss against different piston trajectories with diverse fuels ((a) Methane (b) Propane (c) Ethanol (d) DME (e) n-heptane (f) Ammonia)

It appears that maximum output work can be extracted if piston trajectory has the highest CR and the lowest Ω. However, the values of CR and Ω cannot be selected without limitation. For example, the maximum CR is limited by the mechanical strength of combustion chamber material. Similarly, Ω is also affected by several factors, such as maximal actuation force, the dynamic behavior of actuation system and generated combustion force. Hence, a specific FPE architecture has its own range of practical Ω.

If only considering the motoring process in the prototype FPE, as shown in Figure 1.3, the effect of the combustion force can be excluded. This can be considered as the worst case scenario since no combustion force will be present to help to compress the in-cylinder gas at the opposite end. Given the piston mass as 9kg and assumed maximal hydraulic pressure as 10000 psi, the practical limit of Ω (0.6 to 1.5) can be derived when CR=15, as shown in Figure 3.8 (calculation method can be found in [66]).

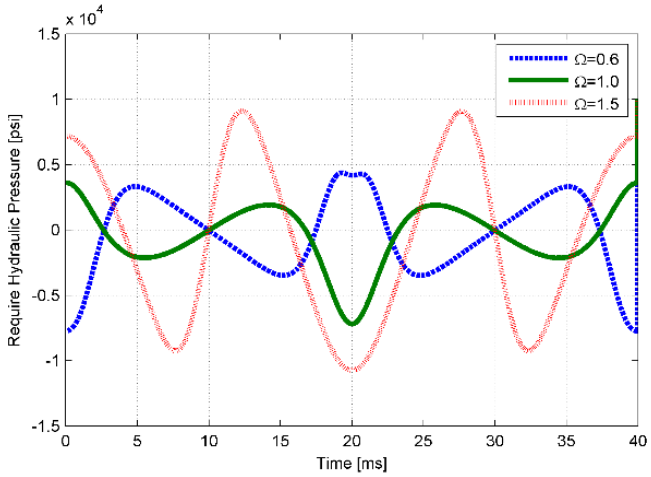

Figure 3.8 Practical limits of Ω and the corresponding required hydraulic pressure

3.3 Comparison between FPE with Virtual Crankshaft and Conventional ICE

In order to further demonstrate the advantages of the piston trajectory-based control, the comparison between the combustion process in piston-trajectory-controlled FPE and the counterpart in crankshaft-based ICE is presented in this subsection. Noted that the piston trajectory of the crankshaft engine is generated by the slider-crank mechanism: the crank radius is set as the amplitude of piston trajectory of FPE; the clearance volume is determined by the minimum volume of the combustion chamber of FPE and the ratio of the connecting rod length to crank radius is set as 4 [29].

First of all, the indicated thermal efficiency of the n-heptane FPE with virtual crankshaft under different compression ratio is compared to the corresponding efficiency in n-heptane crankshaft-based ICE.

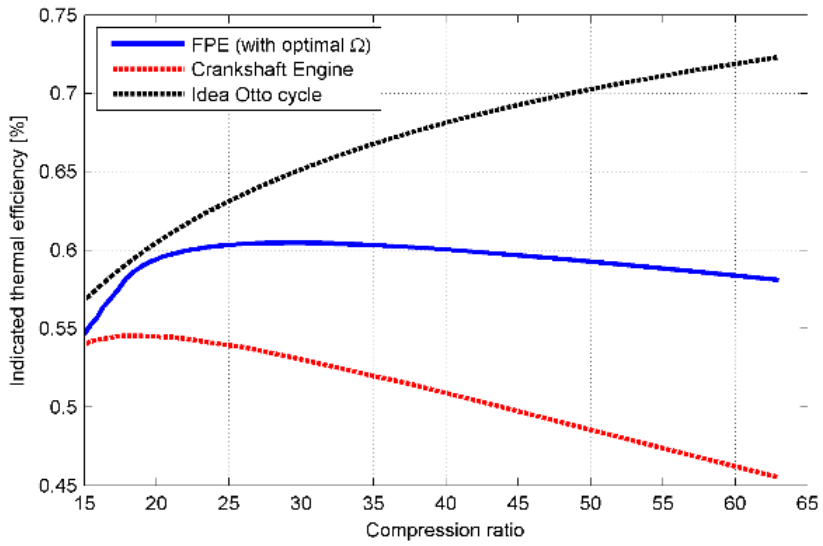

Figure 3.9 Comparison of the indicated thermal efficiency between two n-heptane engines: FPE with virtual crankshaft and the crankshaft engine

As can be seen in Figure 3.9, the indicated thermal efficiency in FPE (with optimal Ω in each compression ratio) is always higher than the one in the crankshaft engine. The gain in efficiency is more obvious while the compression ratio increases. It can be explained since larger CR yields higher in-cylinder temperature which is favorable to transfer more energy to the chamber wall as the heat loss. Hence, the advantage of the FPE, which reduces the amount of heat loss by providing short residential interval around the TDC, will significantly affect the heat loss process and increase the corresponding indicated thermal efficiency.

Another comparison is conducted to represent the better performance of FPE with virtual crankshaft while handling the extremely fuel-lean combustion.

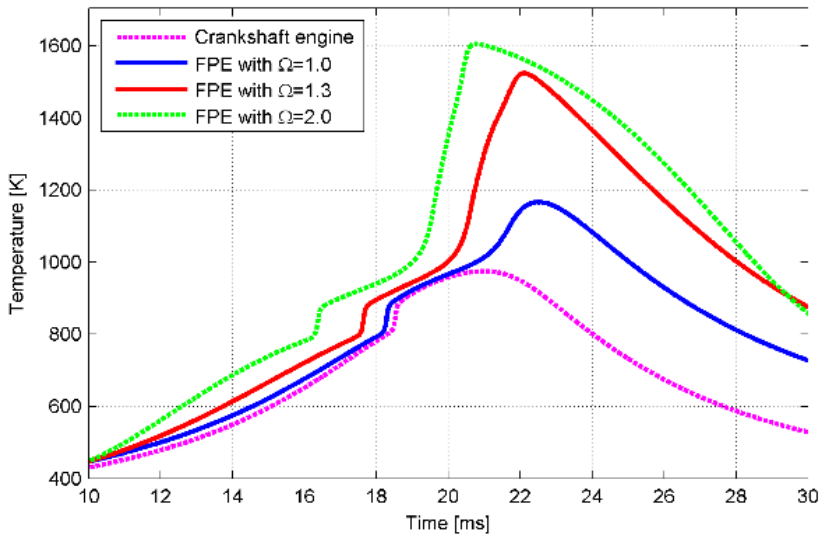

Figure 3.10 Temperature traces of extremely fuel-lean (λ = 4) combustion along different piston trajectory at CR = 12

From Figure 3.10, it is clear that the piston trajectory of crankshaft engine could not trigger strong combustion to extract the sufficient chemical energy from the fuel.

However, the FPE with the active piston motion control could deal with this fuel-lean issue, and not only ignites the combustion but also varies the SOC timing by adjusting the value of Ω. The indicated thermal efficiencies of these four conditions are listed in Table 3.4 below:

Table 3.4 Comparison of indicated thermal efficiency from extremely fuel-lean combustion under different piston trajectory

Piston trajectory (CR = 12)	**Indicated thermal efficiency**	**Efficiency gain**
Crankshaft engine	**12.50%**	**-**
Ω = 1.0	**32.09%**	**19.59%**
Ω = 1.3	**50.13%**	**37.63%**
Ω = 2.0	**48.98%**	**36.48%**

It is worth noting that the indicated thermal efficiency will be reduced if Ω is too large. Due to the fact that large Ω will sustain the piston location near the TDC for a relatively longer time, the corresponding heat loss may be increased. However, such large Ω is still useful to adjust the SOC timing or sometimes is necessary to trigger the extremely fuel-lean combustion.

3.4 Illustration of the Piston Trajectory Influences from a Chemical Kinetics Perspective

Equation (2.15) to (2.17) indicate that species concentrations and temperature affect the corresponding reaction rate directly. In return, higher reaction rate generates more

radical species in the chamber, and more chemical heat release further increases the in-cylinder gas temperature. Therefore, the intrinsic dynamic coupling among them can be described as a positive feedback system (solid square in Figure 3.11). This positive feedback behavior can be reinforced when the temperature, as well as the amount of the radical species, reaches a certain level (dashed square in Figure 3.11). In this case, more elementary reactions are involved in the dynamic system and the chain reaction mechanism is formed, which converts the reactants to the final products rapidly and generates a significant temperature rise as well.

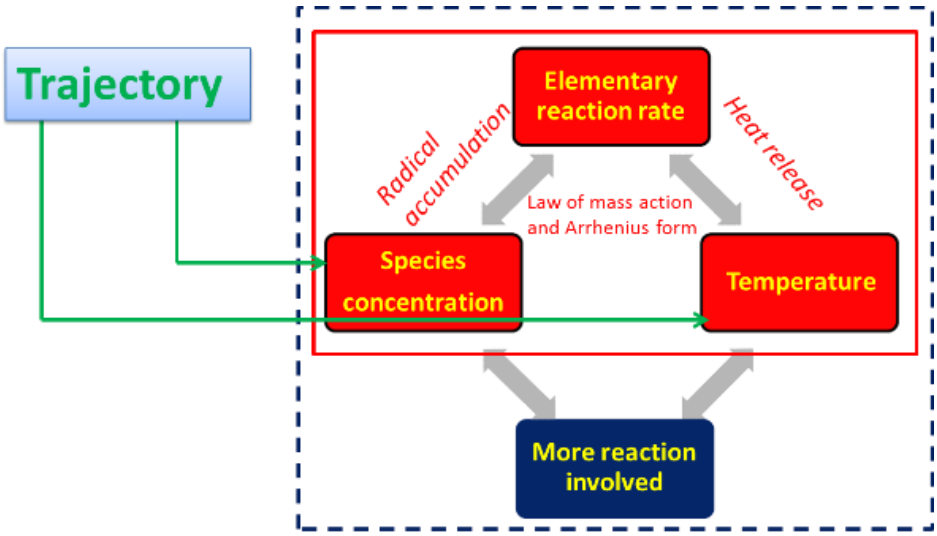

Figure 3.11 Schematic diagram for the trajectory influence on the combustion

In order to explain it further, two piston trajectories, namely $\Omega = 0.4$ and $\Omega = 0.7$ cases in Figure 3.3 are investigated again. For the sake of convenience, a specific temperature traces plot of these two are shown in Figure 3.12.

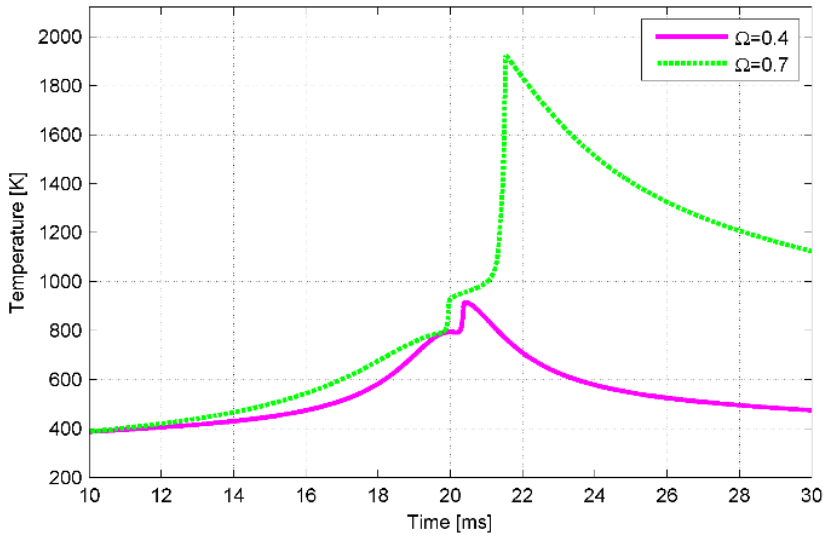

Figure 3.12 Temperature traces of n-Heptane for Ω = 0.4 and Ω = 0.7 (CR = 15.0, air-fuel equivalence ratio λ =2.0 and T_{intake} = 300K)

The only difference between these two cases is the fact that the in-cylinder charge undergoes two piston trajectories with distinct Ω. However, the subsequent combustion processes are completely different since the temperature of the in-cylinder gas almost reaches 2000K in the higher Ω case while incomplete combustion occurs in the lower Ω case. The reason behind this phenomenon is apparent if the process is examined from a chemical kinetics perspective. During the time duration from 10ms to 20ms, the gas temperature trace in Ω = 0.7 case is always higher than the temperature trace in Ω = 0.4 case, which indicates the radical species accumulation process in the former case is much quicker than the latter one attributed to the higher reaction rate during this period. Therefore, even though the in-cylinder temperatures become almost identical at 20ms, only the higher Ω case achieves sufficient amount of the radical species and triggers the combustion process around the TDC while the radical species accumulation process in

the lower Ω case continuous. This conclusion is demonstrated by Figure 3.13, which shows the accumulation process of the radical species OH. The species OH is selected because it is the primary radical species to consume the fuel molecule during the ignition stage, and it significantly affects the subsequent combustion process as well [93].

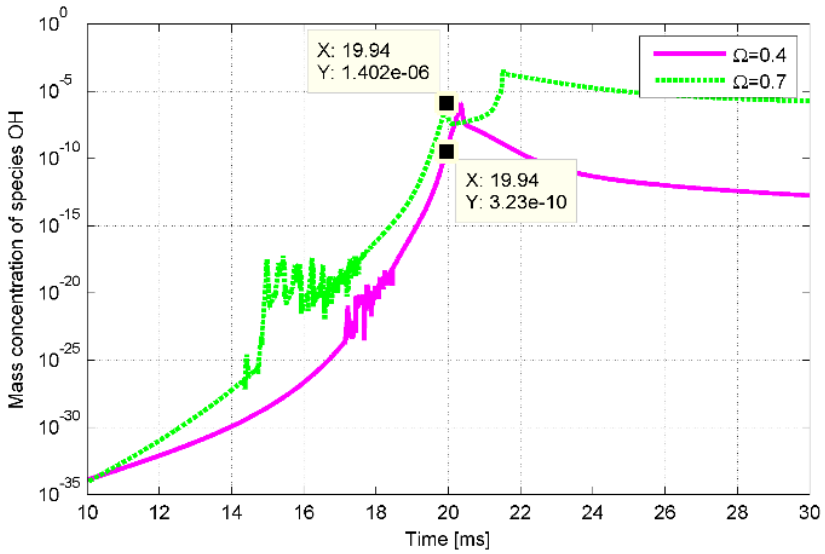

Figure 3.13 OH species histories for Ω = 0.4 and Ω = 0.7

As shown in Figure 3.13, at 19.94ms, the concentration of OH in Ω = 0.7 case is almost ten thousand times of the counterpart in Ω = 0.4 case. After this time instant, the combustion starts in Ω = 0.7 case and the NTC behavior is reflected explicitly along the curve. In contrast, the mass fraction of OH keeps rising after the TDC in Ω = 0.4 case and forms an incomplete combustion process eventually.

Figure 3.14 shows the OH species accumulation processes for these two cases at three different time instants through the reaction paths diagrams.

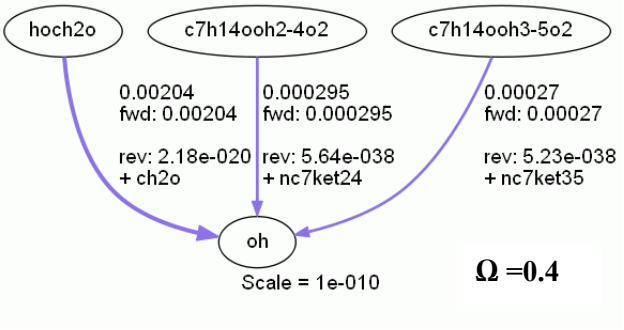

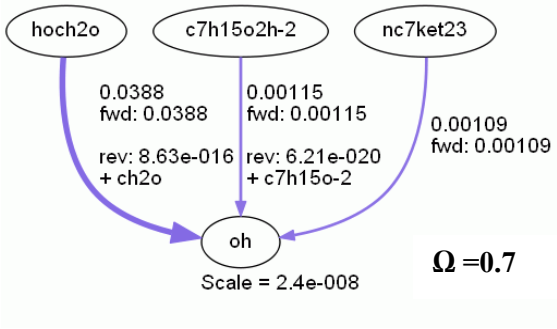

(a) Corresponding reaction paths diagrams at19 ms

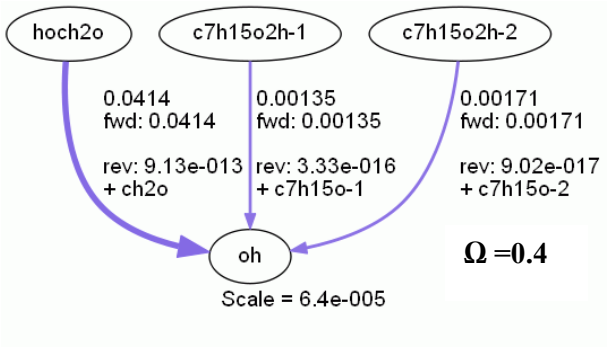

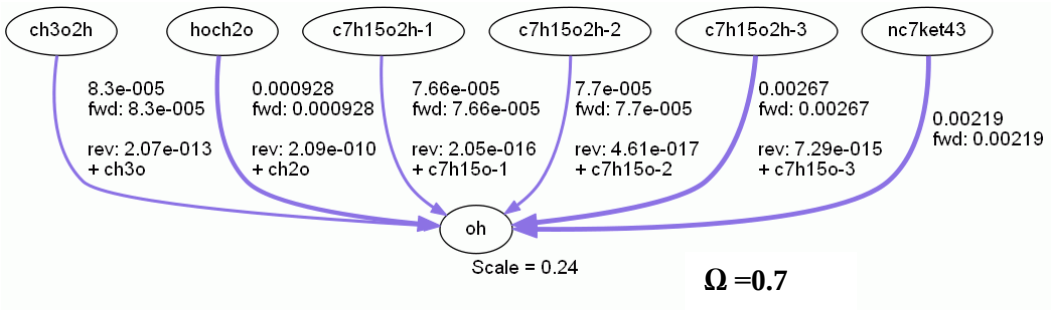

(b) Corresponding reaction paths diagrams at 20ms (TDC)

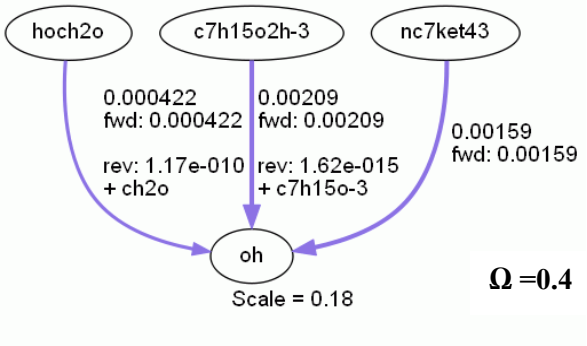

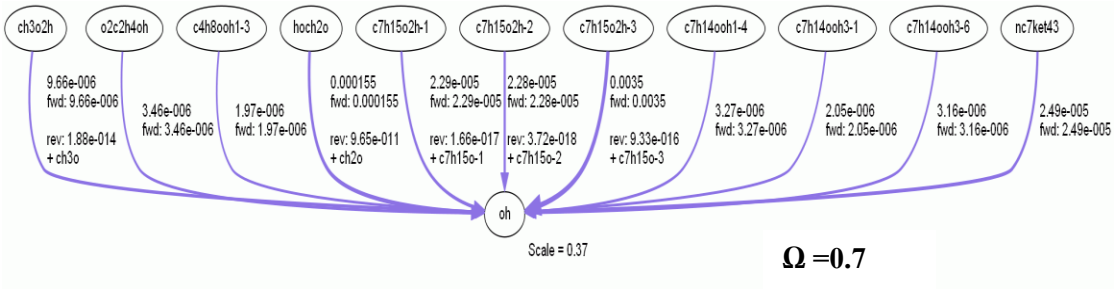

(c) Corresponding reaction paths diagrams at 20.5ms

Figure 3.14 Reaction path diagrams for Ω = 0.4 and Ω = 0.7 at three different time instants

From Figure 3.14 (a), at 19ms, the involved elementary reactions for these two cases are almost identical. However, the general reaction rate in Ω = 0.7 case, which is scaled as 2.4e-8, is higher than the other case, which is scaled as 1.0e-10. This variation of the reaction rates is caused by the different in-cylinder temperatures at this time instant (Figure 3.12).

Afterward, at 20ms, the difference between the general reaction rates of the two cases is greater. As shown in Figure 3.14 (b), the general reaction rate in Ω = 0.4 case is scaled as 6.4e-5 while the rate in other case reaches to 0.24. This significant increase indicates the difference between the amounts of radical species in these two cases (Figure 3.13). It is also apparent that more elementary reactions are involved in Ω = 0.7 case which implies the formation of the chain reactions mechanism.

The chain reactions mechanism is more obvious for $\Omega = 0.7$ case in Figure 3.14 (c), while the corresponding reaction paths diagram for $\Omega = 0.4$ case is almost the same as previously except the higher reaction rate. Consequently, two completely different combustion processes are generated by the two piston trajectories.

3.5 Conclusion

In this chapter, the concept of trajectory-based combustion control has been proved by extensive simulation. The corresponding results indicate clearly that with the ability of precise piston trajectory tracking, the FPE is able to adjust the entire combustion process by varying the volume profile of the combustion chamber and therefore altering the in-cylinder gas temperature and pressure traces, the indicated output work and the heat loss. Due to the closely coupled interactions between the in-cylinder gas dynamics and the fuel chemical kinetics during the engine operation, the trajectory-based combustion control enables us to manipulate the accumulation process of the radical species. Furthermore, this new degree of freedom offers us the capability to determine which elementary reactions in the mechanism will participate in the reaction process and how they react via designing the in-cylinder gas temperature trace. Consequently, the trajectory-based combustion control can be utilized in the real-time control of HCCI combustion as well as other advanced combustion strategies.

Chapter 4

Effects of the Trajectory-based Combustion Control on Engine Emissions

Besides the combustion performance, the trajectory-based combustion control can also reduce the engine-out emission from the FPE. In order to prove such an advantage, the aforementioned chemical kinetics driven model has been modified within two aspects: geometric part and chemical kinetics part. The corresponding simulation results are illustrated in this chapter as well.

4.1 Modification on the Chemical Kinetics Driven Model

4.1.1 Asymmetric Piston Trajectory

As mentioned in the last chapter, by changing the value of Ω, different piston motion patterns between the same TDC point and BDC point can be achieved in the FPE with virtual crankshaft mechanism, as shown in Figure 4.1.

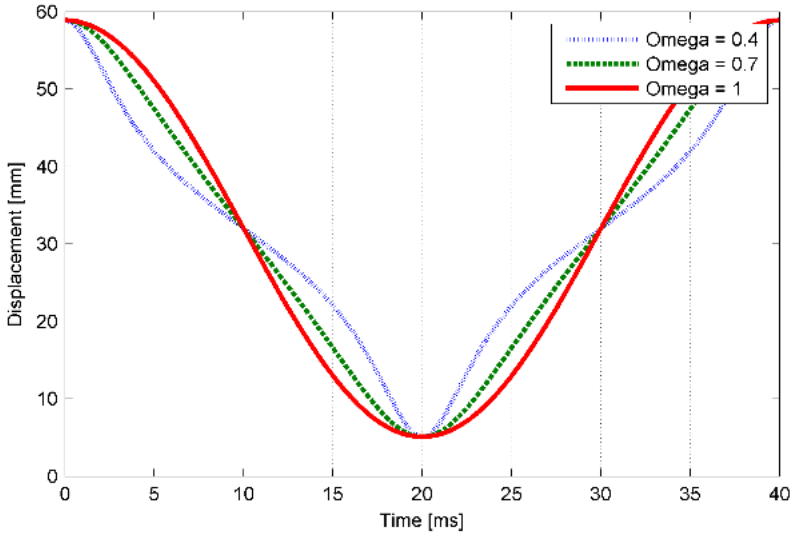

Figure 4.1 Various piston trajectories with different Ω

In addition, due to the ultimate freedom of the piston movement in the FPE, the piston trajectory can even be asymmetric. In other words, the compression process and the expansion process of the FPE can be totally distinct with each other. As shown in Figure 4.2, three trajectories are depicted with the identical compression process, but different expansion processes indicated by various Ω Afterward. The variation of Ω in each trajectory occurs at the TDC point (indicated by 20ms point since the FPE operation frequency is 25Hz in this study) which ensures the smooth transition. This unique feature in the FPE realizes the in-cycle combustion control by assigning different control objectives on the designing of each trajectory section. For example, the compression process can be determined by optimizing the combustion phase and the expansion process can be designed to reduce the heat loss and NOx emission.

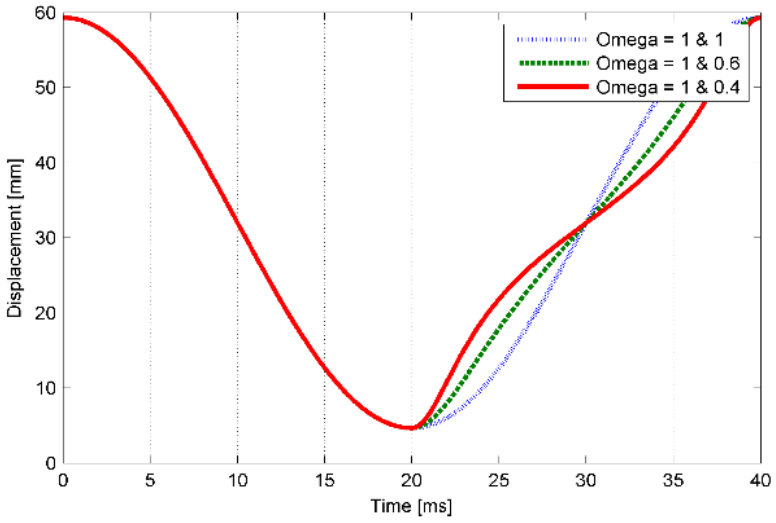

Figure 4.2 Asymmetric trajectories generated by the FPE (identical compression processes but different expansion processes)

4.1.2 Chemical Kinetics Part

The reaction mechanism utilized herein is a reduced n-heptane reaction mechanism [94]. This mechanism is first developed by embedding several sub mechanisms such as the GRI NOx mechanism and a detailed poly-aromatic hydrocarbon (PAH) mechanism, into a base n-heptane mechanism. Afterward, various mechanism reduction methods, including the direct relation graph error propagation (DRGEP) and reaction pathways analysis, are applied to reduce the size of the entire mechanism to 76 species and 366 reactions. Consequently, the generated mechanism not only captures the essential feature of the chemical kinetics reproduced by these detailed reaction mechanisms but also improves computational efficiency significantly. The effectiveness of this reaction mechanism, in terms of the predictions of ignition delay time and flame propagation speed, has been experimentally validated by different facilities, e.g. shock tube, constant volume chamber, and testbed engine.

The chemical kinetics of each emission species can be achieved through the reaction mechanism as well. The base n-heptane mechanism contains elementary reactions which represent the pyrolysis process of n-heptane molecule at low and elevated temperature. These reactions form the governing chemical kinetics for the generation of unburned HC; The PAH mechanism, describing the formation of PAH up to four rings which are the major precursors of the soot emission, is also included in the applied reaction mechanism.

Additionally, the applied reaction mechanism contains 42 reactions involved production and consumption of CO and all of them are listed in the appendix at the end of this paper. In order to capture the essence of the CO chemical kinetics, sensitivity analysis is further conducted among these 42 reactions. Generally, the sensitivity analysis is the process of calculating the normalized sensitivity coefficient S_i for the involved reactions, which can be yielded as:

$$S_i = \frac{P_i}{\omega_{CO}} \frac{\partial \omega_{CO}}{\partial P_i} \tag{4.1}$$

while ω_{CO} represents the concentration of CO and P_i is a multiplier on the forward rate constant of i th reaction.

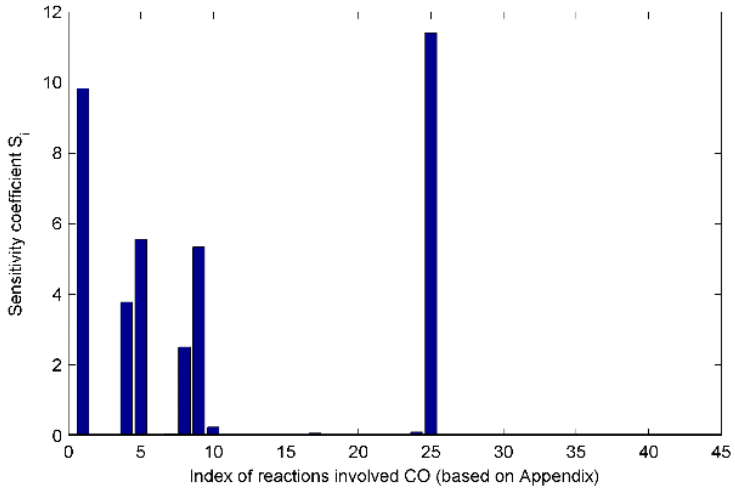

Figure 4.3 Sensitivity analysis for 42 reactions involved CO

The result of the sensitivity analysis is shown in Figure 4.3 and the selected 10 elementary reactions, whose S_i are larger than 0.05, are listed in Table 4.1.

Table 4.1 Governing reactions for CO chemical kinetics

Selected Elementary Reactions
C5H11CO <=> C2H4 + C3H7 + CO
CH3O + CO <=> CH3 + CO2
CO + OH <=> CO2 + H
CO + HO2 <=> CO2 + OH
HCO + O2 <=> CO + HO2
HCO (+M) <=> CO + H (+M)
HCO + OH <=> CO + H2O
CH2CHO + O2 <=> CH2O + CO + OH
CH2CHO (+M) <=> CH3 + CO (+M)
CH3CO (+M) <=> CH3 + CO (+M)

The included GRI NOx mechanism in the employed reaction mechanism is built upon the Zeldovich mechanism [95] plus the generation processes of N_2O and NO_2, which consist of 11 elementary reactions (as can be seen in Table 4.2). Extensive researches have been conducted to demonstrate the capability of this mechanism predicting accurate NOx emission in the real world applications [96].

Table 4.2 Governing reactions for NOx chemical kinetics

Selected Elementary Reactions
N2 + O <=> N + NO
N + O2 <=> NO + O
N + OH <=> H + NO
N2 + O2 <=> N2O + O
N2O + O <=> 2 NO
N2 + OH <=> H + N2O
HO2 + N2 <=> N2O + OH
HO2 + NO <=> NO2 + OH
NO + O (+M) <=> NO2 (+M)
NO2 + O <=> NO + O2
H + NO2 <=> NO + OH

4.2 New Approach to Reduce Engine-out Emissions

In [79], the authors have shown that varying the piston motion patterns between the TDC and the BDC point, indicated by the value of Ω, enables the adjustment of the combustion processes in terms of manipulating the combustion phasing, reducing the heat

loss and increasing the indicated thermal efficiency. This idea is clearly presented in the block diagram of the trajectory-based combustion control, as shown in Figure 4.4.

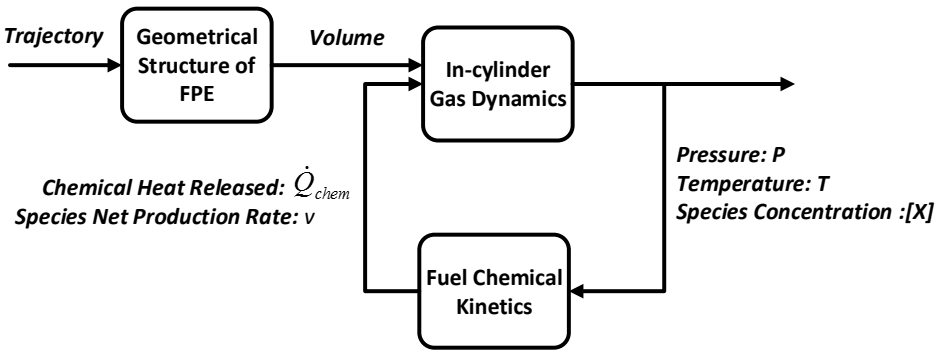

Figure 4.4 Block diagram of the trajectory-based combustion control

Apparently, the piston trajectory works as an input to the entire dynamic system and produces different volume profiles accordingly. Afterward, these variable volume profiles are sent to the feedback loop and influence the interactions between the in-cylinder gas dynamics and the fuel chemical kinetics. Eventually, the system outputs are generated in terms of pressure, temperature and species concentrations.

Considering the fact that production of emissions is also included in the species concentration outputs, the capability of tailoring the combustion in FPE by varying piston trajectories implies a new approach to reduce the emissions.

As can be seen in Figure 4.5, three piston trajectories with an identical compression ratio (CR = 11) but different Ω (show in Figure 4.1) generate completely distinct combustion processes. The air-fuel equivalence ratio (AFER) of the mixture in each case is fixed at 2. It is evident that the trajectory with Ω = 0.4 cannot ignite the intake mixture at all, which produces a large amount of unburned hydrocarbon emission inevitably. However, increasing Ω to 0.7 generates an uncompleted combustion process and converts

the unburned hydrocarbon to both CO and CO_2. A completed combustion process is eventually formed if Ω is increased to 1 and almost all the fuel molecules are converted to final product CO_2. In the last case, the peak temperature of the in-cylinder gas reaches over 2100K indicating the total chemical energy of the fuel has been released through the oxidation of CO to CO_2.

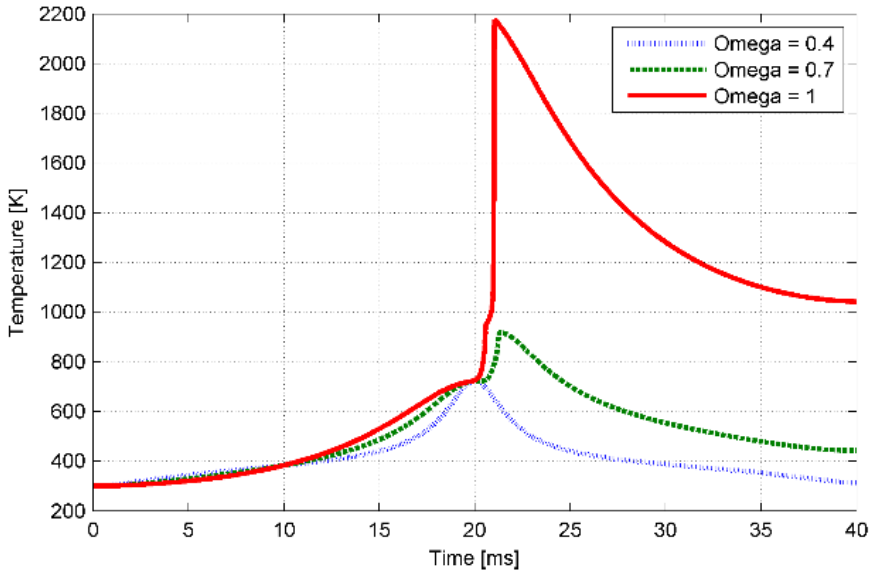

Figure 4.5 Temperatures traces along the piston trajectories in Figure 4.1

These different combustion processes can be explained since larger Ω of piston trajectory has longer resident time when the piston locates around the TDC point, which offers longer period to accumulate the necessary radical species and trigger the combustion. In another word, piston trajectory with great Ω provides a beneficial environment for the air-fuel mixture ignition while small Ω inhibits the accumulation of radical species and postpones the start of combustion or even causes a misfire. In other words, the piston trajectory with large Ω ensures the completed oxidation of fuel molecule to CO_2 and therefore reduces the emissions such as CO and unburned HC.

Additionally, the ultimate freedom of the piston movement in FPE also enables the implementation of asymmetric piston trajectories, as shown in Figure 4.2. In other words, the compression and expansion sections can be synthesized for different objectives respectively. For example, the compression trajectory is designed to trigger the combustion occurring at the TDC point which forms the approximate ideal Otto cycle and guarantees the minimum production of CO and unburned HC; the expansion trajectory is developed to reduce the in-cylinder gas temperature right after the combustion. In this way, not only the heat loss but also the NOx emission, which is sensitive to temperature, can be decreased. The piston trajectories in Figure 4.2 are generated based on these two requirements and the corresponding temperature profiles are shown in Figure 4.6.

It is apparent in Figure 4.6 that each peak temperature is located at the TDC point in all the three cases, which means the combustions are all completed before the beginning of the expansion processes. Additionally, the temperature traces after the TDC point are distinct with each other due to the different expansion processes. The in-cylinder temperature reduces faster after the peak temperature in the third case (solid line) compared to the others. This result is intuitive since the third piston trajectory (presented as the solid line in Figure 4.2) expands more quickly than the other two, which increases the volume of the combustion chamber and cools down the gas temperature more rapidly. Since all the chemical energy has already been extracted at the TDC point, shorter period of higher temperature in the cylinder lowers the dissipation of the thermal energy and enhances the indicated thermal efficiency. The calculated thermal efficiencies for the

three cases support the conclusion above, as can be seen in the inserted box inside Figure 4.6. Additionally, the reduced in-cylinder temperature also decreases the production of NOx. The detailed explanation of the reduction of NOx and CO emission, from the perspective of chemical kinetics, will be shown in the next section.

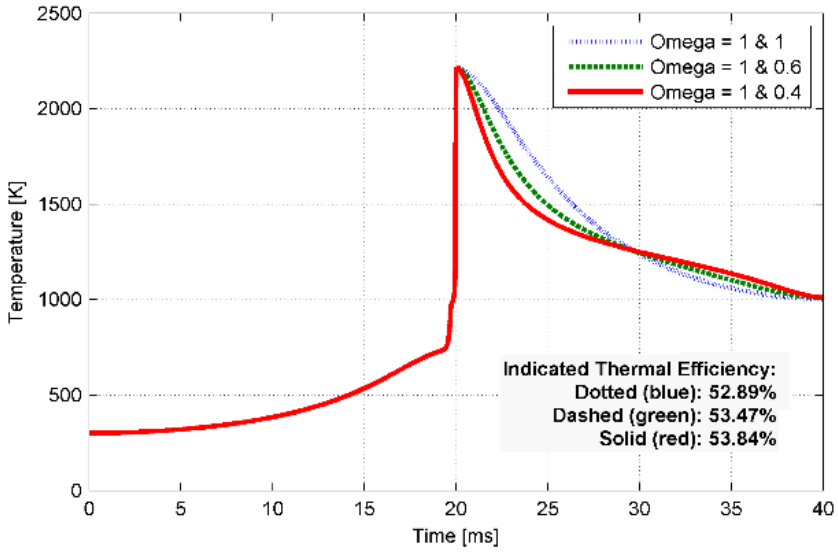

Figure 4.6 Temperature traces along the piston trajectories in Figure 4.2

4.3 Simulation Results and Discussion

4.3.1 CO Emission

The production of CO emission is mainly due to the uncompleted combustion. In other words, not all the carbon atoms in the fuel molecules are converted to the final product CO_2 but generate some other products including unburned HC and CO. One of the critical reasons causes the uncompleted combustion in HCCI combustion is the utilization of fuel-rich mixture. If the AFER is less than 1, insufficient oxygen is involved in the combustion process and the carbon atoms can only be partially oxidized to CO,

which produces significant CO emission. As a result, operating the FPE in the fuel-lean condition is able to reduce CO emission.

However, even in the fuel-lean condition, the completed combustion process is still not guaranteed. As illustrated in Figure 4.5, misfire or uncompleted combustion still exist though the AFER λ equals 2. Fortunately, the piston trajectories in the FPE can be adjusted in order to ensure the completed oxidation of carbon atoms in the fuel molecules.

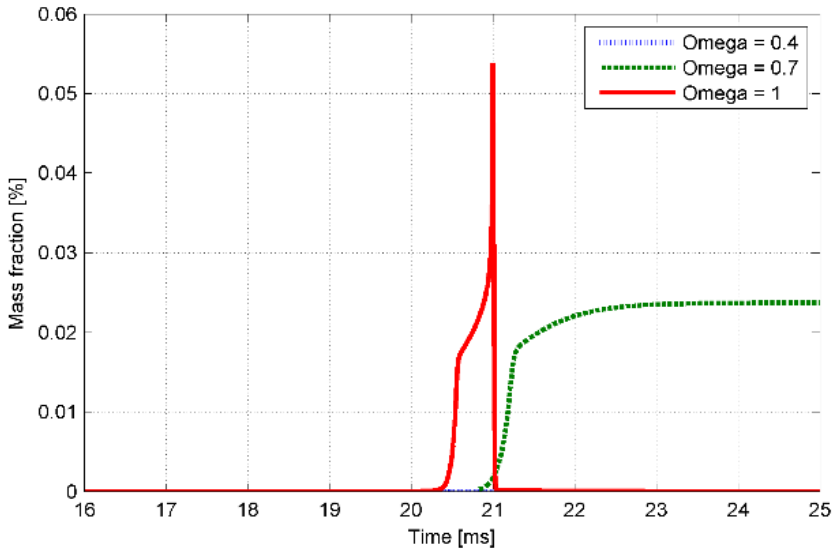

Figure 4.7 CO concentration traces during the combustion processes in Figure 4.5

Figure 4.7 displays the corresponding CO traces during the combustion processes shown in Figure 4.5. Due to the misfire in the trajectory with Ω = 0.4, the low temperature cannot break up the majority of fuel molecules to smaller hydrocarbon, e.g. aldehyde. As a result, very few CO is generated through the low-temperature pyrolysis reactions at pretty slow rates and significant unburned HC is produced, as shown in Figure 4.8 (a).

In the second case whose piston trajectory with Ω = 0.7, an uncompleted combustion occurs (Figure 4.7) and a great amount of CO (over 0.02% in mass fraction scale) is produced mainly by the following reactions (Figure 4.8 (b)):

$$C_5H_{11}CO \leftrightarrow C_2H_4 + C_3H_7 + CO \tag{4.2}$$

$$HCO + O_2 \leftrightarrow CO + HO_2 \tag{4.3}$$

However, the major CO consumption reaction:

$$CO + OH \leftrightarrow CO_2 + H \tag{4.4}$$

is not triggered due to the relatively low temperature and insufficient radical species. Thus, the large amount of CO is not converted to CO_2 but maintained as the emission eventually.

The last case forms a completed combustion after the TDC point. As the solid line shown in Figure 4.5, almost all the carbon atoms are converted to CO right before 21ms and subsequently oxidized to CO_2 rapidly. The corresponding chemical kinetics of this process is shown in Figure 4.8 (c), presenting the major reactions involved in this process. The major CO consumption reaction (4.4), as well as the major heat release reaction during the combustion process, are dominant during the entire process. Consequently, the final production of CO, in this case, is only 2.22e-7% in mass fraction scale. As mentioned previously, piston trajectory with greater Ω provides a favorable environment to trigger the combustion by locating the piston around the TDC point for a longer duration. On the other hand, the advanced start of combustion timing also implies a longer period of high-temperature in-cylinder which increases chemical reaction rates and improves the completeness of combustion.

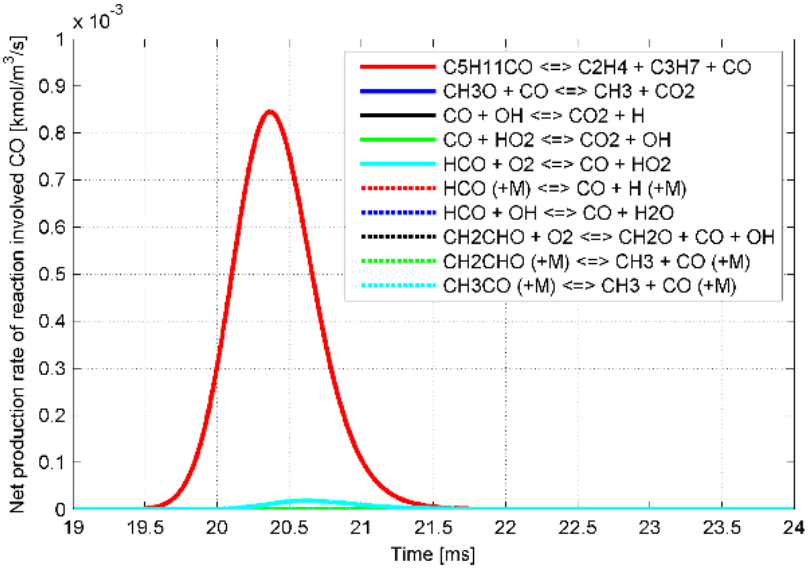
x 10^-3
Net production rate of reaction involved CO [kmol/m^3/s]
Time [ms]
C5H11CO <=> C2H4 + C3H7 + CO
CH3O + CO <=> CH3 + CO2
CO + OH <=> CO2 + H
CO + HO2 <=> CO2 + OH
HCO + O2 <=> CO + HO2
HCO (+M) <=> CO + H (+M)
HCO + OH <=> CO + H2O
CH2CHO + O2 <=> CH2O + CO + OH
CH2CHO (+M) <=> CH3 + CO (+M)
CH3CO (+M) <=> CH3 + CO (+M)

(a)

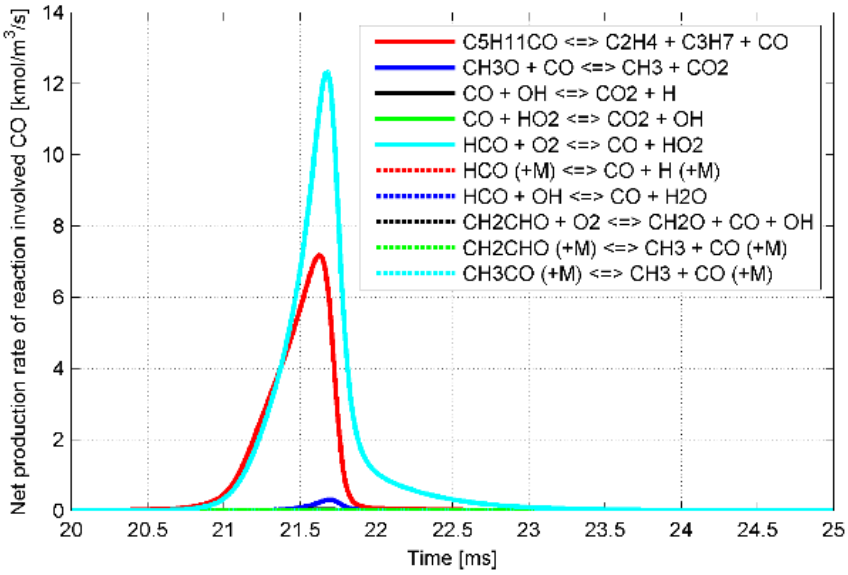
Net production rate of reaction involved CO [kmol/m^3/s]
Time [ms]
C5H11CO <=> C2H4 + C3H7 + CO
CH3O + CO <=> CH3 + CO2
CO + OH <=> CO2 + H
CO + HO2 <=> CO2 + OH
HCO + O2 <=> CO + HO2
HCO (+M) <=> CO + H (+M)
HCO + OH <=> CO + H2O
CH2CHO + O2 <=> CH2O + CO + OH
CH2CHO (+M) <=> CH3 + CO (+M)
CH3CO (+M) <=> CH3 + CO (+M)

(b)

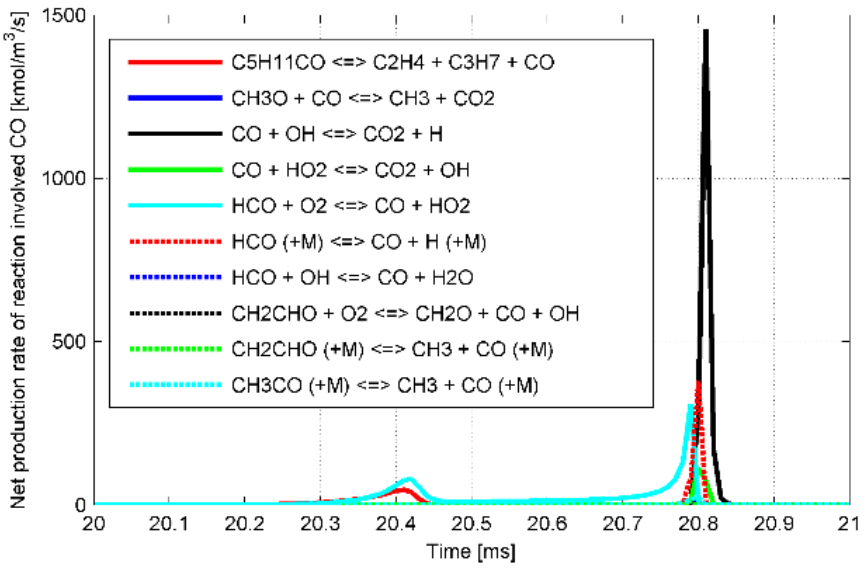

(c)

Figure 4.8 Chemical kinetics of CO emission during the combustion processes shown in Figure 4.5 ((a) $\Omega = 0.4$, (b) $\Omega = 0.7$, (c) $\Omega = 1.0$)

In reality, measured CO emission could be higher than the prediction of the simulations in the fuel-lean condition. This discrepancy is mainly caused by the partial oxidation of the fuel emerging from the crevices in the combustion chamber or from the oil layer on the engine wall [29]. The piston trajectory in the FPE can be further designed to deal with these issues by generating various flow field inside the cylinder and further reduces CO emissions. The detailed research is out of the scope of this paper but will be investigated in the future.

4.3.2 NOx Emission

The predominant composition, over 90% of NOx emissions within the engine exhaust, is nitric oxide (NO), while nitrogen dioxide (NO_2) and nitrous oxide (N_2O) form the rest. Extensive researches have conducted to investigate the formation mechanisms of NOx

emissions [96]. Among them, the most widely-used mechanism describing the NOx production from the practical engine in fuel-lean condition is the Zeldovich mechanism or so-called “thermal mechanism” [95], which is included in the employed reduced n-heptane reaction mechanism.

In the Zeldovich mechanism, the NOx emission is represented as the NO and the majority of the NO is formed by the oxidation of nitrogen under high in-cylinder temperature. The governing elementary reactions predicting this mechanism are shown as below:

$$O + N_2 \leftrightarrow NO + N \tag{4.5}$$

$$N + O_2 \leftrightarrow NO + O \tag{4.6}$$

$$N + OH \leftrightarrow NO + H \tag{4.7}$$

The corresponding reaction rates of these three reactions can be found in [96]. Among these three reactions, the reaction (4.5) works as the initial reaction for the NO formation by generating the radical species N. Additionally, the NO formation rate at low temperature is much slower compared to the typical combustion rate and therefore most of NO is assumed to be produced after the completion of combustion [95]. Such a character implies that NO formation mechanism can be decoupled with the main combustion mechanism and it is possible to deal with the NOx emission after the combustion completes.

There are four factors substantially affecting the NO production in practical engines: air-fuel ratio, in-cylinder temperature, in-cylinder pressure and engine speed. The reason of air-fuel ratio is obvious since leaner air-fuel mixture indicates more nitrogen and

oxygen are involved in the combustion process which increases the likelihood of generating NO. On the other hand, high temperature and high pressure in combustion chamber speed up the rates of corresponding reactions and low engine speed extends the time for reactions which inevitably enhances the NO production. In addition, it is widely-accepted that among of these four, in-cylinder temperature is the dominant one to determine the amount of NO eventually. The relationship between the temperature and the NO emission can be explained by the characteristic time of NO formation as below.

Based on the reactions (4.5) to (4.7), the production rate of NO is yielded as:

$$\frac{d[NO]}{dt} = k_5^+[O][N_2] + k_6^+[N][O_2] + k_7^+[N][OH] - k_5^-[NO][N] - k_6^-[O][NO] - k_7^-[NO][H] \tag{4.8}$$

where [ ] represents the species molar concentration, k_i^+ and k_i^- show the forward and reverse reaction rates of the corresponding reactions.

By assuming species N being on the quasi-steady state, (4.8) can be further simplified as:

$$\frac{d[NO]}{dt} = 2k_5^+[O][N_2]\frac{1-[NO]^2/(K[O_2][N_2])}{1+k_5^-[NO]/(k_6^+[O_2]+k_7^+[OH])} \tag{4.9}$$

where $K = (k_5^+/k_5^-)(k_6^+/k_6^-)$

Since the majority of NO is produced after the completion of combustion, it is appropriate to approximate the concentrations of each species in (4.9) as the corresponding equilibrium values at the local in-cylinder pressure and temperature. Besides, at the very beginning of the NO formation process, the concentration of NO should be much less than the concentration of other stable species, like O_2 and N_2. Using these two assumptions, the initial NO production rate can be simplified as:

$$\frac{d[NO]}{dt}|_{initial} = 2k_5^+[O]_e[N_2]_e \tag{4.10}$$

The equilibrium value of species $[O]_e$ can be derived based on the equilibrium constant of the following reaction: [29]

$$\frac{1}{2}O_2 \leftrightarrow O \tag{4.11}$$

and finally, the initial production rate of NO is derived as:

$$\frac{d[NO]}{dt}|_{initial} = \frac{6\times10^{16}}{T^{1/2}}\exp(\frac{-69090}{T})[O_2]_e^{1/2}[N_2]_e \tag{4.12}$$

which is consistent with the result in [96].

The characteristic time for the NO formation can be calculated as below:

$$\tau_{NO} = \frac{[NO]_e}{d[NO]/dt|_{initial}} \tag{4.13}$$

Additionally, $[NO]_e$ can be yielded as [29]

$$[NO]_e = 4.5\exp(-\frac{10825}{T})[O_2]_e^{1/2}[N_2]_e^{1/2} \tag{4.14}$$

Plugging (4.12) and (4.14) into (4.13), the expression of characteristic time for the NO formation is finally derived as:

$$\tau_{NO} = \frac{8\times10^{-16}T\exp(58300/T)}{p^{1/2}} \tag{4.15}$$

As shown in (4.15), the characteristic time is determined by the in-cylinder gas temperature and pressure. However, the temperature is more important due to its exponential term in (4.15). Figure 4.9 illustrates this conclusion. Obviously, the characteristic time of NO formation is more sensitive to the in-cylinder temperature since

the 200K increase in temperature reduces one order of magnitude of the characteristic time. Additionally, due to the fact that a typical engine cycle lasts less than 100ms, the NO generation is only considerable when the in-cylinder temperature is over 2000K.

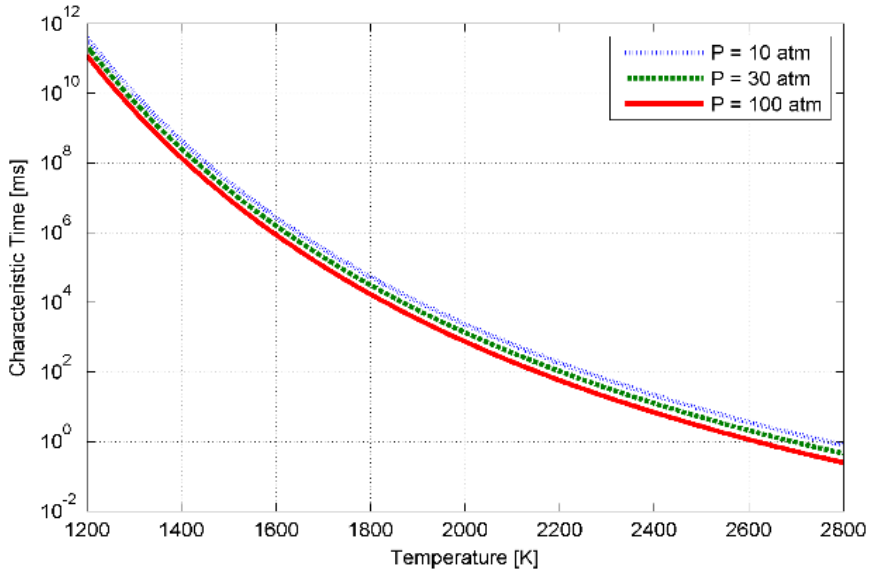

Figure 4.9 Characteristic time of NO formation in log scale at various in-cylinder pressure and temperature

As mentioned in the last section, the piston trajectories in Figure 4.2 are within the asymmetric pattern while the compression process and expansion process are different to each other which generate significant effects on the combustion performance in terms of NOx emission. Therefore the corresponding emissions performances are under investigated.

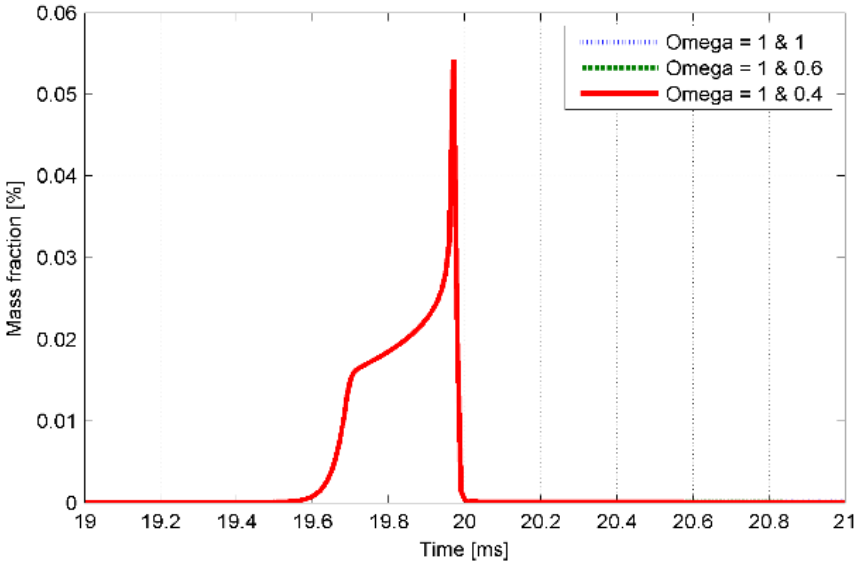

(a)

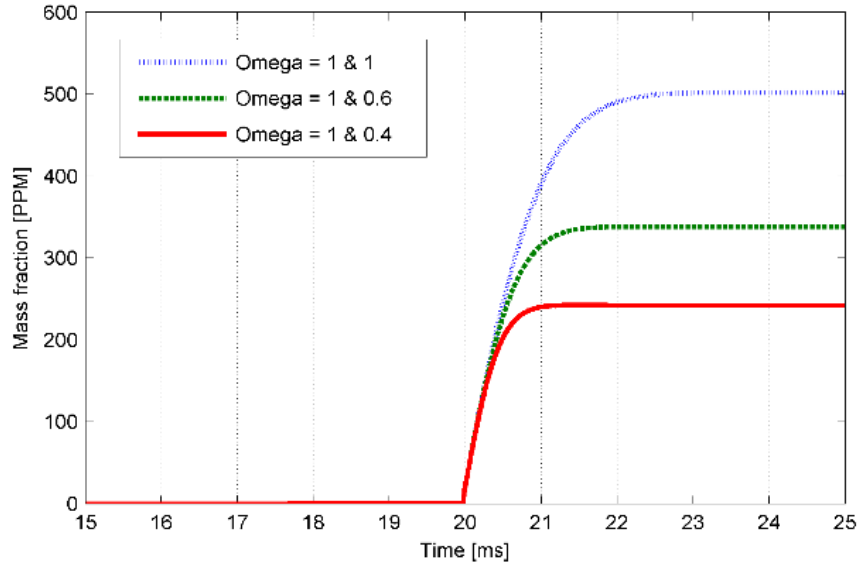

(b)

Figure 4.10 CO concentration (a) and NOx concentration (b) traces from the combustion processes along the piston trajectories in Figure 4.2

Figure 4.10 shows the CO and the NOx emissions traces during the combustion processes in Figure 4.6 respectively. From Figure 4.10 (a), it is evident that all the CO

molecules are oxidized to CO_2 at the TDC point (20ms) in each case which implies the completion of the combustion. Furthermore, the majority production of NOx indeed begins after the TDC point in each case (Figure 4.10 (b)), which supports the assumption that NOx formation mechanism can be decoupled with the main combustion chemical kinetics due to its relatively lower reaction rate at low temperature. In addition, the NOx emission is almost reduced by half (from 500 ppm to 240 ppm) due to the quicker expansion in the solid line compared to the other two. The result is intuitive from the perspective of the chemical kinetics since rapid expansion reduces both the temperature and the pressure in the cylinder and therefore inhibits the formation of NOx Afterward. Additionally, the sudden expansion also increases the combustion chamber volume quickly, which reduces the species concentration involved the reactions and the rates of NOx formation reactions as well. As can be seen in Figure 4.11, the third case, where Ω = 1.0 & 0.4, not only possesses much smaller production rates of each reaction but also has relatively shorter reaction period for active NOx production. More importantly, this NOx emission reduction is achieved without sacrificing on the engine thermal efficiency (in Figure 4.6), which further demonstrates the advantages of the trajectory-based combustion control on emissions control.

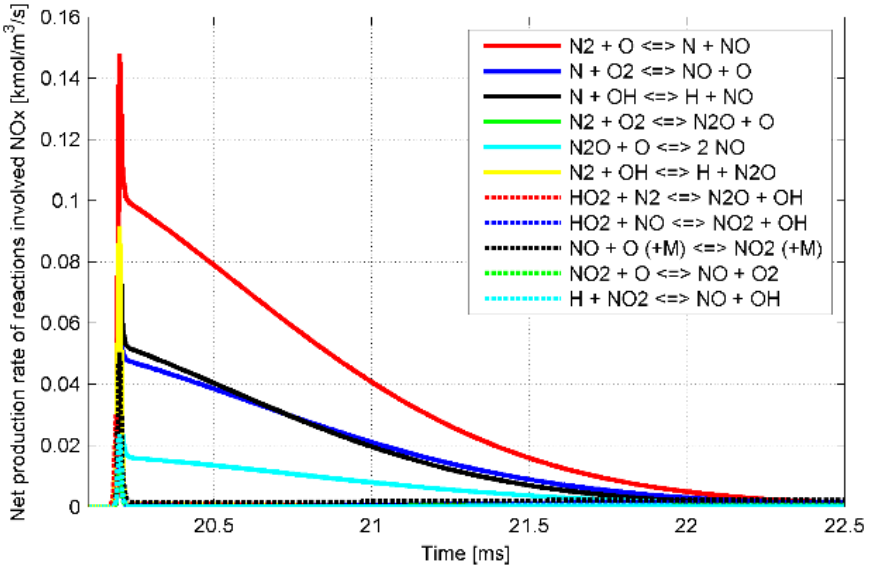
Net production rate of reactions involved NOx [kmol/m3/s]
Time [ms]
N2 + O <=> N + NO
N + O2 <=> NO + O
N + OH <=> H + NO
N2 + O2 <=> N2O + O
N2O + O <=> 2 NO
N2 + OH <=> H + N2O
HO2 + N2 <=> N2O + OH
HO2 + NO <=> NO2 + OH
NO + O (+M) <=> NO2 (+M)
NO2 + O <=> NO + O2
H + NO2 <=> NO + OH

(a)

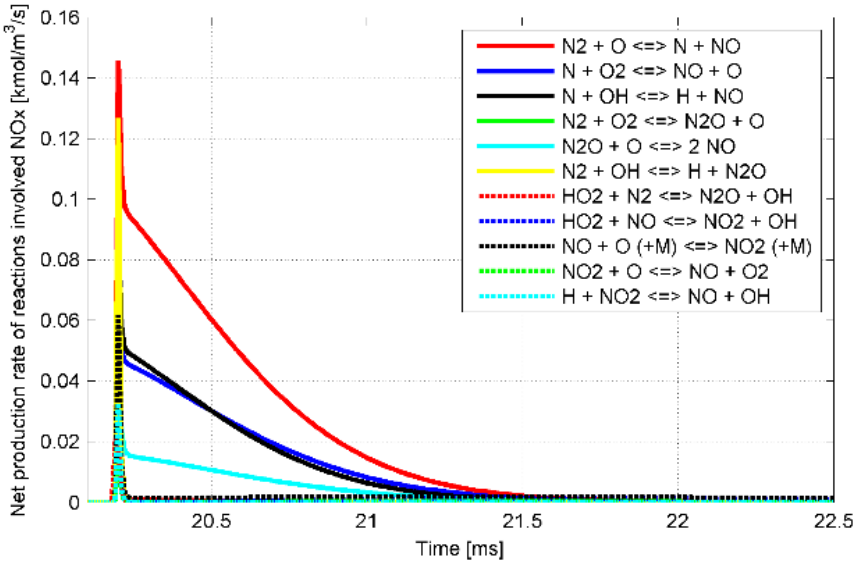
Net production rate of reactions involved NOx [kmol/m3/s]
Time [ms]
N2 + O <=> N + NO
N + O2 <=> NO + O
N + OH <=> H + NO
N2 + O2 <=> N2O + O
N2O + O <=> 2 NO
N2 + OH <=> H + N2O
HO2 + N2 <=> N2O + OH
HO2 + NO <=> NO2 + OH
NO + O (+M) <=> NO2 (+M)
NO2 + O <=> NO + O2
H + NO2 <=> NO + OH

(b)

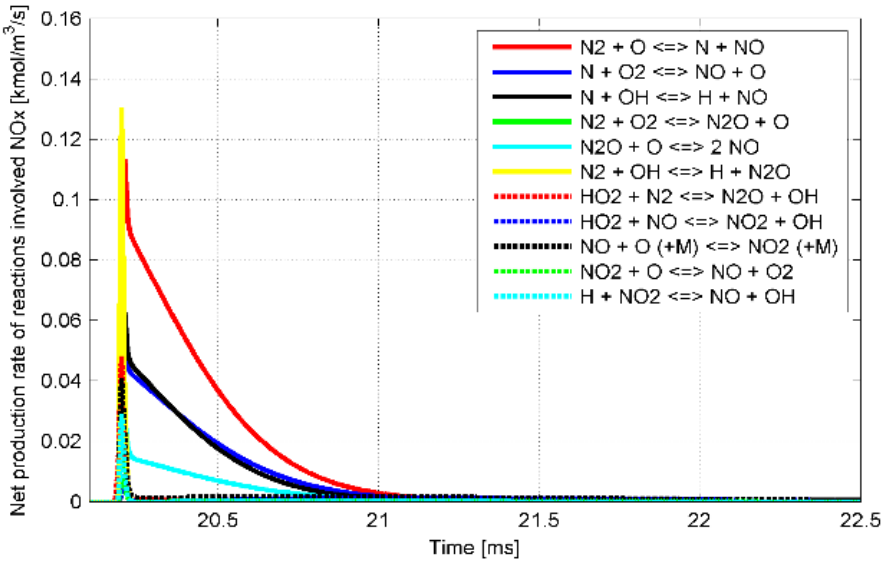

(c)

Figure 4.11 Chemical kinetics of CO emission during the combustion processes in Figure 4.6 ((a) Ω = 1 & 1, (b) Ω = 1 & 0.6, (c) Ω =1 & 0.4)

4.3.3 Optimal Asymmetric Piston Trajectories at Different Working Conditions

In order to further elaborate the emission and efficiency benefits by applying asymmetric piston trajectories in FPE, 3D maps are generated indicating the work output and NOx emissions along different asymmetric piston trajectories. In these 3D maps, each point at the x-y plain represents the two Ωs showing the compression and expansion process respectively. In addition, the z values show the corresponding work output or NOx emissions. A typical example that the FPE works at CR = 12 and AFER λ = 2.0, is shown in Figure 4.12.

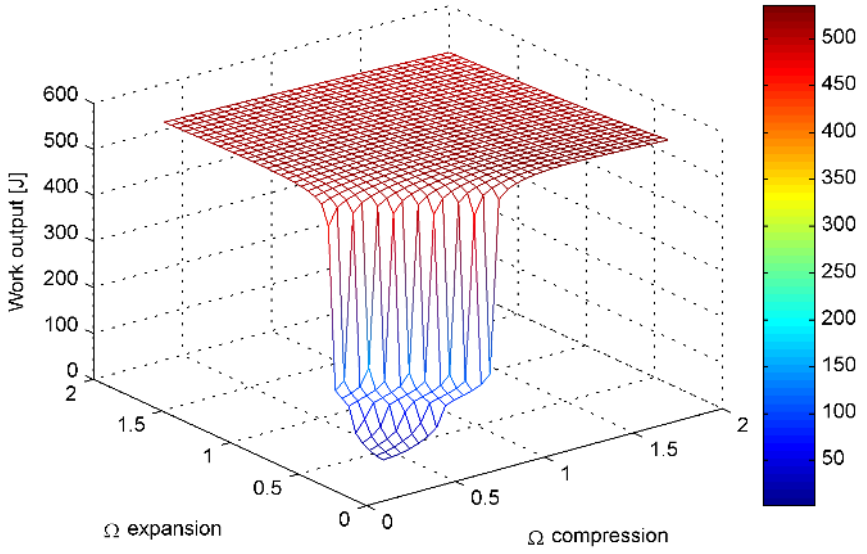

(a)

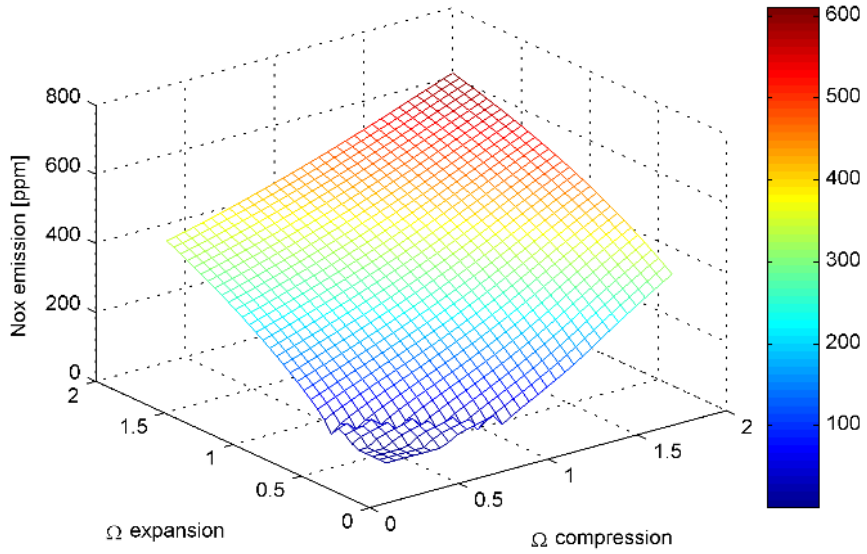

(b)

Figure 4.12 3D maps of FPE performance along different piston trajectories at CR = 12 and AFER λ = 2.0 ((a) work output, (b) NOx emission)

Besides, by checking the simulation results along the diagonal line in the two Ωs domain, the performances of FPE deploying symmetric piston trajectories can be

achieved as well. Table 4.3 lists the comparison of FPE performance by applying the optimal asymmetric piston trajectory and the optimal symmetric piston trajectory respectively.

Table 4.3 FPE performance comparison between the optimal asymmetric and symmetric piston trajectories (CR = 12, $\lambda = 2.0$)

Ω compression	Ω expansion	Work output [J]	NOx emission [ppm]	Efficiency [%]
1.45	0.4	535.24	137.37	52.83%
0.95	0.95	523.31	192.10	51.67%
1.2	0.4	528.24	64.63	52.15%

The first two rows show the optimal asymmetric piston trajectory and the optimal symmetric trajectory at this working condition in terms of maximal work output. As can be seen, using the asymmetric piston trajectory can gain 2.28% work output and reduce NOx emission by 30%. In addition, by reducing the compression Ω from 1.45 to 1.2 in asymmetric trajectory (the third row), the NOx emission can be even further reduced by half while its thermal efficiency is still larger than the symmetric one.

More importantly, the efficiency and emission benefits can also be achieved at other working conditions by leveraging the ultimate freedom of piston motion in the FPE and varying the piston trajectory actively. The corresponding results are listed in Table 4.4 (different CR) and Table 4.5 (different AFER, λ).

Table 4.4 FPE performance comparison between the optimal asymmetric and symmetric piston trajectories (λ = 2.0, different CR)

CR	Ω compression	Ω expansion	Work output [J]	NOx emission [ppm]
CR = 11	2	0.45	507.03	41.57
CR = 11	1.4	1.4	505.67	179.88
CR = 12	1.2	0.4	528.24	64.63
CR = 12	0.95	0.95	523.31	192.10
CR = 13	0.7	0.4	544.74	94.6
CR = 13	0.65	0.65	541.96	200.08

Table 4.5 FPE performance comparison between the optimal asymmetric and symmetric piston trajectories (CR = 12, different λ)

AFER	Ω compression	Ω expansion	Work output [J]	NOx emission [ppm]
λ = 2.5	1.3	0.4	434.24	3.74
λ = 2.5	0.95	0.95	426.31	6.1
λ = 2.0	1.2	0.4	528.24	64.63
λ = 2.0	0.95	0.95	523.31	192.10
λ = 1.5	1.75	0.4	680.15	3500
λ = 1.5	1.2	1.2	664.56	6800

In Table 4.4 and Table 4.5, the red data represent the optimal asymmetric piston trajectories at each working condition. It is quite clear that by actively varying the two Ωs according to different working condition, the FPE gains more output work and produces less NOx emission simultaneously compared to the outcome from the symmetric

trajectory. Thus, it is reasonable to claim that the performance of FPE can be improved significantly in the entire load domain via the trajectory-based combustion control.

4.3.4 Sensitivity Analysis of the Trajectory-based Combustion Control

Usually, the attainable range of Ω in the FPE is limited mainly by the actuation system, such as the peak actuation force or the dynamic behavior of actuators [66]. However, deploying the piston trajectory within this physically available range may still not guarantee the occurrence of the combustion. For example, smaller Ω at lower CR may not provide a sufficiently long period of high temperature to ignite the air fuel mixture and trigger the combustion. As a result, a so-called combustion available range of Ω, within the physically available range, also exists. Furthermore, unlike the physical one, the combustion available range of Ω is varied depend on different working conditions, such as the CR and the AFER. The corresponding simulation results are shown in Figure 4.13 and Figure 4.14.

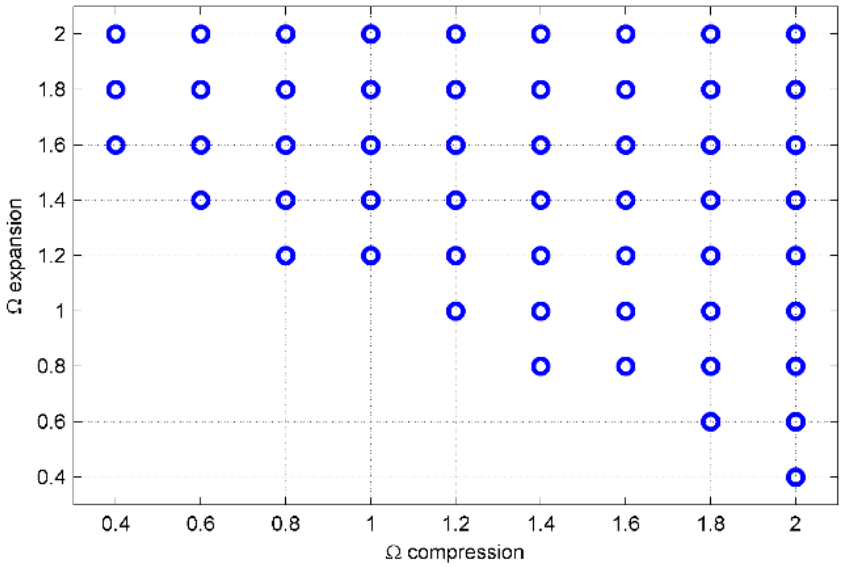

(a)

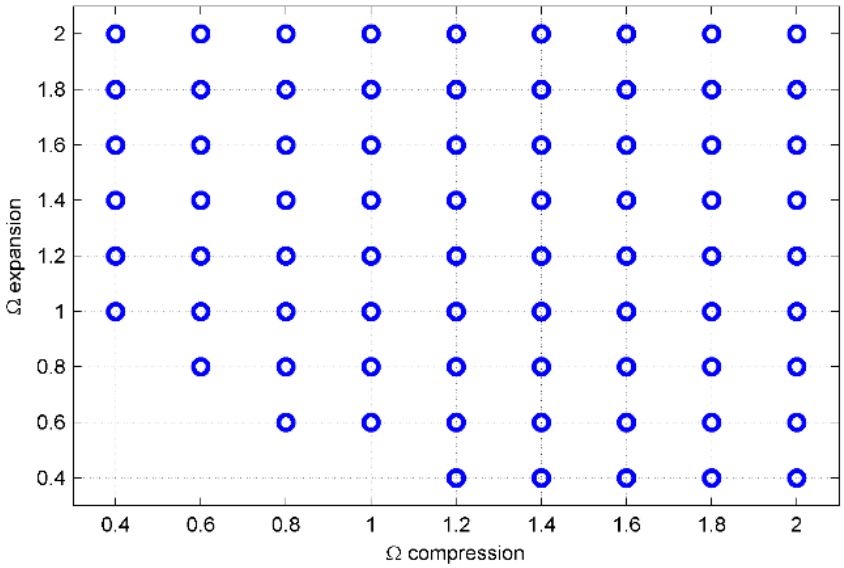

(b)

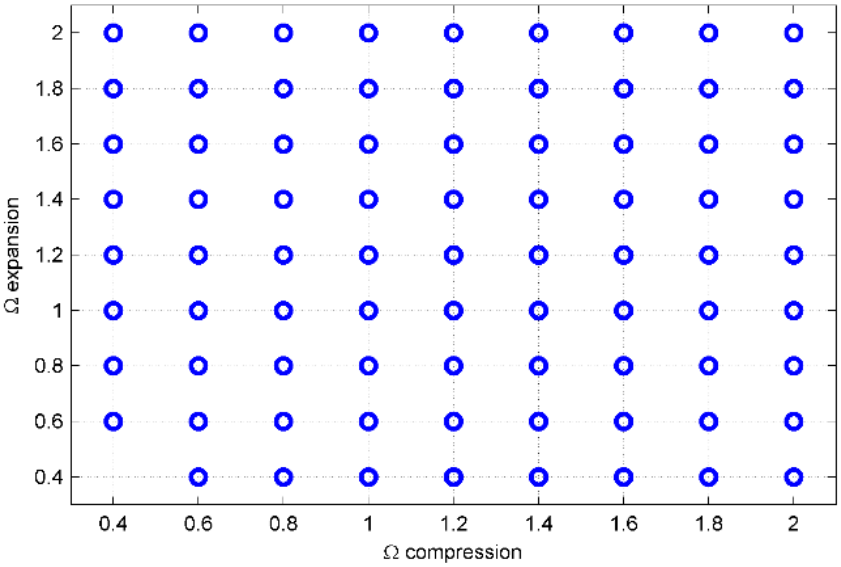

(c)

Figure 4.13 Combustion available ranges of Ω at different CR and λ = 2.0 ((a) CR = 11, (b) CR = 12, (c) CR = 13)

Figure 4.13 represents the combustion available ranges of Ω at different CR and identical AFER. Each circle point in the figures indicates the piston trajectory triggering

the combustion successfully. It is quite intuitive that increasing the CR enlarges the combustion available range of Ω. Enlightened by this observation, in order to ensure the combustion indeed occurring in the FPE, the applied piston trajectory has to be selected from the combustion available range of Ω while CR = 11.

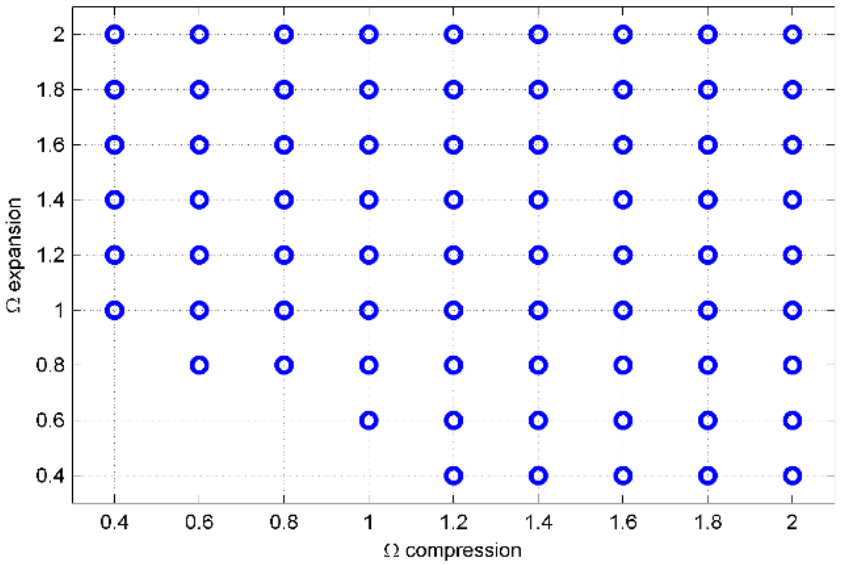

(a)

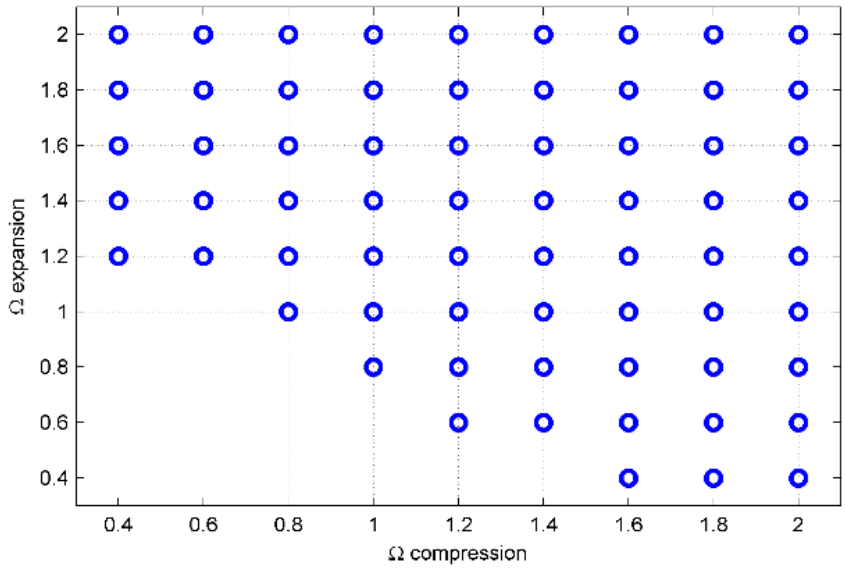

(b)

Figure 4.14 Combustion available ranges of Ω at different λ and CR = 12 ((a) λ = 2.5, (b) λ = 1.5)

Similarly, the combustion available ranges of Ω are also varied according to the AFER, as shown in Figure 4.14. Obviously, lower AFER reduces the range of Ω. This phenomenon can be explained by the larger heat capacity possessed by the fuel molecules, and richer fuel in the air fuel mixture requires the piston locating around the TDC point for a longer duration to increase the in-cylinder temperature high enough and trigger the combustion [97]. Therefore, in order to ensure the occurrence of combustion regardless of the disturbance of AFER, the piston trajectory has to be chosen from the combustion available range of Ω at lower AFER as well.

4.3.5 Comparison of FPE with Conventional ICE

A comparison of engine indicated thermal efficiency and NOx emission between a conventional ICE and an FPE with the optimal piston trajectories are presented in this subsection to further illustrate the advantages of the piston trajectory-based combustion control. Specifically, the piston trajectory of the crankshaft engine is generated through the slider-crank mechanism. Detailed information on these trajectories can be found in [79]. On the other hand, the optimal piston trajectories in FPE under different compression ratio are all asymmetric piston trajectories. Their compression sections are determined to ignite the combustion at the TDC point and their expansion processes are designed to decrease the production of NOx.

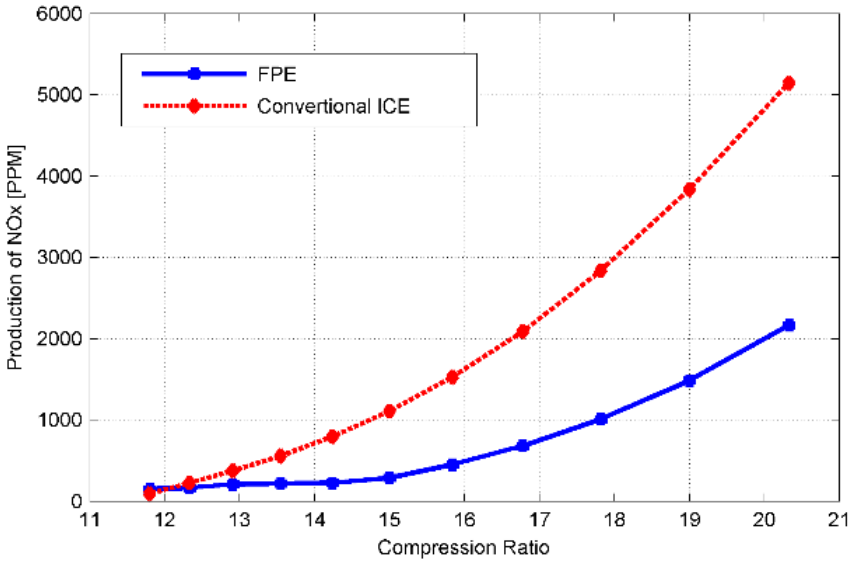

(a)

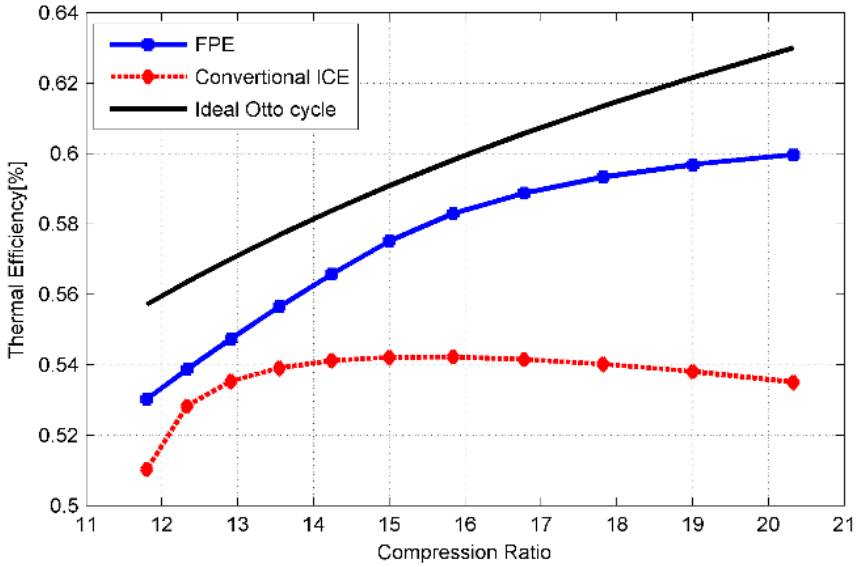

(b)

Figure 4.15 Comparison between FPE and conventional ICE under different compression ratio ((a) production of NOx emission, (b) Indicated thermal efficiency)

As can be seen in Figure 4.15 (a), due to the freedom of the piston motion in FPE, the NOx emission from the FPE are always lower compared to the output of the ICE, except

at CR = 11.8 while the combustion in the ICE is uncompleted. Additionally, the benefit of NOx reduction is further enhanced at the high compression ratio condition. Such result is intuitive since the piston motion of the FPE can be adjusted actively to adapt to different working conditions, e.g. high compression ratio. In addition, by using the same optimal piston trajectories, the indicated thermal efficiency from the FPE are also higher than the counterpart of ICE, as shown in Figure 4.15 (b). In other words, besides the benefits of emission performance, the FPE with optimal asymmetric piston trajectories can also increase the engine efficiency simultaneously across the entire compression ratio domain, which is consistent with our aforementioned analysis.

4.4 Conclusion

In this chapter, the benefit of the trajectory-based combustion control on emissions reduction is presented. Enabled by the FPE, the trajectory-based combustion control is able to manipulate the in-cylinder temperature trace and affect the chemical kinetics of the combustion, including the generation processes of different emissions. A comprehensive model is then developed to reproduce the combustion processes along different piston trajectories. The simulation results clearly show that both CO and NOx can be reduced by implementing appropriate piston trajectories in the FPE. Specifically, unique asymmetric trajectories are designed that decreases the amount of NOx emission and increases the engine thermal efficiency simultaneously. Meanwhile, sensitivity analyses are conducted at different working conditions to demonstrate the robustness of this advanced combustion control method. In addition, the performance of the FPE is also compared to the conventional ICE in terms of indicated thermal efficiency and NOx

emission production which further demonstrates the advantages of the piston trajectory-based combustion control. Considering the fact that the production of emission species are mainly driven by the chemical kinetics, the emission benefits from the trajectory-based combustion control can be readily extended to other emission species in different combustion modes.

Chapter 5

Effects of the Trajectory-based Combustion Control on Renewable Fuel Applications

The utilization of the trajectory-based combustion control is extended to renewable fuels applications in this chapter. Seven renewable fuels are considered including hydrogen, biogas, syngas, ethanol, dimethyl ether (DME), biodiesel, and Fischer-Tropsch fuel. The influences of both CR and piston motion pattern between the two dead centers on the combustion process of those renewable fuels are presented in this chapter, which demonstrates the ultimate fuel flexibility and large tolerance of fuel impurity possessed by the FPE. In addition, the simulation results show that, due to its ultimate fuel flexibility, large tolerance of fuel impurity, and controllable piston trajectory, the FPE, with the trajectory-based combustion control, enables a co-optimization of renewable fuels and engine operation.

5.1 Renewable Fuels

Renewable fuels are referred to gaseous or liquid fuels converted from sustainable feedstock. Typical renewable fuels nowadays include hydrogen, biogas, syngas, ethanol, DME, biodiesel, and F-T fuel. The physical and chemical properties of these seven fuels are listed in Table 5.1 for comparison. In the rest of this section, a comprehensive review is presented, which discusses properties, production technologies and existing challenges of each fuel in detail.

Table 5.1 Properties of seven renewable fuels, gasoline and diesel [2]-[8], [10], [11]

Property	Unit	H_2	Biogas	Syngas	Ethanol	DME	Biodiesel	F-T fuels	Gasoline	Diesel
Molar mass	g/mol	2	~22	~25	46	46	~290	~210	~110	~170
C content	Mass%	0	~44	~14	52.2	52.2	~77	85.7	84	86
H content	Mass%	100	~10	~2	13	13	~12	14.3	16	14
O Content	Mass%	0	~46	~24	34.8	34.8	~11	0	0	0
Density	kg/m^3	0.082	~1.15	~0.95	785	667	880	757	737	831
Cetane number		<0	<0	<0	5-8	>55	47	>70	0-5	40-50
Auto-ignition Temperature	^oC	500	>600	>600	365	350	370	-	260	210
Low heating value	MJ/kg	120	~30	~18	26.87	27.6	~37	43.24	43.47	42.5
Kinematic viscosity	cSt	~100	-	-	1.1-2.2	<0.1	1.9-6.0	-	<1	3
Boiling point	K	20	~150	~100	351	248.1	360	-	310-478	450-643
Vapor pressure (at 298K)	kPa	-	-	-	5.83	530	<10	-	<180	<<10

5.1.1 Hydrogen

Hydrogen (H_2) is the lightest element, which results in some extreme properties, such as high thermal conductivity, rapid burning speed, and quite a high octane number [8]. As a fuel, H_2 has the highest energy content per unit of mass, around 120MJ/kg, and produces zero C-based emissions. Additionally, since H_2 is the most plentiful element on earth, it is also considered as one of the endless energy sources.

Currently, extensive researches have been conducted to investigate the production of H_2 from biomass directly. Those processes are usually classified into two groups: thermal-chemical conversion and biochemical conversion [98]. The former approach involves a series of thermal chemical reactions, such as steam reforming, pyrolysis, and gasification of biomass. The latter one includes fermentative H_2 production, photosynthesis process, and biological water gas shift reaction [99]. Even though it is more environment-friendly and less energy intensive, the biochemical conversion still needs to further improve its conversion efficiency and decrease the related cost [9]. In addition, H_2 can also be produced via water electrolysis, which is more sustainable, if renewable energy, such as solar energy, wind turbine, and hydropower, are employed.

There are some roadblocks preventing the large scale utilization of H_2. The most severe problem is the safety of H_2 storage. Due to its small molecular size and less ignition energy, H_2 could easily be dispersed into the atmosphere and ignited [8].

5.1.2 Biogas

Biogas is a versatile gaseous renewable energy source, which is predominantly produced by anaerobic digestion (AD) of energy crops, agriculture residues, livestock

waste, industry slurry and municipal solid waste. The main components of raw biogas are CH_4, 50-70% in vol., and CO_2, 30-40% in vol., with a smaller amount of H_2S and NH_3 [100]. Due to the large amount of CO_2, the raw biogas has smaller lower heating value and much larger density compared to natural gas.

As one of the most energy-efficient and environment-friendly renewable fuels, the production of biogas through AD offers unbeatable benefits compared to the others. For example, extremely low cost of feedstock decreases its price significantly; the AD process provides an excellent approach dealing with the landfill deposit and waste recovery and therefore improving human health and hygiene. As a result, more countries have explored the utilization of biogas since last century: The United States consumed 147 trillion BTU (155 trillion kJ) of energy from biogas, about 0.6% of the national natural gas consumption in 2003 [101]. In 2008, more than 60% of gaseous vehicle fuel in Sweden is biogas, which powered more than 17,000 vehicles nationally [102]. At the end of 2010, almost 6,000 biogas plants were operated in German [103].

Usually, the raw biogas is used in combined heat and power (CHP) plant after desulfurization and dehydration. In addition, the raw biogas can also be upgraded by concentrating the methane component up to 95% or more [104]. The upgraded biogas, or so-called bio-methane, is widely adopted as the vehicle fuels in many European countries, such as Germany, Sweden, Switzerland, and Norway. However, the upgrading process inevitably increases the price of biogas and limits its market. Other related technological issues also exist including the methane slip problem during the upgrading process and its transportation challenges.

5.1.3 Syngas

Syngas is another gaseous fuel which is converted via gasification, a thermochemical conversion process which partially oxidizes hydrocarbon compounds into different products [105]. Typically, the produced syngas contains multiple gases, such as CO, H_2, CH_4, CO_2, and N_2. Other impurities, such as tar, particulate matter (PM) and char, also exist. The main chemical reactions governing the conversion process can be summarized as follow:

Partial oxidation: $$C + 0.5O_2 \leftrightarrow CO \quad (5.1)$$

Complete oxidation: $$C + O_2 \leftrightarrow CO_2 \quad (5.2)$$

Water gas reaction: $$C + H_2O \leftrightarrow CO + H_2 \quad (5.3)$$

Water gas shift reaction: $$CO + H_2O \leftrightarrow CO_2 + H_2 \quad (5.4)$$

Methane formation: $$CO + 3H_2 \leftrightarrow CH_4 + H_2O \quad (5.5)$$

Currently, gasification is recognized as the most promising technology to be fully commercialized. The gasifiers can be categorized into two groups: fixed bed gasifier and fluidized bed gasifier. The dominant gasifier is the fixed bed downdraft one due to its higher conversion efficiencies and lower production of tar and PM [106]. Typical compositions of syngas from this gasifier are listed in Table 5.2.

Table 5.2 Typical bio-syngas composition produced from downdraft gasifiers operated on low- to medium moisture content feedstock [107]

Component	[%] in volume
H_2	12-20
CO_2	9-15
CH_4	2-3
CO	17-22
N_2	50-54

Besides the gasifier, other aspects, e.g. moisture in the feedstock, temperature, air-fuel equivalence ratio (ER) for gasifying process and gasifying agent, are also critical to determine the quality of gasification [105]. For instance, feedstock with high moisture reduces the calorific value (CV) of the product due to the need of evaporation; higher temperature leads to higher yield of CO and H_2, less tar content and more ash; Higher ER facilitates biomass oxidation and therefore generates less CV product, while low ER results in more tar and other impurities; at last, if gasifying agent is pure oxygen, more combustible gases are produced at a higher cost.

Extensive studies have been conducted to investigate the performance of feeding the syngas into the ICE directly [106]-[108]. It has concluded that in this case, the ICE encounters 20-30% power de-rating in the diesel mode and even larger power loss in the spark ignition mode [107]. The reduction is mainly attributed to the lower CV of the syngas and less volume of the syngas/air mixture entering the engine cylinders. Increasing CR is an effective way to address this issue. It has been demonstrated that a

15-20% improvement of power de-rating could be achieved if high CR engine is utilized [108].

5.1.4 Ethanol

Ethanol is mainly produced from renewable biomass through the fermentation process. It has been accepted as a fuel for ICE even before the gasoline [109]. Currently, ethanol is still a promising alternatives fuel due to its compatibility of existing ICE. Besides, ethanol has a higher octane number, which enables the ICE to operate at higher CR [10]. The utilization of ethanol in the ICE can also reduce emissions, e.g. CO, unburned HC, SO_x, and NO_x, due to its higher oxygen content, almost zero sulfur content and less lower heating value (LHV) [109].

The production of ethanol is drastically increased from 4.5 billion gallons to 23.4 billion gallons in 2010 globally [110]. Conventionally, ethanol is produced from the food crops, which are easily transformed to simple sugar through milling, liquefaction, and saccharification. Then, the simple sugar is further fermented to ethanol via specific microorganisms. The corresponding chemical process is represented as follow:

$$(C_6H_{10}O_5)_n(sugar, cellulose) + nH_2O \rightarrow nC_6H_{12}O_6 \tag{5.6}$$

$$C_6H_{12}O_6 \rightarrow 2CH_3CH_2OH(ethanol) + 2CO_2 \tag{5.7}$$

Concerns are raised for this approach due to the food supply issues worldwide. Therefore, conversion of ethanol from the non-food lignocellulosic plant, or so-called “second generation feedstock”, is extensively explored [5]. Consequently, besides

reactions (5.6) and (5.7), the conversion process of second generation feedstock is also affected by following reactions:

$$(C_5H_8O_4)_n\,(hemicellulose) + nH_2O \rightarrow nC_5H_{10}O_5 \tag{5.8}$$

$$3C_5H_{10}O_5 \rightarrow 5CH_3CH_2OH\,(ethanol) + 5CO_2 \tag{5.9}$$

To date, how to extract simple sugar from these lignocellulosic materials in a cost-effective way, is still a bottleneck for this technology. Usually, such feedstock has been treated through acid hydrolysis and/or enzymatic hydrolysis before the fermentation process [5], which are very energy- and cost-intensive. Other conversion methods, e.g. thermochemical transformation of lignocellulosic materials and ethanol production from microalgae and seaweeds, are also proposed, which have not entered into practice yet.

5.1.5 Dimethyl Ether (DME)

DME is the simplest ether with a chemical formula of CH_3OCH_3. Its physical properties are quite similar to other liquefied petroleum-based gas, such as propane and butane. DME is usually compressed to the liquid phase and works as a substitute for diesel fuel [5]-[7]. At the present time, most DME is produced by dehydrogenation of methanol from natural gas or syngas:

Methanol synthesis: $$CO + 2H_2 \leftrightarrow CH_3OH \tag{5.10}$$

Methanol dehydration: $$2CH_3OH \leftrightarrow CH_3OCH_3 + H_2O \tag{5.11}$$

Water-gas shift: $$H_2O + CO \leftrightarrow H_2 + CO_2 \tag{5.12}$$

Net reaction: $$3H_2 + 3CO \leftrightarrow CH_3OCH_3 + CO_2 \tag{5.13}$$

Besides, DME also owns other unmatched advantages:

- *Human Health:* DME is accepted as a non-toxic and noncarcinogenic volatile organic compound.
- *Economy:* due to its similar properties of liquefied petroleum gas, DME can use the existing gas infrastructures for transport and storage.
- *Environment impact:* The absence of C-C bond in DME and its high oxygen content result in less PM and NOx.

Nonetheless, the relatively lower heating value of DME requires the ICE operating at a higher CR to fully extract its chemical energy. Meanwhile, the existence of multiple impurities, such as methanol and water, also asks for specific treatment before it is feed to conventional ICE.

5.1.6 Biodiesel

Biodiesel is a yellowish liquid whose chemical structure is mainly mono-alkyl esters of fatty acids [5]. It is considered as one of the best non-toxic and bio-degradable drop-in biofuels. From 2003 to 2013, the worldwide production of biodiesel has increased significantly, from 213 million gallons to 6289 million gallons [111].

At the very beginning, the biodiesel was produced from vegetable oil or animal fat directly by mechanical extraction. However, mainly due to the high viscosity of the derived oil, it was abandoned. Afterward, many alternative approaches, e.g. blending, micro-emulsions and transesterification, were proposed [112]. At the present time, the dominant technology is transesterification, governed by reaction (14), where R_1, R_2, and R_3 are different or the same aliphatic hydrocarbon groups [5].

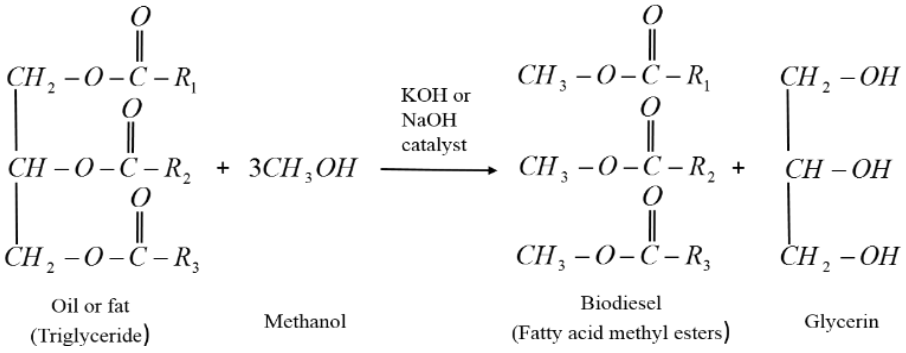

(5.14)

Even though the properties of produced bio-diesel are excellent, the high cost of the corresponding feedstock, such as vegetable oil and animal fat, still prevents the transesterification from wide commercialization. This drawback results in the exploration of the second generation feedstock, including used vegetable oil, non-edible plant oils, and even waste restaurant oil [2], [5]. Due to the high content of free fatty acid in those second generation feedstock, the corresponding production technologies are also upgraded. The third generation feedstock, such as algae, bacilli, fungi, and yeast [8], is also proposed to further reduce bio-diesel price. Nonetheless, lots of challenges still exist for the third generation feedstock in terms of cost and efficiency.

It is widely accepted that bio-diesel can be injected into the diesel engine directly, with no or minor hardware modification. Even though the fuel economy may reduce around 10% due to its less low heating value [113], the emissions performance, in terms of SOx, NOx, and PM, is much better than its petroleum-based counterparts [114].

5.1.7 Fisher-Tropsch Fuels

Fisher-Tropsch fuel, or F-T fuel, is the name of a variety of liquid hydrocarbons which are produced from syngas through Fisher-Tropsch synthesis, established by Germany scientists, Franz Fisher and Hans Tropsch, back to 1920s [115]:

$$nCO + 2nH_2 \rightarrow (-CH_2-) + nH_2O \quad (5.15)$$

$$nCO + (2n+1)H_2 \rightarrow C_nH_{2n+2} + nH_2O \quad (5.16)$$

$$nCO + (n + m/2)H_2 \rightarrow C_nH_m + nH_2O \quad (5.17)$$

As can be seen, the production of F-T fuels can be separated into three steps: syngas generation, syngas processing and finally Fischer-Tropsch synthesis. It was evaluated that the syngas generation, especially from the biomass, accounts for more than half of the capital investment and operating cost [116]. Variable aspects affect the yield and quality of the F-T fuels, including reaction temperature, reaction pressure, feed gas composition and catalyst type.

Since its majority components are straight-chain alkanes, the F-T fuels own very high quality as a substitute for diesel fuel. In addition, attributed to its relatively S-free content and few aromatic compounds, the F-T fuels generate nearly zero SOx and PM emissions. Furthermore, due to its high cetane number, the F-T fuels can also be blended into traditional diesel to further improve its quality.

5.2 Simulation Results and Discussion

The main focus of this chapter is to investigate the effects of the piston trajectory on the combustion process of different renewable fuels. In the FPE, the piston trajectories can be varied with respect to both CR and Ω. By changing CR, all seven selected fuels can be ignited in the simulation, which proves FPE's ultimate fuel flexibility. Furthermore, simulations of syngas and F-T fuels show that this freedom can also expand

available range of fuel compositions. The FPE can even enhance the engine tolerance of fuel impurities by varying the CR, proved by the simulation of DME and ethanol.

In addition, the capability of varying Ω in the FPE enables the reduction of required CR to ignite renewable fuels, which is proved by both results of biogas and biodiesel. On top of that, the simulation results of DME also show that the freedom of Ω can be further utilized to optimize the combustion process at a fixed CR.

Afterward, the simulation of H_2 is conducted, concentrated on the optimization of FPE operation by implementing asymmetric piston trajectories. Such asymmetric piston trajectories are designed based on the chemical kinetics of the fuel, variable loading conditions, and corresponding NOx emission.

5.2.1 Effects of CR

CR is such an important parameter for ICE due to its significant influence on engine efficiency. In addition, some researchers even claimed that by changing CR, almost any liquid fuels can be utilized in the ICE [42]. Different variable CR mechanisms have been proposed for ICE [42], [62]-[64] and [117]. Most of them modify the crank/connecting rod mechanism with mechanical linkages and actuation systems. Those technologies offer some flexibility for CR control, but still subject to the mechanical constraints and the response time of the actuation system.

FPE, however, offers continuously variable CR control with the assistance of the virtual crankshaft, and thus realizes the ultimate fuel flexibility. In other words, all renewable fuels can be employed into the FPE.

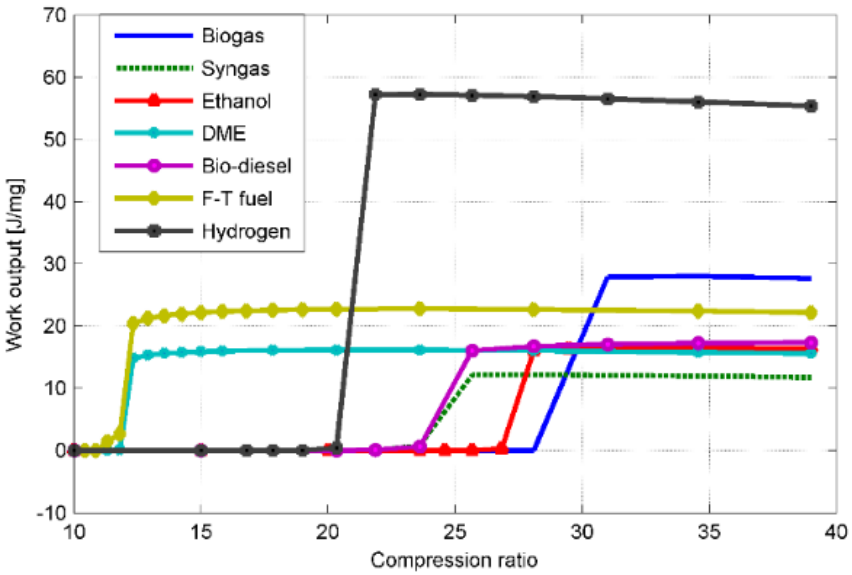

Figure 5.1 Work output per unit mass vs different CR (seven different renewable fuels, AFR = 2, identical Ω = 1)

As can be seen in Figure 5.1, under the HCCI combustion mode, all the seven renewable fuels considered herein can be ignited by employing an appropriate CR into the FPE. The minimal CR to ignite each renewable fuel is listed in Table 5.3.

Table 5.3 Minimal CR to ignite each renewable fuels in FPE (Ω = 1)

Fuels	Components	CR
Biogas	90% CH_4 and 10% CO	31
Syngas	20% CO, 18% H_2, 2% CH_4, 10% CO_2 and 50% N_2	26
Bio-ethanol	100% C_2H_5OH	28
DME	100% DME	12
Bio-diesel	100% Methyl Decanoate	25
F-T fuel	50% n-heptane, 50% iso-octane	12
Bio-hydrogen	100% hydrogen	22

Clearly, the required CRs for each renewable fuel are completely different. Nonetheless, all of these CRs can be obtained in one FPE without any hardware modification. In addition, Figure 5.1 also shows that H_2 has much higher energy density compared to the other fuels. Biogas, which consists of 90% methane, and F-T fuels are followed from this perspective. Fewer output works per mass are produced by DME, ethanol, and bio-diesel, partially because of higher oxygen contents in their molecules. At last, syngas has the least energy density since it comprises more incombustible components, such as CO, CO_2 and a large amount of N_2.

Besides, variable CR also enhances FPE's capability of dealing with different compositions of renewable fuel. For example, the compositions of the syngas can be varied significantly due to the moisture content of the feedstock, employed ER during gasification, gasification temperature and utilized gasification agent, as listed in Table 5.4.

Table 5.4 Typical compositions (in vol.) of various syngas under different conditions [105], [118]

Conditions	**CO**	**H_2**	**CH_4**	**CO_2**	**N_2**
Normal	20	18	2	10	50
High ER	10	9	1	15	65
High moist	9	22	1	8	60
High T	30	20	1	9	40
Oxygen agent	45	35	6	14	0

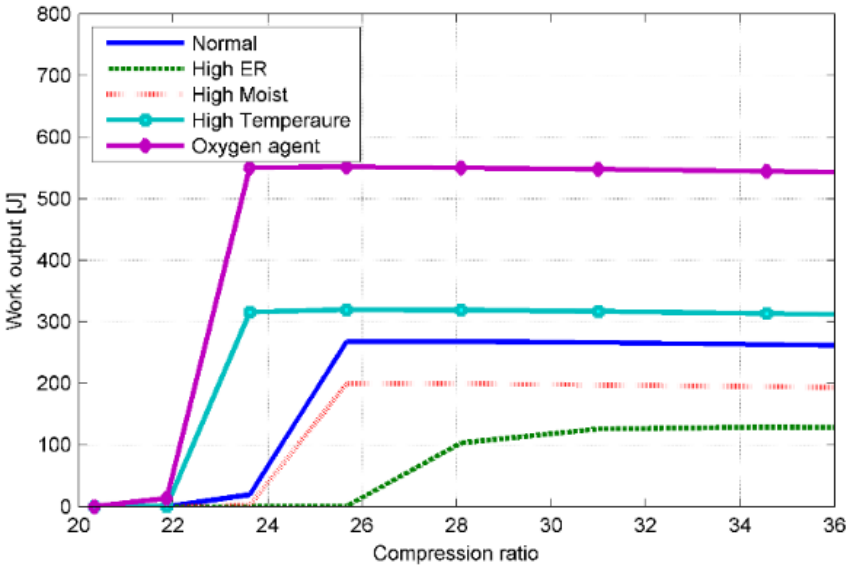

Figure 5.2 Work outputs vs different CR (syngas produced in different conditions, AFR = 2, identical $\Omega = 1$)

Generally, if the gasification proceeds at a higher temperature or with pure oxygen agent, more combustible components, such as CO and H_2, are produced. In this way, the syngas is easier to be ignited by compression and generates more output work as shown in Figure 5.2. If the feedstock has a high content of moisture, more energy is consumed to evaporate the moisture before the gasification, which results in less yield of combustible components. At last, if high ER is employed, more biomass feedstock will be converted to completed products, such as CO_2 and H_2O. Consequently, high CR is required to ignite such syngas and least output work is produced. The last two types of syngas are usually considered as non-combustible syngas for conventional ICE [104]. However, by varying the CR using the virtual crankshaft mechanism, the FPE can still ignite the last two types of syngas and produce output work, though its amount is still relatively low.

A similar trend can be achieved in F-T fuels, which is indicated by a combination of n-heptane and iso-octane with different volume percentages respectively (Figure 5.3).

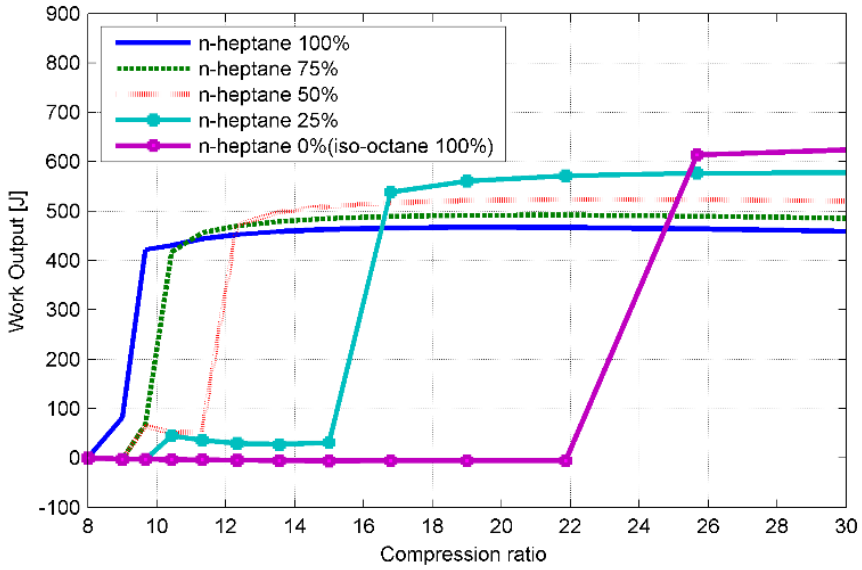

Figure 5.3 Work output vs different CR (F-T fuels with different compositions, AFR = 2, identical $\Omega = 1$)

Besides large variation in compositions, the existences of impurities are also recognized as another roadblock preventing the wide application of renewable fuel. For instance, the production of DME usually generates methanol simultaneously. Complicated after-treatment processes are conducted aimed to remove methanol, which inevitably increases the price of DME. Another example is ethanol, which is completely miscible with water. Usually, multiple distillation processes are needed to dehydrate the produced ethanol in order to make it satisfying the requirement as a vehicle fuel.

Variable CR provides an effective method to increase the tolerance of undesired components in renewable fuels, as shown in Figure 5.4 (DME case) and Figure 5.5 (ethanol case) respectively.

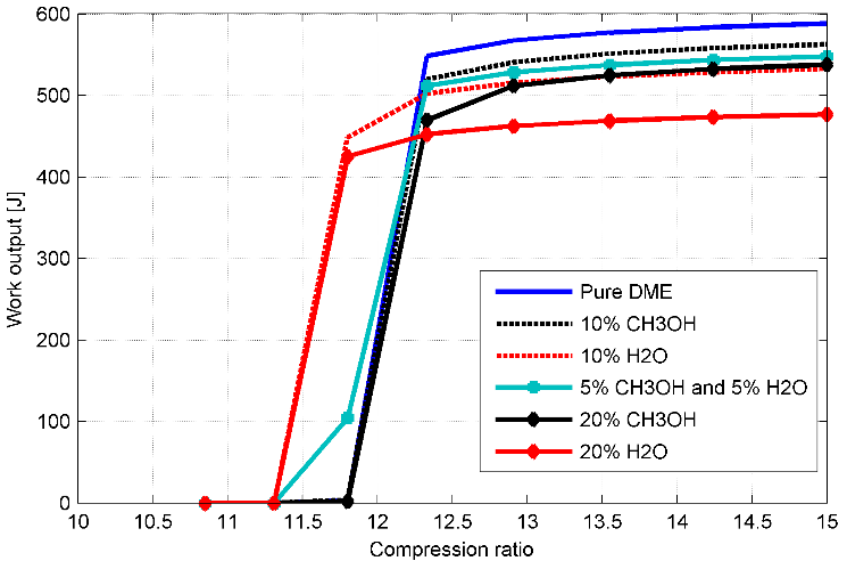

Figure 5.4 Work output vs different CR (DME with different impurities, AFR = 2, identical Ω = 1)

As can be seen in Figure 5.4, no matter how many methanol and water are contained in DME (within 20% impurities), the FPE can always trigger the combustion by providing a suitable CR. Compared to the current purity requirement of DME using in the ICE (usually 95~98% in vol.) [119], such large tolerance of fuel impurity enhances the application of DME and reduces the corresponding cost. However, less work output is indeed a problem, when a larger amount of water and/or methanol exists in DME.

It may be surprised at the first glimpse that smaller CR is required to ignite DME with water. However, this phenomenon can be explained since more reactive radicals, such as H, O, and OH, are generated from H_2O during the ignition process. A similar trend can be observed in ethanol case as well (Figure 5.5). These results offer unintuitive insights for renewable fuel production. It seems that there is no need to completely dehydrate the final products since an appropriate amount of water inside fuel can somewhat improve the ignition and reduce the requirement for after treatment.

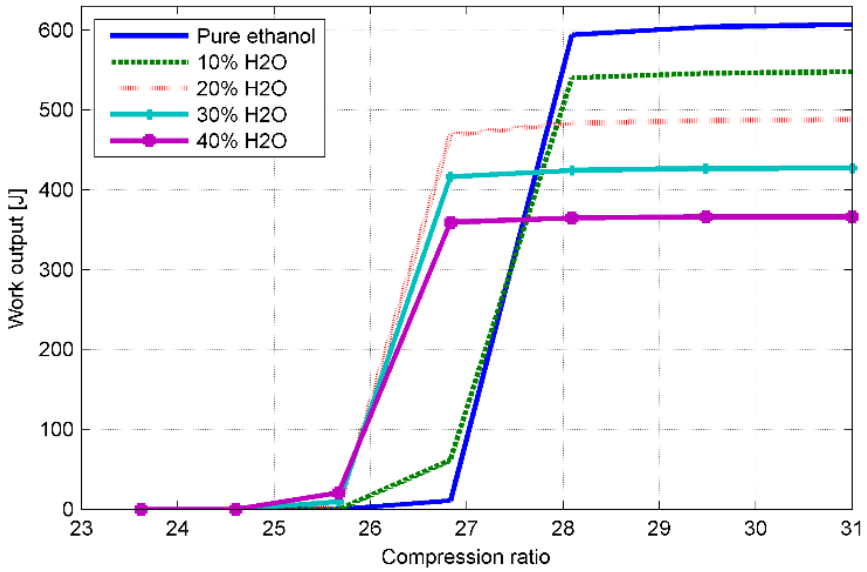

Figure 5.5 Work output vs different CR (ethanol with different water contents, AFR = 2, identical $\Omega = 1$)

In a sum, the capability of varying CR possessed by FPE not only offers FPE ultimate fuel flexibility but also reduces the refinement requirements for those renewable fuels. Consequently, a co-optimization can be achieved. On one hand, the production of renewable fuels can be optimized by taking their chemical and physical properties, environmental impact, and related economy influence into a full consideration. On the other hand, an optimal CR can always be designed and implemented into the FPE to fully leverage the utilization of the employed renewable fuel.

5.2.2 Effects of Ω

The minimal required CRs in Table 5.3 are derived only according to chemical kinetics. However, it is possible that those CR are still too high that the FPE cannot sustain a long-term operation due to the mechanical strength of engine material. Besides,

high CR condition also adversely impacts engine's NVH behavior. As a result, the FPE is expected to operate at the lowest permissible CR.

The FPE provides another degree of freedom on piston trajectory to further reduce the CR listed in Table 5.3. With the virtual crankshaft, the piston motion pattern between the TDC and BDC points, indicated by Ω, can also be varied to realize this function. An example of biogas is shown in Figure 5.6.

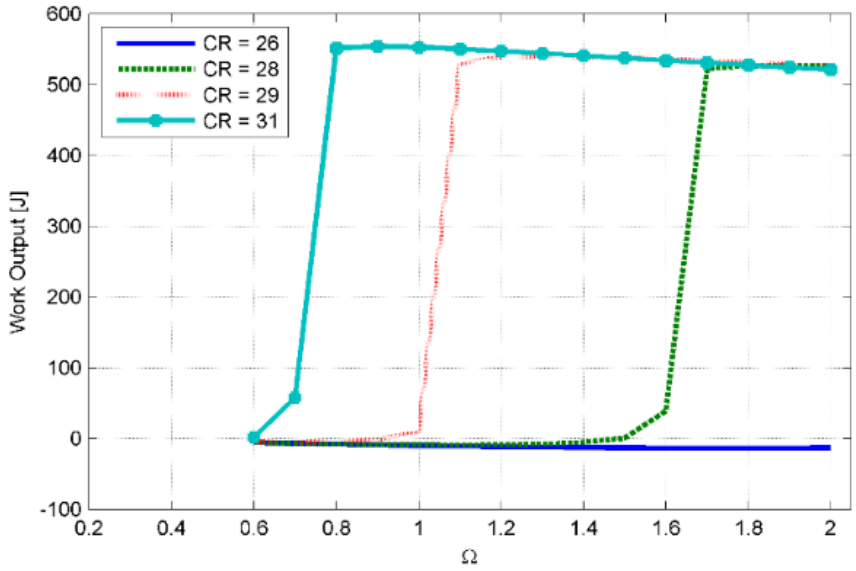

Figure 5.6 Work output vs different Ω (biogas, AFR = 2)

It is clear from Figure 5.6 that by increasing Ω, the ignition of biogas can be achieved at CR = 28, rather than CR = 31 as listed in Table 5.3. The result is even more impressive compared to conventional HCCI engines for upgraded biogas, of which CR is usually in the range of 30 ~ 40 [120]. This reduction can be explained via the characteristic of various piston trajectories with different Ω. Obviously, larger Ω represents a longer period of piston locating around the TDC point. As a result, even though the CR is smaller, the longer period for piston staying around the TDC point still guarantees the

accumulation of sufficient radical species to trigger the chain reaction mechanism and thus ignite the air-fuel mixture. A similar trend is obtained in biodiesel case. As shown in Figure 5.7, the required minimal CR is reduced from 25 to 22.

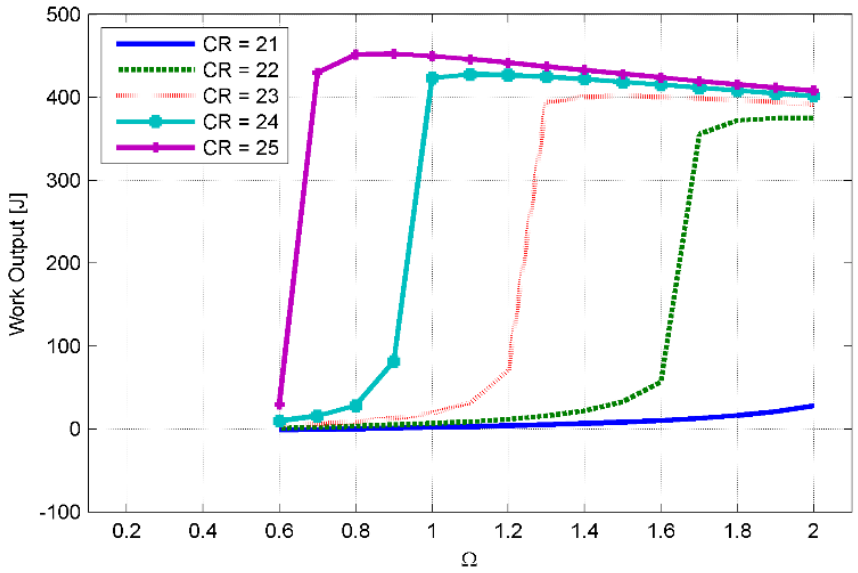

Figure 5.7 Work output vs different Ω (biodiesel, AFR = 2)

On the other hand, the ability to vary Ω in the FPE can also benefit the combustion itself at a fixed CR.

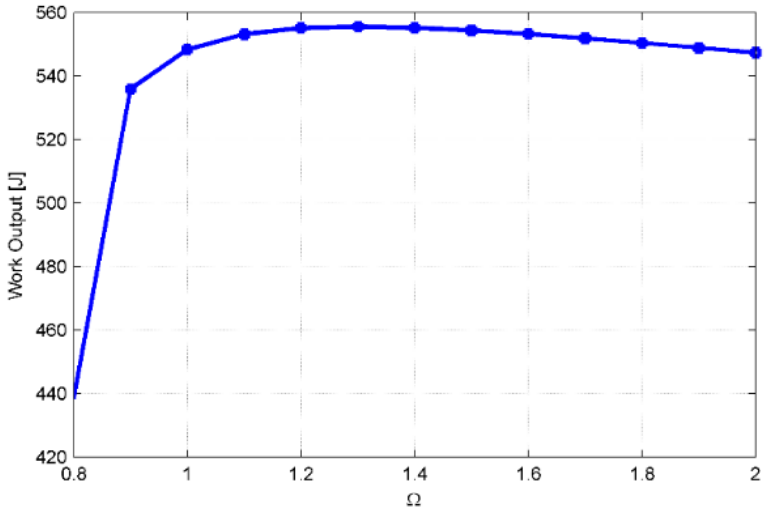

Figure 5.8 Work output vs different Ω (DME, AFR = 2, CR = 12)

Figure 5.8 shows the combustion of DME along different piston trajectories with distinct Ω but identical CR = 12. Obviously, the optimal Ω under this CR is 1.3, which produces 555.57J output work at about 49.3% thermal efficiency. In addition, similar simulation is also conducted using piston trajectory of conventional ICE at same CR. The corresponding thermal efficiency is 44.5%, which agrees with the results reported in [121]. In this case, the variable Ω in the FPE enables about 5% improvement in thermal efficiency. It is worth noting that at higher CR, the improvement of thermal efficiency achieved by this freedom will be further enhanced, as shown in [79].

5.2.3 Asymmetric Piston Trajectory

The most appealing advantage of the trajectory-based combustion control is that the implemented trajectory can even be asymmetric. In this way, two control objectives can be assigned to piston trajectory separately. For instance, the compression trajectory can be designed to optimize the combustion phasing. The expansion trajectory can be determined to reduce NOx emission. An example of H_2 is illustrated in Figure 5.9 and Figure 5.10. In this example, each asymmetric piston trajectories are described by two Ωs: Ω_{comp} represents the Ω of compression trajectories and Ω_{exp} shows the value along expansion process.

Figure 5.9 shows the corresponding output work along different asymmetric piston trajectories. As can be seen, if Ω_{comp} is too small, a specific Ω_{exp} is required to ignite the H_2. For example, if Ω_{comp} is as small as 0.6, the minimally required Ω_{exp} is 1.2, reflected by the blue line in Figure 5.9 (a). On the other hand, if Ω_{comp} is large enough (≥ 1.4), any Ω_{exp} in the range of 0.6 to 2.0 can be implemented to trigger the combustion. The above

results can be explained by the relationship between the Ω and the duration while piston locating around the TDC. Any trajectory with Ω_{comp} larger than 1.4 already provides enough time for ignition while the piston locating around the TDC point along the compression process. Consequently, a quick expansion can be implemented Afterward to reduce the heat loss by selecting the smallest Ω_{exp} available. To the contrary, if Ω_{comp} is too small to provide enough time for ignition, the subsequent Ω_{exp} has to be increased to trigger the combustion.

In addition, as long as the combustion is triggered successfully, the amounts of output works are very close to each other, as shown in Figure 5.9 (a). Specifically, the variation is within 25J in the entire Ω domain. Figure 5.9 (b) is a zoomed-in view, which illustrates the output works more clearly. Obviously, the maximal output work is achieved when Ω_{comp} = 1.8 and Ω_{exp} = 0.6, of which output work is 522.81 J, with 55.9% thermal efficiency. To compare, the simulation is also repeated using the ICE's trajectory. The latter result turns out that the combustion cannot occur in this situation. In addition, a study, investigating the HCCI combustion in an FPE with uncontrollable pistons, claimed that 48% thermal efficiency is achieved when the engine was powered by H_2 and operated at similar CR [120]. As a result, by using the designed asymmetric piston trajectory, almost 8% improvement in thermal efficiency can be achieved. However, the derived asymmetric trajectory (Ω_{comp} = 1.8, Ω_{exp} = 0.6) may still not be the optimal one, if NOx emission is taken into account.

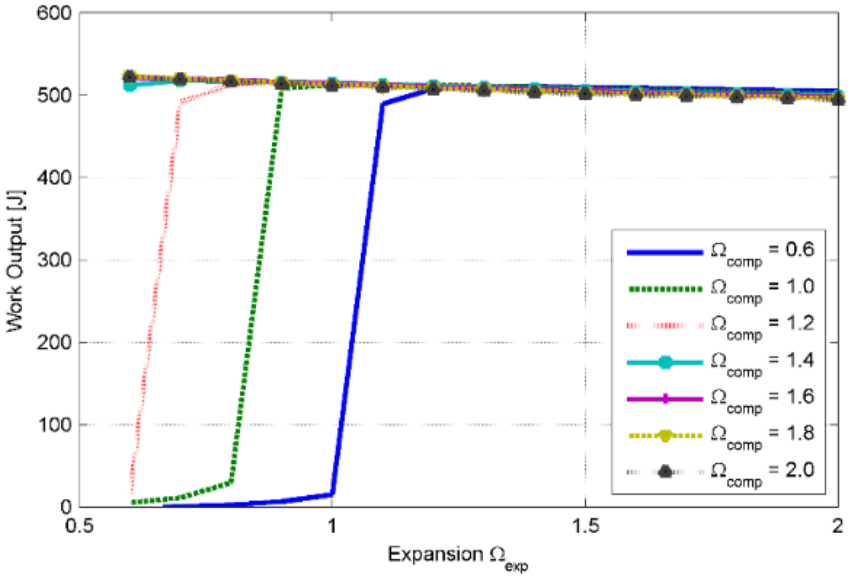

(a)

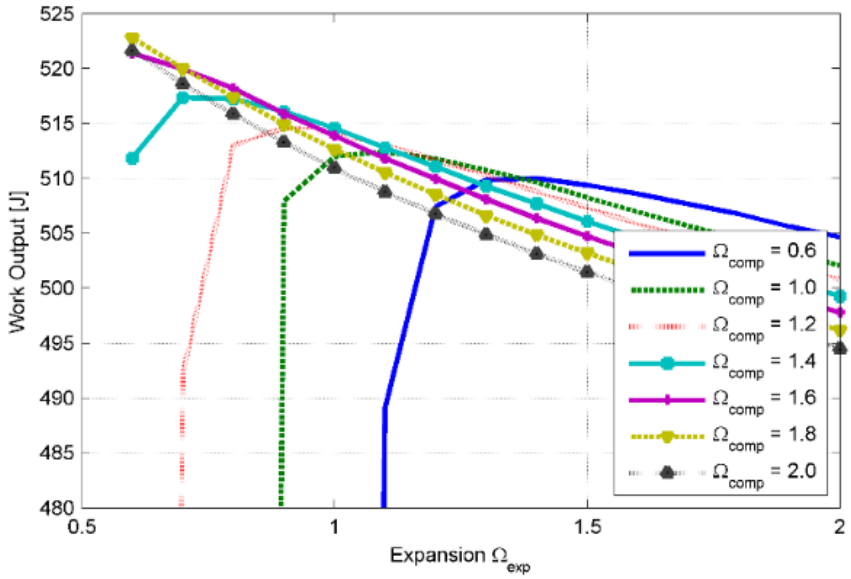

(b)

Figure 5.9 Work output along asymmetric piston trajectories, indicated by two Ωs (H2, AFR = 2, CR = 22, (b) is the zoom-in view of (a))

NOx emission is such a critical aspect due to the increasingly public concerns on the environment. Figure 5.10 represents the corresponding NOx emission following the same

setup in Figure 5.9. As can be seen, the NOx emissions of all the simulation cases are within the range of 30 to 140 ppm, which are significantly less than the typical range of NOx emission, 100 to 500 ppm, in the conventional engine (almost 70% reduction) [120], [122]. Usually, the smallest NOx emission is achieved by the smallest available Ω_{exp}. Those trajectories provide the quickest expansion, and therefore reduce in-cylinder temperature immediately and freeze the NOx production reactions [95].

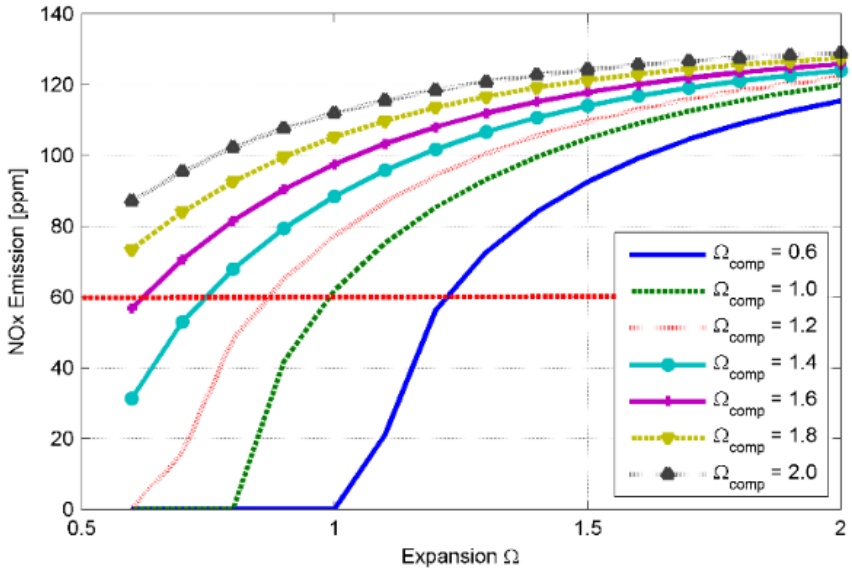

Figure 5.10 NOx emission along asymmetric piston trajectories, indicated by two Ωs (H2, AFR = 2, CR = 22)

As a result, the final optimal Ω pair has to be determined by considering both effects of output work and NOx emission. For instance, the aforementioned Ω pair (Ω_{comp} = 1.8, Ω_{exp} = 0.6), even though it produces the maximal output work, cannot be selected if the NOx emission is required to be less than 60 ppm. Thus, the optimal Ω pair should be Ω_{comp} = 1.6 and Ω_{exp} = 0.6, which produces 56.82 ppm NOx emission and slightly less output work, which is 521.39 J at 55.7% thermal efficiency. The corresponding optimal

asymmetric piston trajectory, in-cylinder temperature profile, P-V diagram, and NOx production are shown in Figure 5.11.

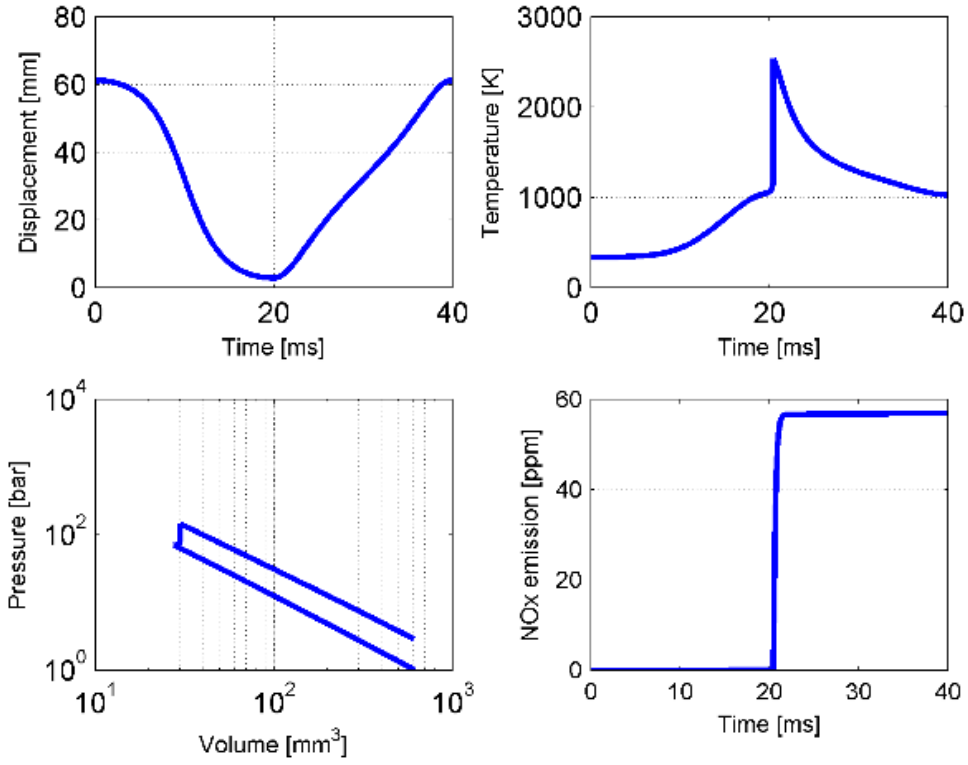

Figure 5.11 Combustion performance along piston trajectory Ωcomp = 1.6, Ωexp = 0.6, (H2, AFR = 2, CR = 22)

Certainly, the derived optimal Ω pair should be adjusted according to CR. For example, if the CR is increased from 22 to 24 for the same setup in Figure 5.9 and Figure 5.10, the corresponding optimal Ω pair is then varied to $\Omega_{comp} = 0.6$, $\Omega_{exp} = 0.6$, as can be seen in Figure 5.12. Intuitively, specific optimal asymmetric piston trajectories can also be generated for other renewable fuels.

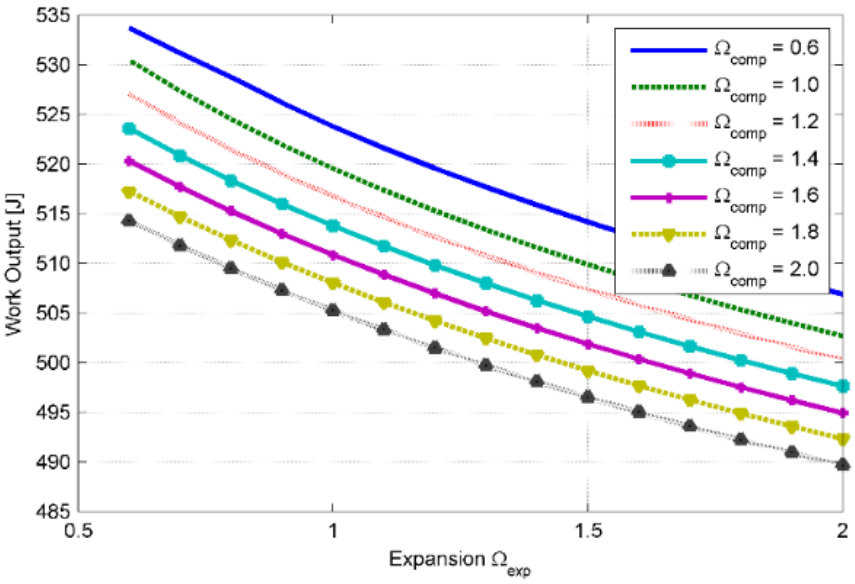

(a)

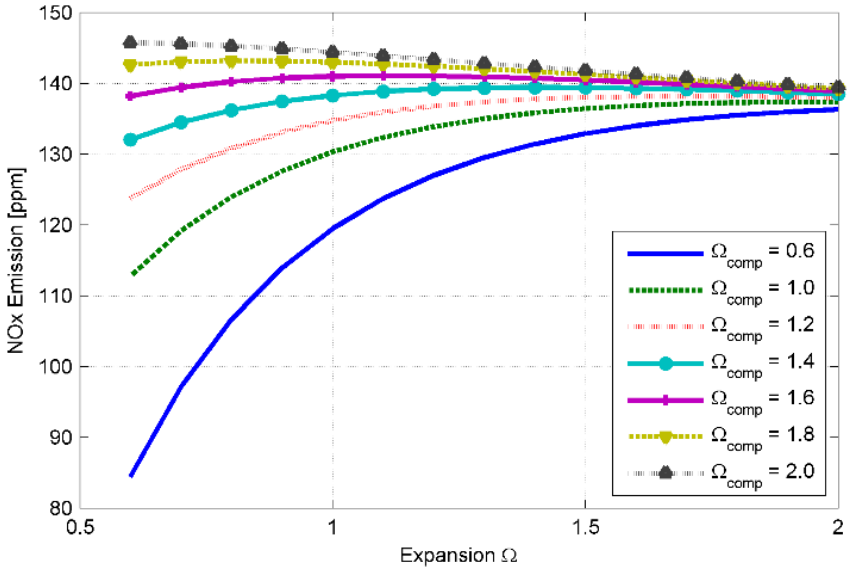

(b)

Figure 5.12 Combustion performance along asymmetric piston trajectories, indicated by two Ωs (H2, AFR = 2, CR = 24, (a) output work (b) NOx emission)

In summary, the controllable piston trajectory in the FPE is able to extract the chemical energy from the renewable fuels in an effective and clean manner. Such

asymmetric piston trajectories are very difficult to realize in conventional ICEs. However, it is easy to achieve in the FPE with the assistance of the virtual crankshaft mechanism, by designing an appropriate trajectory reference accordingly. The above results show that by applying the optimal asymmetric piston trajectories, the thermal efficiency of the FPE is enhanced significantly, while the NOx emission can be reduced simultaneously. Furthermore, the virtual crankshaft also enables real-time control of the piston motion. In this way, the optimal asymmetric piston trajectory can even be modified according to the load variation in real time.

5.3 Conclusion

In this chapter, the trajectory-based combustion control, enabled by the FPE with the virtual crankshaft mechanism, is applied to renewable fuels. Seven renewable fuels, e.g. hydrogen, biogas, syngas, ethanol, DME, biodiesel, and F-T fuels are considered herein. The results show that the FPE has the ultimate fuel flexibility. In addition, a suitable CR can also be selected not only to guarantee the ignition but also to widen the tolerance of undesired composition in renewable fuels. Furthermore, an appropriate piston motion pattern between the two dead centers can also be determined to reduce the required CR for each renewable fuel and to further enhance engine efficiency (5% improvement in DME case). At last, optimal asymmetric piston trajectory can be designed for specific renewable fuels, which enables a significant reduction in the NOx emission (70% reduction in H_2 case) and an improvement in the thermal efficiency (8% improvement in H_2 case) simultaneously.

In summary, the trajectory-based combustion control realizes the co-optimization of fuels and engine operation. Within this context, the production of utilized fuels, no matter renewable or traditional, can be optimized from the perspectives of their own physical and chemical properties, environmental impacts and economic costs. Subsequently, the engine operation can also be optimized by implementing an optimal piston trajectory into the FPE, which is synthesized according to specific characteristics of the utilized fuel, variable loading requirements, and stringent emission regulation.

Chapter 6

Development of the Control-oriented Model for the Trajectory-based Combustion Control

With the trajectory-based combustion control, the extra degree of freedom of the piston trajectory not only realizes the real-time control of the HCCI combustion but also enables the optimization of the related chemical reactivity and heat transfer processes [123]. Nonetheless, the aforementioned chemical kinetics driven model is not suitable for the control purpose. The included detailed reaction mechanisms usually consist of hundreds of species and thousands of reactions and the related models, therefore, possess heavy computational burdens, even under the assumption of the homogeneous environment. Meanwhile, a large amount of species in the detailed mechanisms also increases the order of the dynamic model and causes a significant challenge for the subsequent optimization.

On the other hand, existing HCCI control-oriented models usually assume engine's compression and expansion strokes are polytropic, and employ empirical correlations, e.g. temperature thresholds or integral of Arrhenius equations, to predict the start of combustion (SOC) [87], [124]-[128]. In addition, the heat release of HCCI combustion is either assumed as an instantaneous process [87] or simulated via Wiebe function [124]-[128]. Even though the computational cost is decreased significantly, these assumptions over-simplify the utilized chemical kinetics. Considering the fact that the HCCI

combustion is mainly driven by the chemical kinetics, the existing control-oriented models lack the necessary information to predict the dynamics of the combustion process and the emissions production.

Therefore, in order to implement the piston trajectory-based HCCI combustion control in the FPE in real-time and achieve the optimization of piston trajectory according to variable working conditions, a new control-oriented model with short computation time and sufficient chemical kinetic information is needed. Such a model is proposed in this chapter.

6.1 Modeling Approach

The proposed control-oriented model consists of three components. First, a new mechanism producing variable piston trajectories is introduced. Unlike slider-crank mechanism [29], the new mechanism adds an additional degree of freedom to the piston motion and represents the unique characteristic of the FPE. Secondly, a physics-based model is developed to describe the in-cylinder gas dynamics adequately. In addition, a specific reaction mechanism is also employed in the model to represent the chemical kinetics of the fuels. It is worth mentioning that a specific phase separation method is utilized while developing the reaction mechanism, aimed to reduce the computational cost and sustain sufficient chemical information simultaneously.

6.1.1 Variable Piston Trajectories

Unlike the conventional ICE, the FPE has no constraints on its piston motion due to the absence of the mechanical crankshaft mechanism. As a result, variable piston

trajectories with different CRs and motion patterns between the BDC and TDC points can be easily achieved in an FPE. Hence the conventional slider-crank mechanism is inappropriate to describe these piston trajectories and a new mechanism is needed to represent the piston motion.

As mentioned before, the FPE piston trajectory can be represented as the x-axis displacement of a point moving around an ellipse in the Cartesian coordinate, as shown in Figure 6.1.

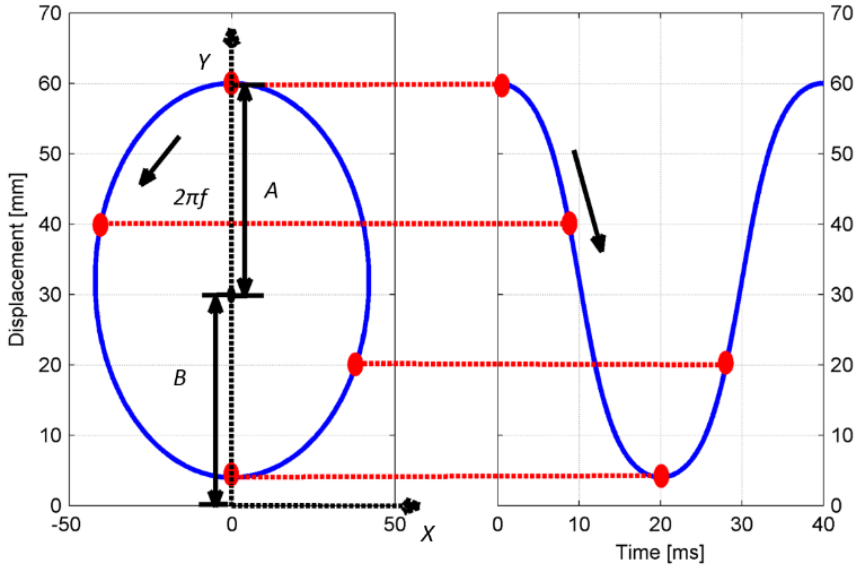

Figure 6.1 Description of FPE piston motions

The corresponding piston trajectories *S* can be yielded as:

$$S = \frac{A \cdot \Omega \cdot \cos(2\pi f \cdot t)}{\sqrt{\Omega^2 \cdot \cos(2\pi f \cdot t)^2 + \sin(2\pi f \cdot t)^2}} + B \tag{6.1}$$

where *A* is the major axis of the ellipse, *B* is the location of the ellipse center as the bias, *f* represents the frequency of the engine operation, Ω (= minor axis / major axis) implies the shape of the ellipse and *t* stands for the time.

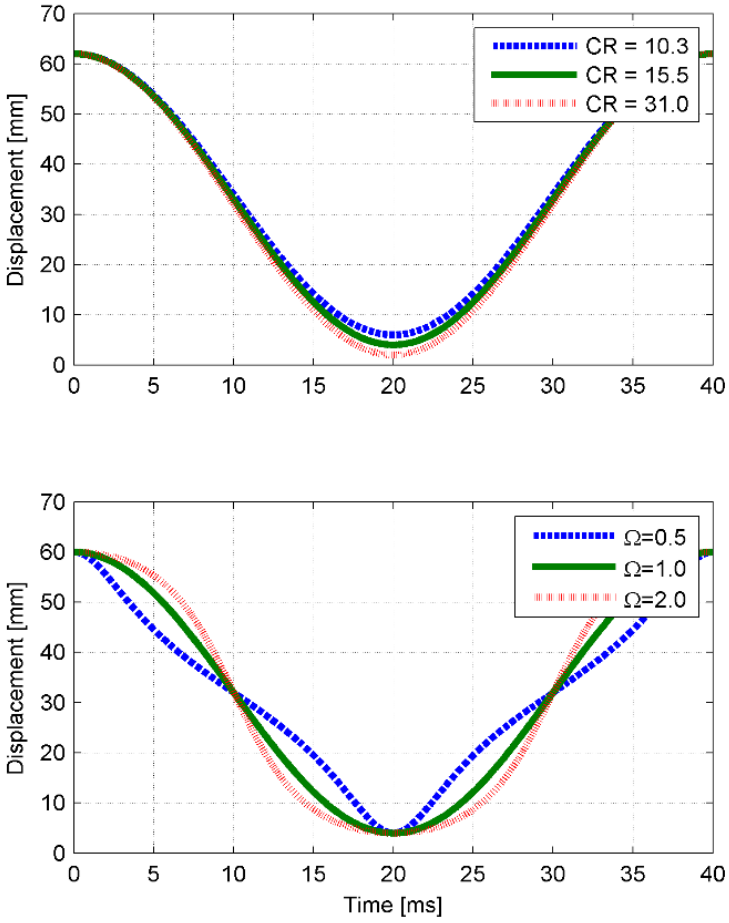

Figure 6.2 Piston trajectories with different CR (top) and Ω (bottom)

Figure 6.2 shows the corresponding results of piston trajectories with various CRs and different piston motion patterns between the TDC and BDC points. It has been shown that the FPE enables significant improvement in the thermal efficiency and reduction of NOx emissions simultaneously by implementing appropriate piston trajectories accordingly [79], [80] and [129].

6.1.2 Physics-based Model

The physics-based model is developed based on the first law of thermodynamics applied to a closed system, while the scavenging process is neglected. The states include

pressure P, temperature T and each species concentration $[X_i]$ inside the reaction mechanism. In this subsection, the rate equations of pressure P and temperature T are introduced, and the rates of each species concentrations $[X_i]$ will be discussed in the next subsection.

6.1.2.1 Pressure rate equation

From the ideal gas law, the pressure of the in-cylinder gas, P, and its time derivative can be represented as below: (R is the universal gas constant)

$$P = \sum_i [X_i] \cdot R \cdot T \tag{6.2}$$

$$\dot{P} = P \cdot \sum_i [\dot{X}_i] / \sum_i [X_i] + P \cdot \dot{T} / T \tag{6.3}$$

6.1.2.2 Temperature rate equation

In order to derive the rate equation for the in-cylinder gas temperature T, the first law of the thermodynamics for a closed system and the ideal gas law has to be combined as follow.

The first law of the thermodynamics for a closed system is:

$$\frac{d(mu)}{dt} = -\dot{Q} - \dot{W} \tag{6.4}$$

where m is the total mass in the cylinder, u is the specific internal energy of the in-cylinder gas, $\dot{Q}$ is the heat transfer rate and $\dot{W}$ is the expansion work rate.

Furthermore, the heat transfer process is assumed as a convection process:

$$\dot{Q} = h_{hl} \cdot A_{wall} \cdot (T - T_{wall}) \tag{6.5}$$

where T_{wall} is the wall temperature, A_{wall} is the heat transfer surface area and h_{hl} is the heat transfer coefficient, which is determined by a modified Woschini correlation [29]:

$$A_{wall} = 2 \cdot \frac{\pi}{4} \cdot b^2 + \alpha \cdot \pi \cdot b \cdot S \tag{6.6}$$

$$h_{hl} = 3.26 \cdot b^{-0.2} \cdot P^{0.8} \cdot T^{-0.55} \cdot w^{0.8} \tag{6.7}$$

In (6.6) and (6.7), b represents the bore of the engine, S is the piston trajectory, α is an FPE architecture parameter (= 2, when the FPE uses the opposed piston architecture) and w is the average in-cylinder gas velocity.

Besides, the rate of expansion work is calculated as:

$$\dot{W} = P \cdot \dot{V} \tag{6.8}$$

where V is the combustion chamber volume, which is determined by the piston trajectory S:

$$V = \frac{\pi}{4} \cdot b^2 \cdot \alpha \cdot S \tag{6.9}$$

Now, given the fact that the specific enthalpy h can be obtained from the specific internal energy u:

$$h = u + P \cdot v \tag{6.10}$$

where v is the specific volume of the in-cylinder gas.

Combining (6.4), (6.8) and (6.10), the following equation can be obtained:

$$\frac{d(m \cdot h)}{dt} = \dot{m} \cdot P \cdot v + \dot{P} \cdot V - \dot{Q} \tag{6.11}$$

Due to the closed system assumption, (6.11) can be further simplified as:

$$\frac{d(m \cdot h)}{dt} = \dot{P} \cdot V - \dot{Q} \tag{6.12}$$

On the other hand, the total enthalpy of the in-cylinder gas can also be derived via the sum of each species enthalpy:

$$m \cdot h = \sum_i N_i \cdot \hat{h}_i \tag{6.13}$$

where N_i is the mole number of species i and $\hat{h}_i$ is mole-based specific enthalpy of species i. Furthermore, the rate of $\hat{h}_i$ can be calculated as:

$$\dot{\hat{h}}_i = c_{p,i}(T) \cdot \dot{T} \tag{6.14}$$

where $c_{p,i}(T)$ is the mole-based constant pressure heat capacity of species i at temperature T.

Therefore, the time differential of the total enthalpy is:

$$\begin{aligned} \frac{d(m \cdot h)}{dt} &= \sum_i (\frac{dN_i}{dt} \cdot \hat{h}_i) + \sum_i (\frac{d\hat{h}_i}{dt} \cdot N_i) \\ &= V \cdot \sum_i ([\dot{X}_i] \cdot \hat{h}_i) + \dot{V} \cdot \sum_i ([X_i] \cdot \hat{h}_i) + V \cdot \dot{T} \cdot \sum_i ([X_i] \cdot c_{p,i}(T)) \end{aligned} \tag{6.15}$$

Combining (6.12) and (6.15) and plugging (6.3) into the combination, the temperature rate, $\dot{T}$ is derived as follow:

$$\dot{T} = \frac{-\sum_i ([\dot{X}_i] \cdot \hat{h}_i) - \dot{V} \cdot \sum_i ([X_i] \cdot \hat{h}_i)/V + P \cdot \sum_i [\dot{X}_i] / \sum_i [X_i] - \dot{Q}/V}{\sum_i ([X_i] \cdot c_{p,i}(T)) - P/T} \tag{6.16}$$

6.1.3 Chemical Kinetics

As can be seen from (6.3) and (6.16), other information, e.g. the values of $c_{p,i}$ and $\hat{h}_i$ as well as the history of species concentrations $[X_i]$, are required to solve these equations.

This information can be obtained from the chemical kinetics part of the model, which is formed by the reaction mechanism.

Frist, several thermodynamic properties of each species, such as $c_{p,i}$ and $\hat{h}_i$, are functions of temperature T in the reaction mechanism via the NASA polynomial parameterization [85]:

$$\frac{c_{p,i}(T)}{R} = a_0 + a_1 T + a_2 T^2 + a_3 T^3 + a_4 T^4 \tag{6.17}$$

$$\frac{\hat{h}_i(T)}{RT} = a_0 + \frac{a_1}{2} T + \frac{a_2}{3} T^2 + \frac{a_3}{4} T^3 + \frac{a_4}{5} T^4 + a_5 / T \tag{6.18}$$

where a_0 to a_5 are six parameters calibrated by NASA. To further reduce the computational cost, all the functions above are re-fitted into three order polynomial of T in the proposed model.

In addition, the history of each species concentration $[X_i]$ is derived via integrating the following differential equation:

$$[\dot{X}_i] = \frac{d}{dt}\left(\frac{N_i}{V}\right) = \frac{\dot{N}_i}{V} - \frac{\dot{V} N_i}{V^2} = w_i - \frac{\dot{V}}{V}[X_i] \tag{6.19}$$

where w_i is the production rate of species i from the reaction.

The heavy computational burden of the model with detailed chemical kinetics is usually caused by the tedious calculation processes, such as (6.17), (6.18) and (6.19). This burden is exacerbated significantly as the number of species and the number of reactions increase. In order to reduce the computational burden and keep sufficient chemical kinetics information, an engine operating cycle is separated into several phases

(Figure 6.3) and in each phase, a specific reaction mechanism with the minimal size is applied to predict the combustion process as precisely as possible:

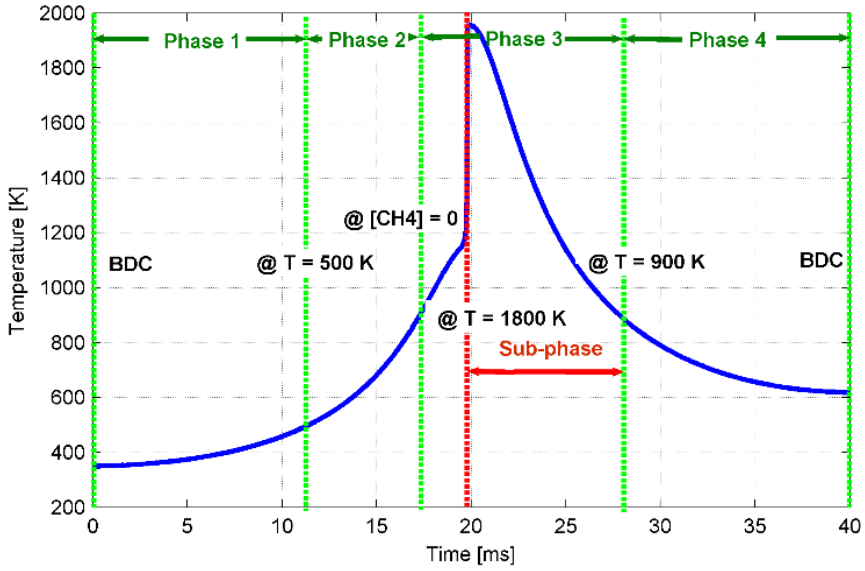

Figure 6.3 Phase separation within an engine cycle

Phase 1: this phase begins when piston locates at the BDC and ends when *T* reaches 500K. During this interval, few chemical reactions occur due to the low temperature and therefore, no reaction mechanisms need to be applied here.

Phase 2: A simplified reaction mechanism will be employed in this phase to represent the ignition process until all the fuel molecules are converted to intermediate species. Specifically, in this model, methane (the major component of natural gas) is assumed as the fuel and the corresponding ignition mechanism is a one-step reaction converting all the methane into CO and H_2, as the intermediate species:

$$R_1 : CH_4 + 0.5O_2 \rightarrow CO + 2H_2$$

where its reaction rate is derived through the Jones-Lindstedt mechanism (JL) [130]:

$$RR_1 = 4.4\times10^9 \cdot [CH_4]^{0.5} \cdot [O_2]^{1.25} \exp(-\frac{15095}{T}) \tag{6.20}$$

The corresponding production rate of each species in this phase are:

$$\begin{cases} w_{CH_4} = -RR_1 \\ w_{O_2} = -0.5RR_1 \\ w_{H_2} = 2RR_1 \\ w_{CO} = RR_1 \\ w_{CO_2} = 0 \\ w_{H_2O} = 0 \end{cases} \tag{6.21}$$

For other fuels, specific reaction mechanisms for their ignition process can be found [131]-[133]. By applying those mechanisms, the proposed control-oriented model can be extended to different fuels.

Phase 3: Afterward, the intermediate species CO and H_2 will react to generate final products CO_2 and H_2O as well as to release the major of thermal energy. The corresponding reaction mechanism utilized in this phase is shown as below:

$$R_2 : CO + H_2O \rightarrow CO_2 + H_2$$
$$R_3 : H_2 + 0.5O_2 \rightarrow H_2O$$

where the reaction rates for both reaction steps are determined respectively [130], [134]:

$$RR_2 = 2.75\times10^7 \cdot [CO] \cdot [H_2O] \exp(-\frac{10065}{T}) \tag{6.22}$$

$$RR_3 = 1.5\times10^9 \cdot [H_2][O_2]^{0.5} \exp(-\frac{17609}{T}) \tag{6.23}$$

Similarly, the production rates of each species in this phase are the sum of all involved reaction rates:

$$\begin{cases} w_{CH_4} = 0 \\ w_{O_2} = -0.5RR_3 \\ w_{H_2} = RR_2 - RR_3 \\ w_{CO} = -RR_2 \\ w_{CO_2} = RR_2 \\ w_{H_2O} = -RR_2 + RR_3 \end{cases} \tag{6.24}$$

Sub-phase: when the temperature is over 1800K, the production of NOx should be taken into account. The thermal NOx generation mechanism [95] is added here since it is the most suitable mechanism for high temperature and rich oxygen environment. By kinetic analysis, an overall expression for the rate of thermal NOx formation is derived and modified from Bowman et al [96]:

$$w_{NO_x} = \frac{2.0\times10^{15}}{T^{0.5}}[N_2][O_2]^{0.5}\exp(\frac{-69090}{T}) \tag{6.25}$$

Phase 4: after the in-cylinder temperature T decreases to 900K, almost all the reaction products remain constants. Therefore, there is no need to consider the chemical kinetics any further and the rest of the cycle will be simulated as ideal expansion process with the heat transfer until the piston reaches the BDC again. It is also possible that not all the fuel molecules are consumed due to the relatively low temperature or extremely fuel-lean condition. In this case, phase 3 cannot be triggered and the process enters phase 4 directly.

To summarize, the phase separation method transforms the entire chemical kinetics of the HCCI combustion into a sequence based on the thermal state, e.g. temperature, and the species concentration. Such a sequence guarantees the specific chemical kinetics in one phase has little effects on the simulation of the other phases. As a result, by applying the specific reaction mechanism in each phase, the proposed model not only increases the

computational speed (30% in this study) by avoiding unnecessary parallel computations with the entire chemical kinetics but also reduces the order of the control-oriented model, which facilitates the subsequent optimization process.

6.2 Simulation Result and Discussion

The simulation results of the proposed model are shown in this section and compared with the outcomes of two existing models, namely a simplified model [87] and a detailed model [79]. The simplified model is developed based on the assumption that the entire chemical kinetics can be represented by a global reaction step reproducing the combustion of methane. Consequently, this model utilizes the integral of the Arrhenius reaction rate equation to predict the SOC timing. In addition, the subsequent heat release is assumed to be instantaneous after the combustion occurrence. To the contrary, the detailed model represents the chemical kinetics of methane through a detailed reaction mechanism, GRI-Mech 3.0 [135], and takes every elementary reaction into account. The development of the simplified model and the detailed model can be found in [87] and [79] respectively. To have a fair comparison, initial conditions, in terms of air-fuel-ratio, thermal states of the intake air and piston trajectory profile, are fixed for the simulations of the three models.

6.2.1 Computational Cost

First of all, the computational costs of the three models are compared. The corresponding simulations are conducted using a laptop with 2.60GHz Intel(R) Core ™ i5-3230M processor and 4.00 GB installed memory. As shown in Table 6.1, the detailed

model needs 2070ms to simulate an engine cycle, which lasts only 40ms. The proposed model spends 98ms, which reduces the computational time by 95.27%. This improvement should be more significant if long-chain hydrocarbon fuels or renewable fuels are applied in the proposed model. However, the simplified model only takes 7ms to reproduce the combustion process within an engine cycle, which is still far beyond the other two.

Table 6.1 Comparison of the computational times of three models

Utilized model	**Computation time [ms]**
Detailed model	2070
Proposed model	98
Simplified model	6

6.2.2 Accuracy of the Prediction

Another comparison of these three models benchmarks the accuracy of the model predictions of HCCI combustion in terms of in-cylinder gas temperature profiles and NOx productions.

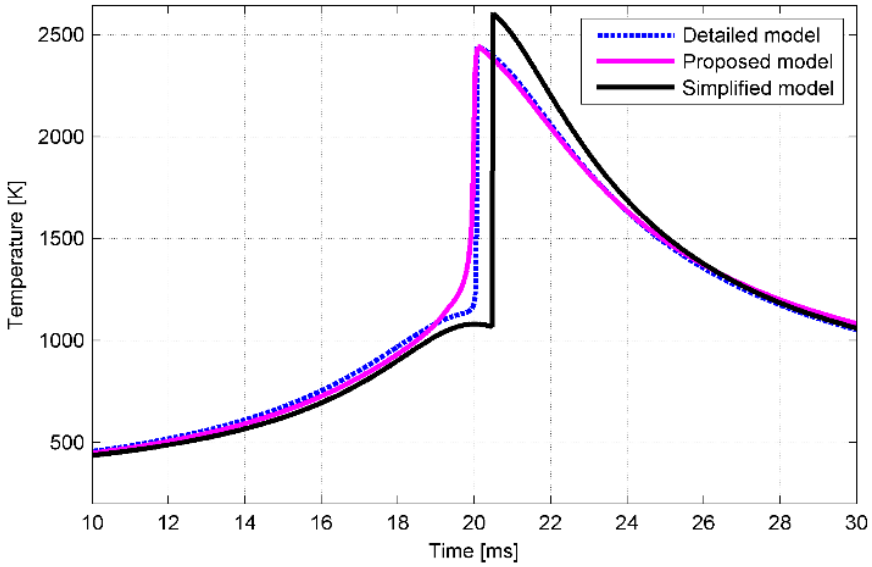

Figure 6.4 Comparison of temperature profiles from three models (AFR = 2, CR = 31 and Ω =1)

As shown in Figure 6.4, the simulation result from the proposed model has a good agreement with the detailed model, which demonstrates its effectiveness. Both two models predict similar peak temperature (2444K for the detailed model and 2442K for proposed model) and SOC timing (20.06ms for the detailed model and 19.97ms for proposed model). On the other hand, the simplified model fails to represent the combustion precisely with over-estimated peak temperature (2601K) and SOC timing (20.48ms) due to the over-simplified chemical kinetics: the global reaction step neglects the heat release of the reactions occurring in the low temperature, which causes the late prediction of the SOC timing. Additionally, due to the assumptions that the entire chemical energy is released instantaneously, the temperature rise in the simplified model is much greater than reality since the heat loss during the combustion process and the possibility of the incomplete combustion are ignored.

Besides, the simplified model cannot provide any information on NOx emission. As shown in Figure 6.5, even though the NOx generation is only considered after the in-cylinder temperature reached 1800K in the proposed model, its final production of NOx still resembles the outcome of the detailed model. Such phenomenon attribute to the unique characteristic of the thermal NOx mechanism, which can be decoupled from the general combustion processes [96]. However, the critical information about the NOx emission is totally lost in the simplified model since the global reaction step only involves the fuel consumption.

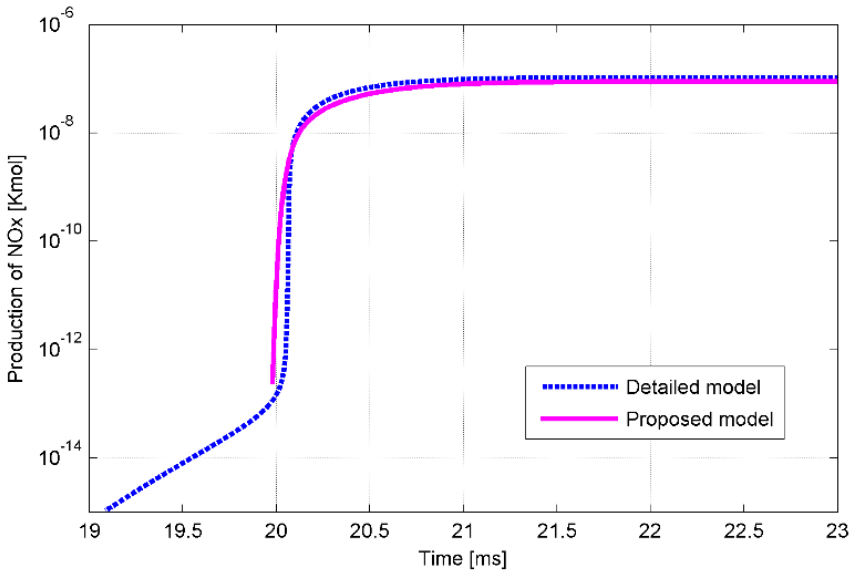

Figure 6.5 Comparison of NOx production from the two models (AFR = 2, CR = 31 and Ω =1)

Hence, despite the least computational cost, the simplified model is not suitable for the control objective due to its discrepancy in the prediction of the combustion process and lack of information on emission production. On the other hand, the proposed control-oriented model offers a good balance between the computational cost and the accuracy of

prediction, therefore makes itself a suitable candidate for the controller design and subsequent optimization for the piston trajectory-based HCCI combustion control.

6.2.3 Comparison at Different Working Conditions

As the power source for automobiles or other mobile applications, the FPE should function adequately under the entire operation domain. Additionally, by applying the piston trajectory-based HCCI combustion control, the FPE is expected to operate at various CRs as well as different piston motion patterns between the TDC and BDC points, as shown in Figure 6.2. Therefore, the proposed control-oriented model is required to sustain the good agreement with the detailed model at various working conditions. Otherwise, tedious parameters calibration process, especially on the chemical kinetics part, should be conducted, which undermines the advantage of the proposed control-oriented model. In this subsection, both simulation results of the proposed model and the detailed model are compared herein, which effectively shows the fidelity of the proposed model at various working conditions. Inspired by Figure 6.2, the simulation results are mainly categorized into two groups: 1. Various CR and 2. Different piston motion patterns, indicated by Ω.

6.2.3.1 Various CR.

The simulation results of the two models are compared at a range of CR, from 28 to 39. Lower CR raises challenges for the ignition of methane under a fuel-lean HCCI conditions and higher CR is avoided by the limitation of the physical strength of the material. Various equivalence air-fuel ratios (AFRs) are also shown herein to reflect different load conditions. Three parameters are selected to demonstrate the accuracy of

the prediction between these two models, e.g. the peak temperature T_{peak}, the SOC timing, and the final NOx production. Figure 6.6 to Figure 6.8 show the relative error of these three terms respectively.

As shown in Figure 6.6, the relative error of the T_{peak} is in the range of -15% to 3%. However, if the range of applied CR is narrowed from 30 to 39, the range of relative errors can be decreased from -5% to 3%. Obviously, the performance of the proposed control-oriented model is slightly undermined at the lower CR and higher AFR. These two conditions physically enhance the difficulty for the fuel ignition. After the CR drops to 28 and the AFR raises over 3, the ignition of the air-fuel mixture falls into a boundary condition, while the occurrence of the combustion is quite sensitive to the temperature and the species concentrations. Thus, it is inappropriate to continuously use the proposed control-oriented model to simulate the combustion process in those working conditions.

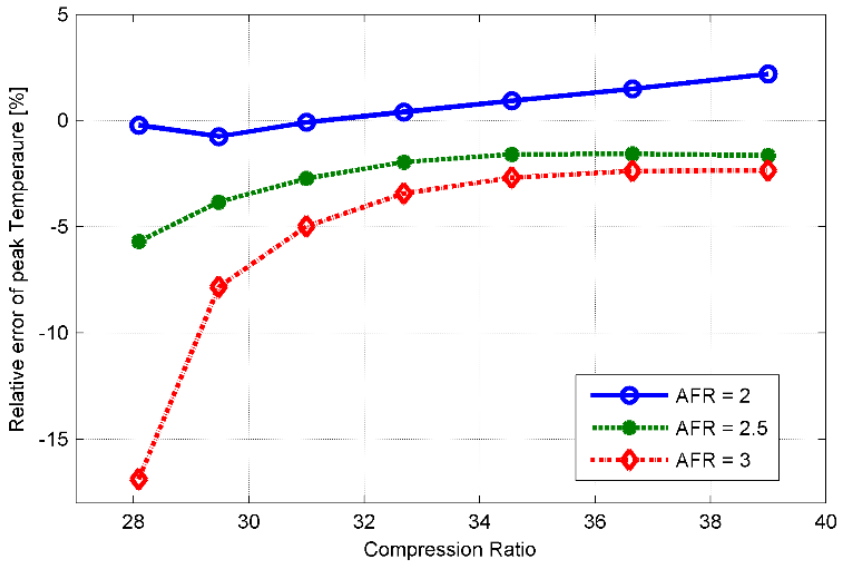

Figure 6.6 Relative error of peak Temperature from the two models at various CRs and different AFRs

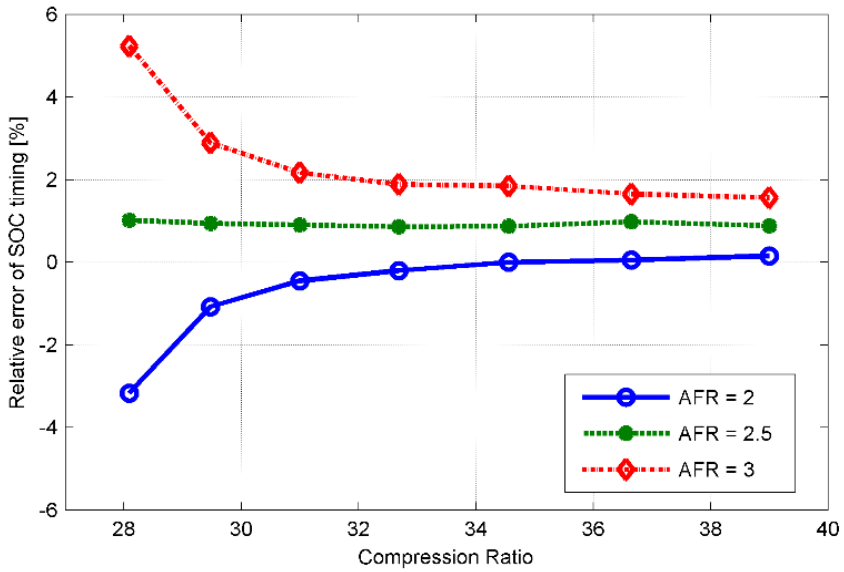

Figure 6.7 Relative error of SOC timing from the two models at various CRs and different AFRs

Figure 6.7 shows the relative error of the SOC timing between the proposed model and the detailed model. The range of the relative error of SOC timing is from -4% to 5%. Similar to the prediction of the T_{peak}, the performance of the proposed model is even better at high CR and lower AFR (relative error range from -1% to 2%). Besides, the overall relative error of SOC timing is smaller than the counterpart of the T_{peak}, which reveals the fact that the proposed model can precisely capture the combustion phasing at different working conditions. This sort of information is critical since the combustion phasing of the HCCI combustion plays a key role in the control of the HCCI engine.

The comparison of the NOx emission between these two models is illustrated in Figure 6.8. Obviously, the same trend of the NOx emissions is produced via the two models and the orders of magnitude of the results are similar as well. Since the NOx production is quite sensitive to the in-cylinder temperature, the agreement of the two results is diminished at higher CR, which induces aggressive temperature rise in the

cylinder. Besides, various AFRs influence the chemical kinetics of the NOx production due to the available chemical heat release. Parameters adaption for (25) based on the AFR can be conducted to improve the performance of the proposed model on the prediction of the NOx emissions at different AFRs.

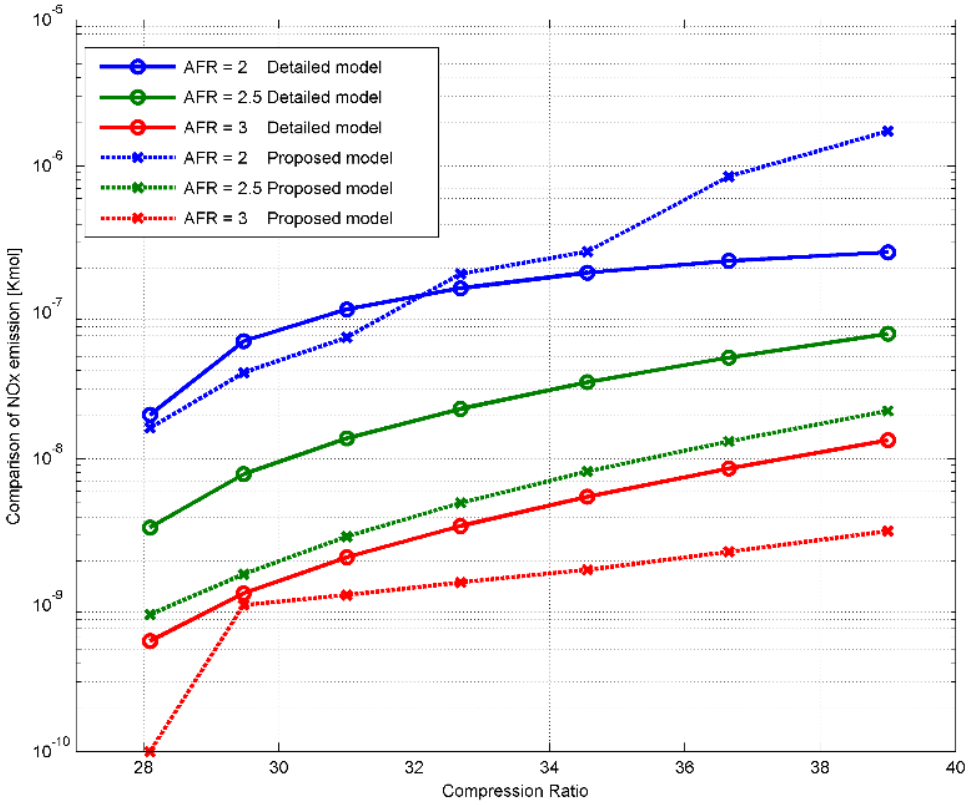

Figure 6.8 Comparison of NOx production from the two models at various CRs and different AFRs

6.2.3.2 Different Ω

Figure 6.9, Figure 6.10 and Figure 6.11 show the comparison of the two models on the aforementioned three terms at various Ω. The range of the selected Ω is from 0.75 to 2.0. It is obvious from Figure 6.9, the performance of the proposed model drops when the AFR is higher and the Ω is smaller. Similar to the CR case, these two conditions make it

more difficult to ignite the methane. Especially, the piston trajectory with smaller Ω shortens the residential time of the piston around the TDC point (Figure 6.2), which decreases the high-temperature duration of the engine cycle and inhibit the corresponding ignition process. To the contrary, piston trajectory with larger Ω promotes the ignition process and facilitates the methane combustion. As a result, the proposed model performs well under these conditions.

The comparison of the SOC timing in various Ω is shown in Figure 6.10. As can be seen, the range of the relative error is within -2% to 2.5%. In this case, the proposed model captures the combustion phasing precisely. Similar conclusion for the NOx emission of the proposed model at various Ω can be reached, as shown in Figure 6.11.

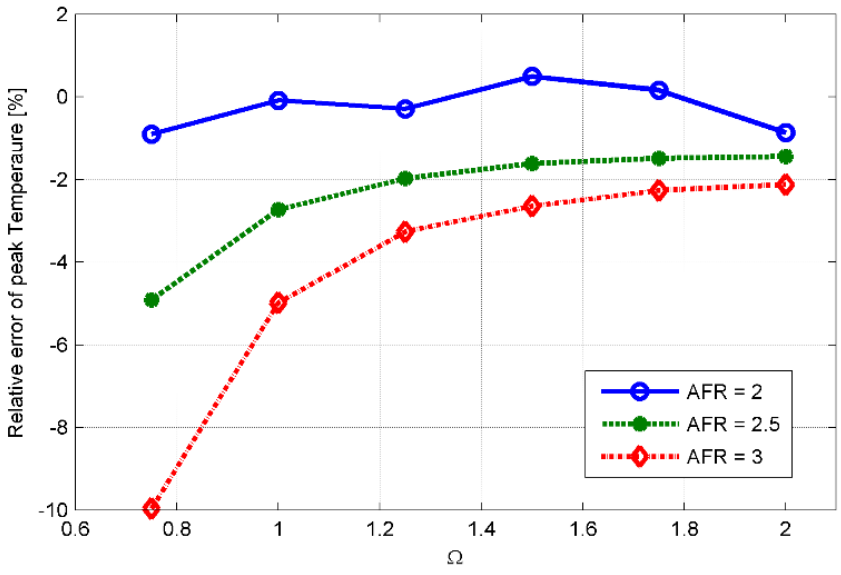

Figure 6.9 Relative error of peak Temperature from the two models at various Ωs and different AFRs

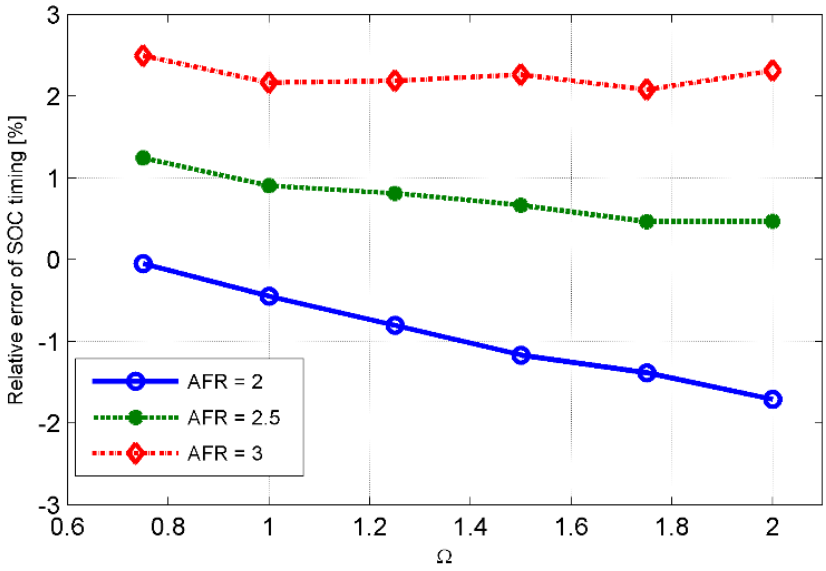

Figure 6.10 Relative error of SOC timing from the two models at various Ωs and different AFRs

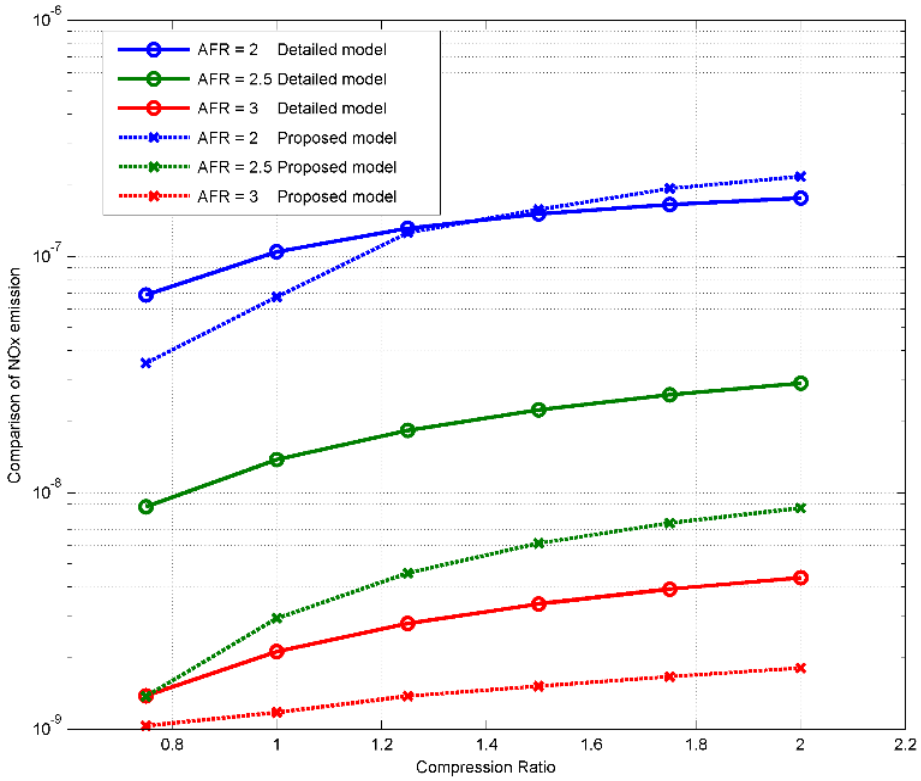

Figure 6.11 Comparison of NOx production from the two models at various Ωs and different AFRs

6.3 Conclusion

In this chapter, a new control-oriented model with a unique phase separation method is developed to realize the trajectory-based HCCI combustion control. In order to reduce the computational burden and keep sufficient chemical kinetics information for HCCI combustion, the engine cycle is separated into four phases and in each phase, a specific reaction mechanism with the minimal size is applied. With the unique phase separation method, the proposed control-oriented model not only shows a good agreement with the detailed physical-based model, in terms of in-cylinder gas temperature and NOx emissions but also reduces the computation time by 95%. In addition, such a good agreement is sustained at various working conditions, including different CRs, multiple AFRs and various piston motion patterns Ω.

Chapter 7

Optimization of the Trajectory-based Combustion Control

After achieving the control-oriented model [136], we are in a good position to proceed the optimization of the trajectory-based combustion control. In this chapter a systematic approach to designing the optimal piston trajectory, according to variable working conditions and versatile fuel properties, is presented. Both offline and online optimization methods are investigated herein. Refer to the offline optimization, two methods are generally utilized: one is converting the original problem to parameters optimization; the other is transforming it to a constrained nonlinear programming and solving it via the sequential quadratic programming (SQP) method. The corresponding optimization results and detailed discussions are followed, which clearly demonstrate the advantage of the trajectory-based HCCI combustion with regard to FPE output work and NOx emission. For the online optimization, a searching process aimed to determine the optimal piston motion pattern according to variable working conditions is presented. With the unique searching process, the simulation studies show that the optimal control of the HCCI combustion phasing can be realized in real time.

7.1 Offline Optimization

7.1.1 Optimization Approach

As can be seen from the last chapter, the control-oriented model that is used to reproduce the combustion of methane is already in the order of 10 (2 from the thermodynamic part and 8 from the chemical kinetics part). Meanwhile, due to the

stiffness of the differential equations representing the chemical kinetics, the small time step is required for numerical computation. The high order of the dynamic models and the requirement of small time step increase the difficulties to achieve the optimal trajectory using the indirect method for the dynamic optimization problems, such as Pontryagin's minimum principle (PMP) [137] or dynamic programming (DP) [138]. So even for offline optimization, a computationally efficient method is required.

Two optimization methods are then proposed to solve this problem. One is to parameterize the piston trajectories, namely the control input, in each combustion cycle as a function of several parameters and then convert the original optimization problem into the parameter optimization framework. In chapter 2, a new description method describing the ultimate freedom of the piston motion in FPE has been proposed [79]. As a result, two parameters, i.e. CR, which stands for compression ratio, and Ω, which shows different piston motion patterns between the BDC and the TDC points, are employed to form the functions.

Specifically, for each trajectory with fixed CR (i.e. only changing Ω), the corresponding cost function (defined based on work output and emissions) can be calculated via the states and the outputs of the control-oriented model by implementing the piston trajectory as the control input. This process generates a mapping between the Ω and the value of the cost function. An analytical function will be further obtained by interpolating the mapping and hence the optimal input (Ω) can be achieved. The advantage of the proposed method is the drastic reduction of the computational burden

since the whole trajectory is represented by only one parameter Ω. However, it also limits the available piston trajectories to those represented by the functions of Ω.

One class of piston trajectories that are of special interest: asymmetrical trajectories, unfortunately, cannot be represented by a single Ω. It is worth mentioning that appropriate asymmetrical trajectories can significantly increase the engine thermal efficiency and reduce emissions production simultaneously [80]. In order to take such asymmetrical trajectories into account, the derived functions of piston trajectories are modified, and two parameters, Ω_1 and Ω_2, are included to represent the compression trajectory and the expansion trajectory respectively. This will form a two parameters optimization problem if the CR is fixed in purpose.

The other optimization method proposed here is the direct optimization method which is able to further enlarge the candidate pool of various piston trajectories. Unlike the previous one, the direct method discretizes the piston trajectory within an engine cycle into n points and represents it as a numerical vector u with n elements. In this way, the value of each element shows the instantaneous displacement of the piston trajectory. Then, by sending the vector u into the control-oriented model, the corresponding states and the outputs of the model, such as in-cylinder pressure, in-cylinder temperature, and concentrations of species, can be calculated and represented as the vectors with the same number of elements:

$$\Phi\left(\begin{bmatrix} u_1 \\ u_2 \\ . \\ . \\ . \\ u_{n-1} \\ u_n \end{bmatrix}\right) = \begin{bmatrix} P_1 & T_1 & [X_{CH_4}]_1 & \dots & [X_{N_2}]_1 \\ P_2 & T_2 & [X_{CH_4}]_2 & \dots & [X_{N_2}]_2 \\ . & . & . & & . \\ . & . & . & & . \\ . & . & . & & . \\ P_{n-1} & T_{n-1} & [X_{CH_4}]_{n-1} & \dots & [X_{N_2}]_{n-1} \\ P_n & T_n & [X_{CH_4}]_n & \dots & [X_{N_2}]_n \end{bmatrix} \tag{7.1}$$

where $\Phi(u)$ indicates the mapping using the control-oriented model; P, T, $[X_{CH4}]$, etc. are the states and output vectors, with n elements, of the model respectively. It is worth noting again that the reason why the mapping process can be applied herein is due to the repetitive nature of the FPE operation. Hence, the time differential equations in the control-oriented model can be numerically solved in cycle base and the corresponding results form the mapping process.

As a result, the entire dynamic optimization problem is transformed into a static nonlinear programming problem with the general form:

minimize $f(\Phi(u), u)$ (7.2.1)

over $u \in R^n$

subject to $h(u) = 0$ (7.2.2)

$g(u) \le 0$ (7.2.3)

$u^L \le u \le u^U$ (7.2.4)

where $f(\Phi(u), u)$ is the cost function which is derived through the control input and the corresponding outputs of the control-oriented model; u is the designed trajectory vector with n elements; $h(u)$ represents the equality constraints of the input vector and $g(u)$

shows the inequality constraints; u^L and u^U are the lower and upper boundaries of trajectory vector, which is determined by the TDC and the BDC point, respectively.

Afterward, the derived nonlinear programming problem is solved based on the sequential quadratic programming (*SQP*) method [138], [139], which is one of the state-of-art algorithms to solve large-scaled constrained nonlinear optimization problems. Generally, the SQP algorithm is a gradient-based method and has to finish two tasks: finding direction vector d_k in the design space and selecting suitable step-size α_k. Then, the new design vector u_{k+1} can be updated as $u_{k+1} = u_k + \alpha_k d_k$ and such iterations continue until the convergence is achieved. In the SQP method, the direction vector d_k at k-th iteration is determined by solving a QP subproblem:

$$\text{minimize} \qquad \frac{1}{2} d_k^T H_k d_k + \nabla f(\Phi(u_k), u_k)^T d_k \tag{7.3.1}$$

$$\text{over} \qquad d_k \in R^n$$

$$\text{subject to} \qquad \nabla h(u_k)^T d_k + h(u_k) = 0 \tag{7.3.2}$$

$$\nabla g(u_k)^T d_k + g(u_k) \le 0 \tag{7.3.3}$$

$$u^L \le u_k + d_k \le u^U \tag{7.3.4}$$

where H_k is a positive definite approximation of the Hessian matrix of the Lagrangian function, which can be derived through the BFGS method [140]; $\nabla f, \nabla h, \nabla g$ are the corresponding gradient vectors at u_k. In to solve this QP sub problem, the active set strategy is utilized herein [140]. Afterward, the step size α_k is achieved by minimizing the descent function, which is developed via cost function $f(\Phi(u),u)$ and constraints $h(u)$ and $g(u)$, along with the direction d_k [141].

7.1.2 Simulation Results and Discussions

7.1.1.1 Parameterizing Piston Trajectories by single Ω

As mentioned above, by given CR, various piston trajectories, with different piston motion patterns between the TDC and BDC points, can be presented as a function of Ω. Hence, the complicated dynamic optimization problem is transformed into a one-dimensional optimization problem. As a preliminary study, the control objective is assigned to maximize the FPE work output *W* per engine cycle:

$$Maximize: J_1 = W = \int P \cdot dV \tag{7.4}$$

Using the control-oriented model, simulation is conducted by assigning the FPE working condition as air-fuel equivalence ratio (AFR) = 2.5, CR = 29 and sweeping the Ω from 0.4 to 2.4 with a step of 0.01. The values of the work output versus the different Ωs are then plotted in Figure 7.1.

As can be seen in Figure 7.1, the optimal Ω in terms of the maximal work output is around 1.11 at this working condition. Any piston trajectory with smaller Ω will cause incomplete combustion and therefore generate lower work output. On the other hand, piston trajectories with larger Ω will extend the residence time of piston around the TDC with high temperature and inevitably increase heat loss during the expansion process. In addition, a function $J_1 = f(\Omega)$ can be obtained via the least square curve fitting. It is worth noting that using the derived analytic function instead of the mapping not only offers similar optimal Ω but also reduces storage memory significantly.

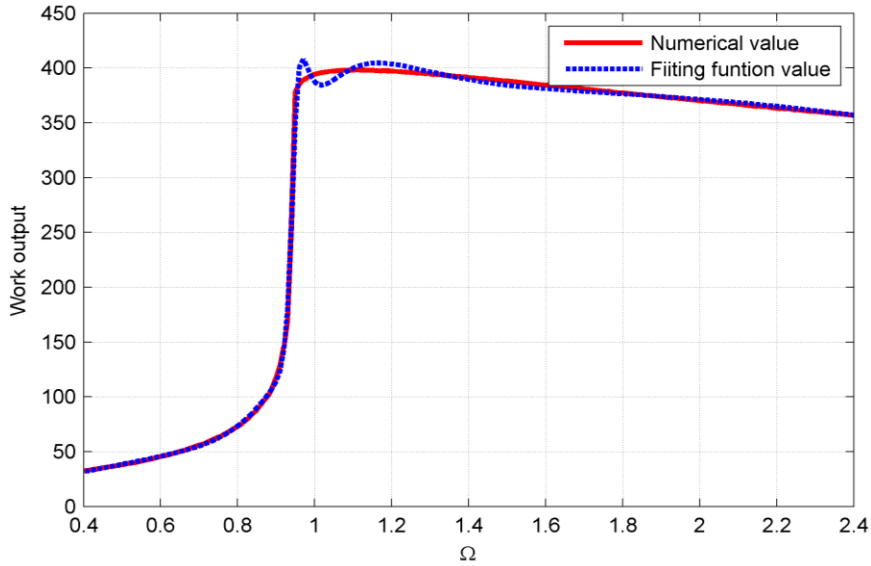

$$f(\Omega)=\frac{1.9269\Omega^{7}-0.4053\Omega^{6}-6.9724\Omega^{5}+3.2980\Omega^{4}+6.6328\Omega^{3}-2.1572\Omega^{2}-4.7820\Omega+2.4652}{\Omega^{7}-1.8378\Omega^{6}+1.4077\Omega^{5}-2.2512\Omega^{4}+0.1240\Omega^{3}+6.4704\Omega^{2}-7.2462\Omega+2.3355}$$

Figure 7.1 Mapping of work output per cycle versus Ω and the corresponding fitting cost function $J_1 = f(\Omega)$

Furthermore, the value of optimal Ω also relies on the value of given CR. Figure 7.2 illustrates the relationship between the optimal Ω and the corresponding CR. Obviously, the optimal Ω is reduced while the CR increases. This result is intuitive since the air-fuel mixture is compressed more aggressively at higher CR and forces the combustion event occurring early. Therefore, the trajectory with lower Ω, which possesses shorter residential time while piston locates around the TDC point, reduces the high-temperature duration within the engine cycle and decreases the heat loss as well [79].

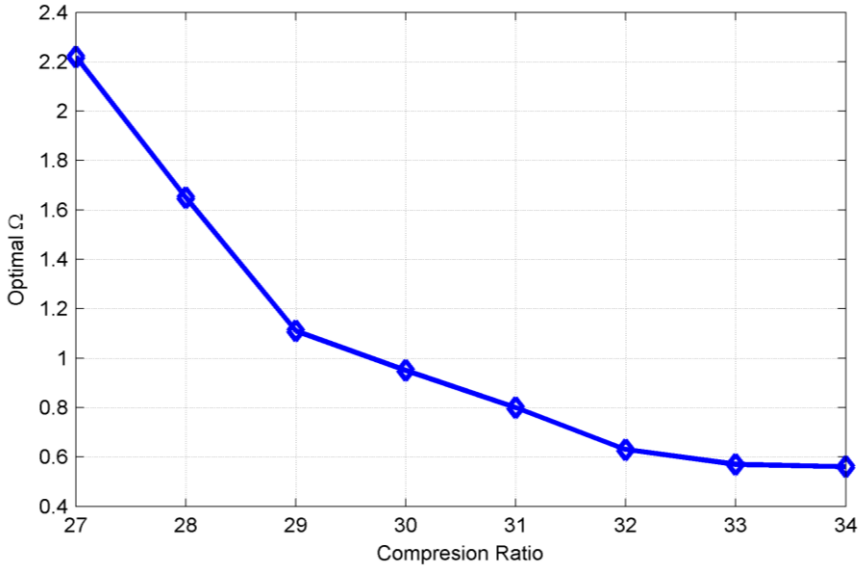

Figure 7.2 Optimal Ωs at different CR

7.1.1.2 Parameterizing Piston Trajectories by Two Ωs

One of the most attractive characteristics of the FPE is that arbitrary piston trajectory can be implemented in the engine. So, in-cycle combustion control can be realized by assigning different control objectives to different trajectory sections. For example, the compression process can be determined by optimizing the SOC timing and the expansion process can be designed to reduce the heat loss and emission [80]

Enlightened by this knowledge, the previous one-dimensional optimization problem (at fixed CR) is further extended to a two-dimensional one, in which the cost function J_2 is represented by a function of two parameters, compression process Ω_1 and expansion process Ω_2 respectively. Furthermore, the effect of NOx emissions is also be considered while developing the new cost function J_2. The corresponding cost function is then represented as below:

$$Maxmize: J_2 = w_1 \frac{W}{W_{\max}} - w_2 \frac{C(NOx)}{C_{\max}(NOx)} = f(\Omega_1, \Omega_2) \tag{7.5}$$

where W and $C(NOx)$ are the work output and final NOx emission along the trajectory determined by Ω_1 and Ω_2; W_{max} and $C_{max}(NOx)$ are the simulated maximum work output and NOx emission respectively working as the normalized coefficients in the cost function J_2. In addition, w_1 and w_2 are weigh coefficients and their sum is one.

The corresponding simulation results of this 2-dimensional optimization problem, while CR = 29, AFR = 2.5 and w_1 = 0.8, is shown in Figure 7.3.

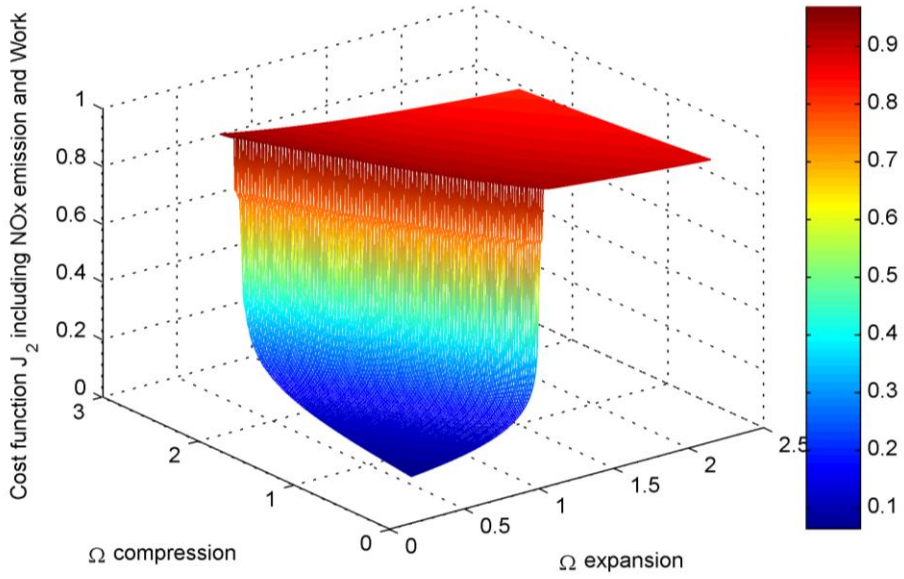

(a)

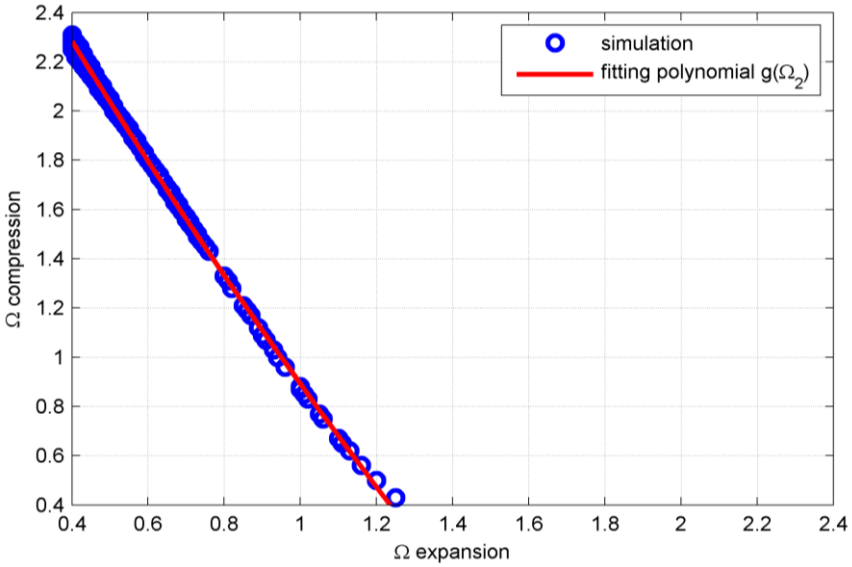

(b)

Figure 7.3 Mapping of cost J_2 as a function of two Ωs at $w_1 = 0.8$ (a) 3D plots (b) fitting plot

It is worth noting that each circle in Figure 7.3 (b) shows a specific Ω pairs generated a cost function J_2 whose value is larger than 0.9. Obviously, the optimal Ω pair is located inside these circles. In order to achieve the optimal Ω pair, a function $g(\Omega_2)$ approximately representing the locations of all of these circle can be fitted as:

$$\Omega_1 = g(\Omega_2) = 0.2562\Omega_2^2 - 2.6194\Omega_2 + 3.3622 \tag{7.6}$$

In this way, the order of this two-dimensional optimization problem is further reduced. In other words, using (7.6) and the control-oriented model, the cost function J_2 can be calculated for each Ω_2. Consequently, the optimal (Ω_1, Ω_2) pair is finally obtained by solving this one-dimensional optimization problem and the corresponding simulation result is listed in Table 7.1. For the sack of comparison, the optimal symmetric piston trajectory (Ω = 1.11) is also listed in the table. It is clear that by deploying the optimal

asymmetric piston trajectory, the FPE is able to reduce the NOx emission by half and increase the work output slightly at the same time.

Table 7.1 Comparison of optimal asymmetric and symmetric trajectories

Ω_1	Ω_2	Work [J]	NOx Emission [mol/m^3]
2.35	**0.40**	**401.91**	**2.32e-6**
1.11	**1.11**	**398.28**	**4.07e-6**

Similarly, the optimal (Ω_1, Ω_2) pair is also varied as the CR. Figure 7.4 shows the fitting plots of cost function J_2 at two different CRs. The differences among these two plots and Figure 7.3 (b) clearly prove that the variation of optimal (Ω_1, Ω_2) pair depends on the value of CRs. Table 7.2 shows the comparison of the optimal asymmetric and symmetric piston trajectory in these three CR which apparently proves the benefits of the former one, in terms of larger output work and less NOx emission.

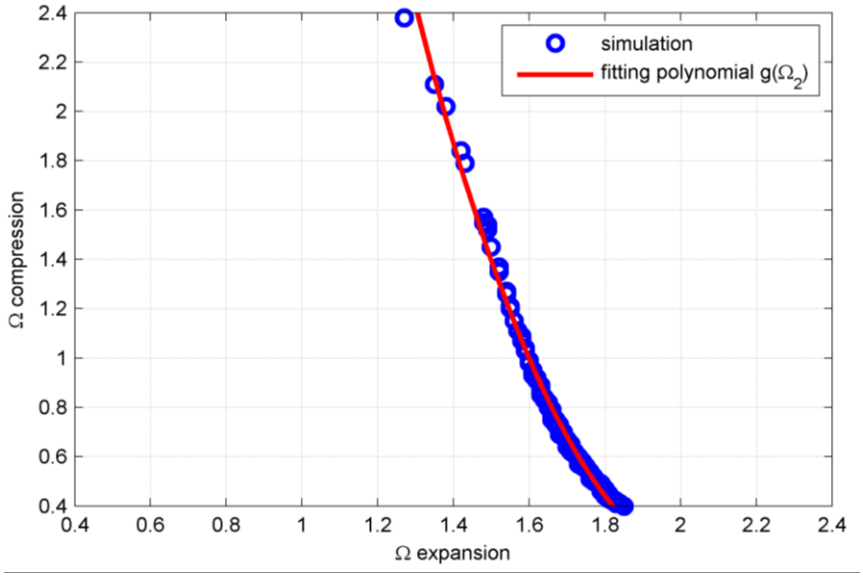

(a)

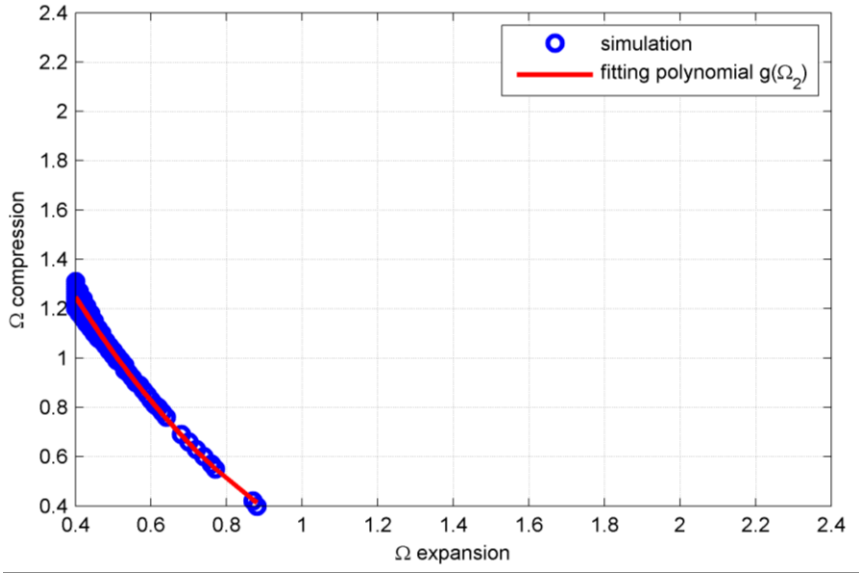

(b)

Figure 7.4 Fitting plot of cost J_2 as a function of two Ωs (a) CR=28; (b) CR=31

Table 7.2 Comparison of optimal asymmetric and symmetric trajectories at different CR

CR	Ω_1	Ω_2	Work [J]	NOx Emission [mol/m^3]
28	**0.44**	**1.84**	**384.82**	**3.87e-7**
28	**1.66**	**1.66**	**380.15**	**1.82e-6**
29	**2.35**	**0.40**	**401.91**	**2.32e-6**
29	**1.11**	**1.11**	**398.28**	**4.07e-6**
31	**1.34**	**0.42**	**414.28**	**2.07e-6**
31	**0.82**	**0.82**	**412.02**	**6.90e-6**

7.1.1.3 Direct Method

In this method, the original optimization problem is converted to a static constrained nonlinear programming problem as shown in (7.7).

$$\text{Minimize:} \qquad f(\Phi(u),u) = -\sum_{i=1}^{100} P_i \frac{(u_{i+1}-u_i)}{dt} + r \cdot \max(0,[X_{NO_x}]_{101} - 3e-6) \qquad (7.7.1)$$

$$\text{over} \qquad u \in R^{101}$$

$$\text{subject to} \qquad h(u) = 0 \qquad (7.7.2)$$

$$g(u) \le 0 \qquad (7.7.3)$$

$$u^L \le u \le u^U \qquad (7.7.4)$$

where r is a large positive number, 10e8, as a penalty if the final NOx emission is greater than 3e-6 mol/m^3; dt is the step time derived from the number of the vector, n = 101, and the given period of an engine cycle, which is 40 ms (shown in Figure 7.5). Clearly, the cost function takes both work output and NOx emission into account.

Furthermore, u^L and u^U are the lower and upper boundaries of trajectory vector u, which are prescribed as the TDC point and the BDC point (in this case, the TDC point is set as 2.1mm and the BDC point is set as 61.9mm to make sure the CR = 29); *h(u)* represents the equality constraints of the input vector u, which limits the first and final elements as u^U ,and the middle element as u^L; *g(u)* shows the inequality constraints of u, which ensures the velocity, calculated by any two subsequent elements of u, is less than 8m/s.

The corresponding optimal trajectory is compared with the previous asymmetric trajectory in Figure 7.5, as well as their temperature profiles and P-V diagram. It is

apparent that the new optimal trajectory possesses even shorter residential time around the TDC and shorter expansion Afterward. In this way, the new optimal trajectory significantly reduces the total amount of heat loss within the entire cycle as well as the NOx emission. With the proposed trajectory-based HCCI combustion, it is also interesting to note that the TDC is not a single point anymore. Instead, the piston can stay at the TDC location for the desired duration (shortest possible combustion duration) and it doesn't have to be in the middle of the time period. Such characteristics benefit the engine thermal efficiency by realizing the ideal constant volume combustion process. As a result, compared to the optimal asymmetric trajectory, the optimal one achieved from the direct method further increase the work output from 401.91J to 416.70J and keep the NOx emission almost at the same level, which are 2.45e-6 and 2.31e-6 respectively. However, to realize this optimal piston trajectory, large piston acceleration is required (around 3e5 m/s^2). This is difficult to achieve in the actual FPE. In the future, more physical constraints, such as peak acceleration and peak pressure, will be added to the optimization. Meanwhile, the direct methods will further be used to design the optimal piston trajectories at different work conditions for other fuels.

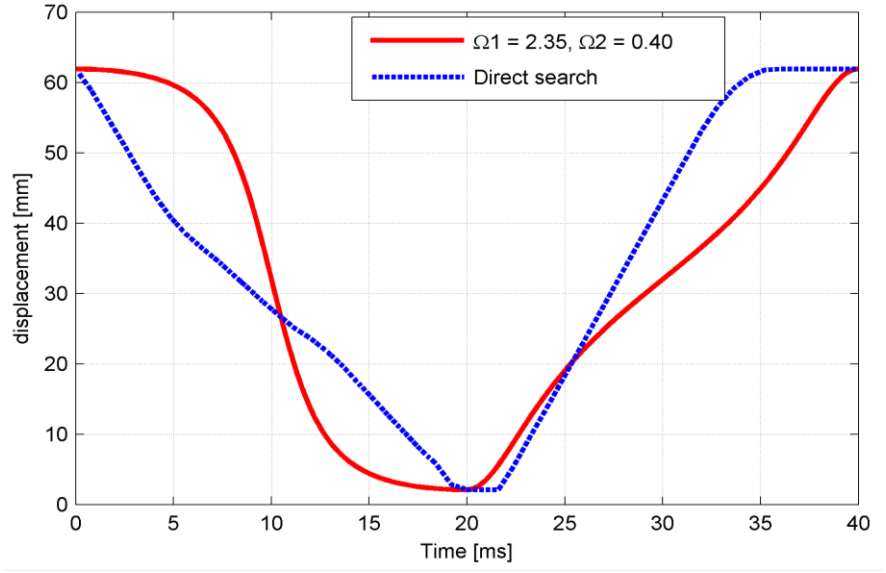
Ω1 = 2.35, Ω2 = 0.40
Direct search
displacement [mm]
Time [ms]
0
10
20
30
40
50
60
70
0
5
10
15
20
25
30
35
40

(a)

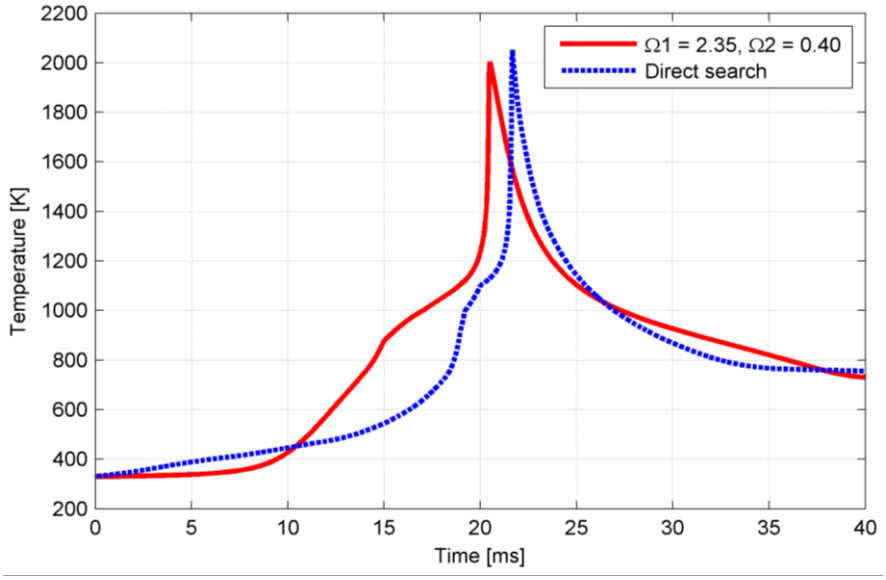
Ω1 = 2.35, Ω2 = 0.40
Direct search
Temperature [K]
Time [ms]
200
400
600
800
1000
1200
1400
1600
1800
2000
2200
0
5
10
15
20
25
30
35
40

(b)

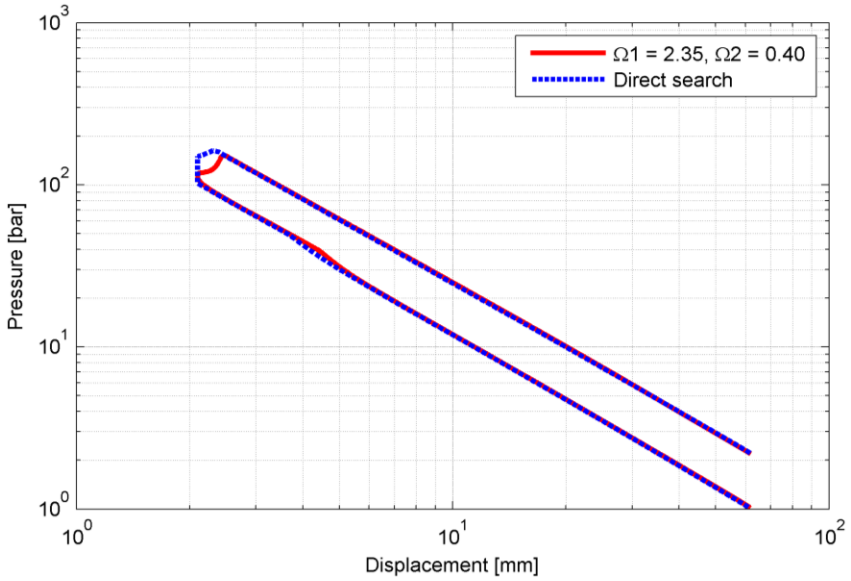

(c)

Figure 7.5 Comparison of optimal piston trajectories achieved from the direct method and two different Ωs at CR = 29 and AFR = 2.5 (a) Displacement (b) Temperature (c) P-V diagram

7.2 Online Optimization

One of the most challenging parts of HCCI implementation is the control of combustion phasing. In the FPE with the piston trajectory-based HCCI combustion control, the ultimate freedom of piston motion can be used as an additional control means to regulate combustion phasing. In this subsection, a searching process of the optimal piston trajectory enabling the best combustion phasing is presented. Additionally, due to the lack of crankshaft mechanism, the widely-used parameter CA50, which represents the HCCI combustion phase in the conventional ICE, is replaced by T50, representing the time instant when 50% fuel chemical energy has been released in this study.

As shown in Figure 7.6, a single-input-single-output feedback loop is utilized to achieve the optimal Ω of the piston trajectory. The objective is to force the T50 locating

at the TDC point in order to realize the ideal Otto cycle and reduce the ringing intensity. To achieve this objective, a heat release analyzer is developed in order to calculate the simulated T50. Afterward, the error between the calculated T50 and the targeted value is sent to a PI controller and the adjustment of Ω is calculated. In this way, the new piston trajectory is generated and the corresponding error in the following cycle will be reduced.

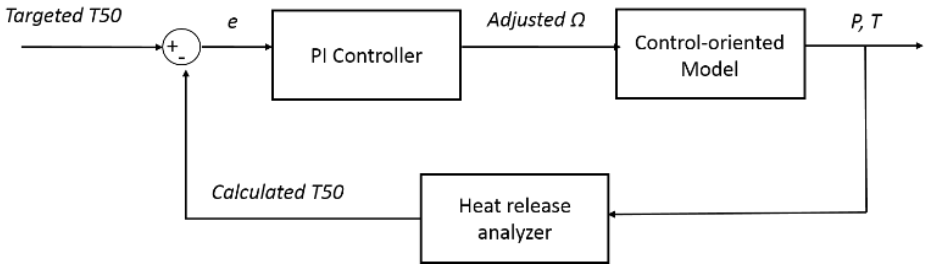

Figure 7.6 Block diagram of the feedback loop searching the optimal piston trajectory with desired combustion phasing

The heat release analyzer calculates the chemical heat release by integrating the instantaneous heat release rate, which is obtained from the piston trajectory and the in-cylinder gas temperature and pressure [29]:

$$\dot{Q}_{HR} = \frac{\gamma}{\gamma - 1} \cdot P \cdot \dot{V} + \frac{1}{\gamma - 1} \cdot V \cdot \dot{P} - \dot{Q} \tag{7.8}$$

where γ is the heat capacity ratio of the in-cylinder gas, which is set as 1.31 [66] and $\dot{Q}$ is the heat transfer rate. The combustion is assumed to occur if the heat release reaches a preset threshold and the T50 value can then be calculated.

As shown in Figure 7.7, when CR = 31, AFR = 2.0, the first piston trajectory, whose Ω = 3.0, triggers combustion early than the TDC point which increases the ringing intensity significantly. Using the feedback loop described above, the Ω of the piston

trajectories in following cycles are reduced from 3.0 to 0.9 and the T50 values are moving closer to the TDC point, as shown in Figure 7.8 (the negative value of the calculated T50 indicates the corresponding instant is before the TDC time). Hence, the fine tuning of the combustion phase is realized by adjusting the piston trajectory and the optimal piston trajectory, which locates T50 at the TDC point, is determined eventually. The optimal piston trajectory is then sent to the detailed model and the comparison between the proposed model and the detailed model presents good agreement again, as shown in Figure 7.9.

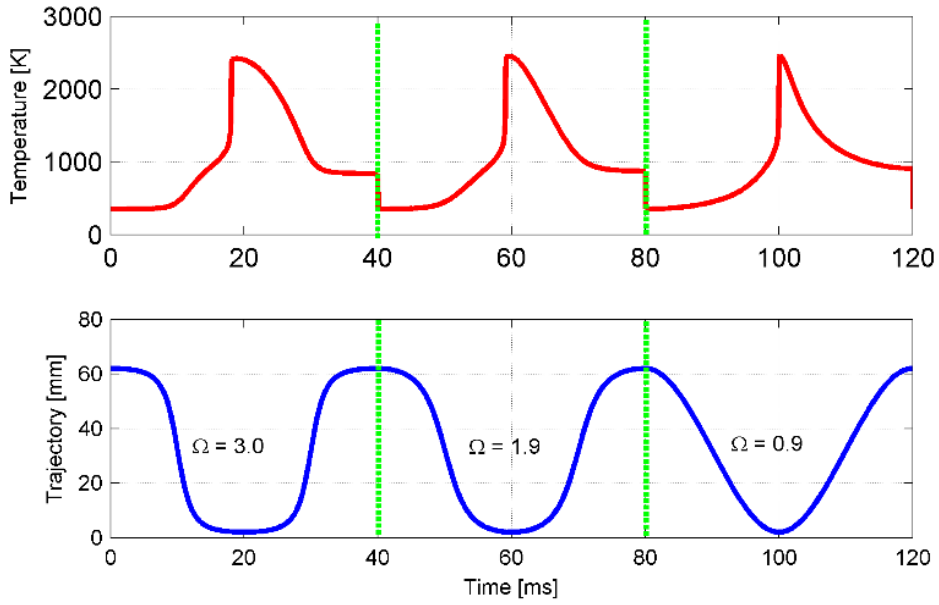

Figure 7.7 Searching process for the optimal piston trajectory (AFR = 2, CR = 31)

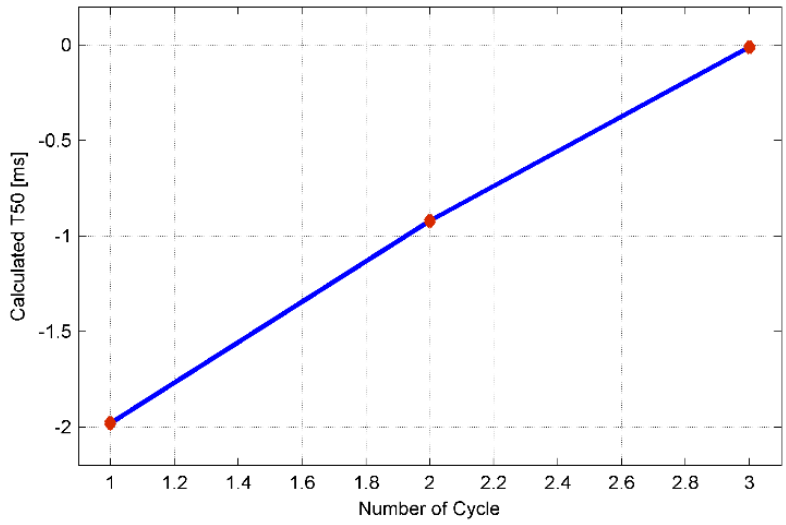

Figure 7.8 Calculated T50 for each engine cycle

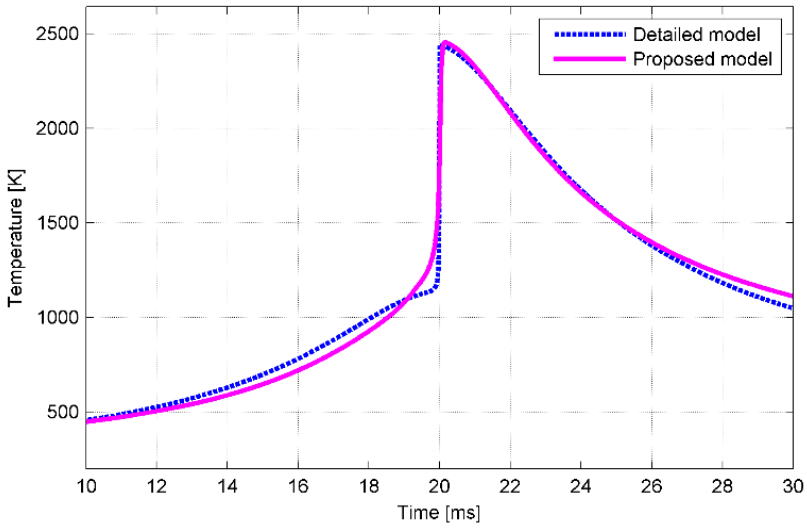

Figure 7.9 Temperature traces of combustion along the optimal piston trajectory using the detailed model and the proposed model respectively

The performance of the feedback loop searching method is also investigated during the variation among multiple working conditions. As shown in Figure 7.10, the left side of the green dashed line represents different working conditions with various AFRs under CR = 31 and the right side represents different working conditions with same AFRs

under CR = 34. As can be seen, no matter how the CR or the AFR is changed, the feedback loop searching method with the proposed model can always achieve an optimal Ω, realizing the desired combustion phasing, after 3 or 4 cycle's simulation, which only lasts 0.3 to 0.4s. In other words, a real time optimal control of the HCCI combustion phasing is achieved through the feedback loop searching method with the assistance of the proposed control-oriented model. As a comparison, the detailed model is also implemented into the feedback loop searching method to determine the optimal Ω for the combustion phasing control. However, the turnaround time of this process is about 20s, which is far beyond the requirement for the real time application.

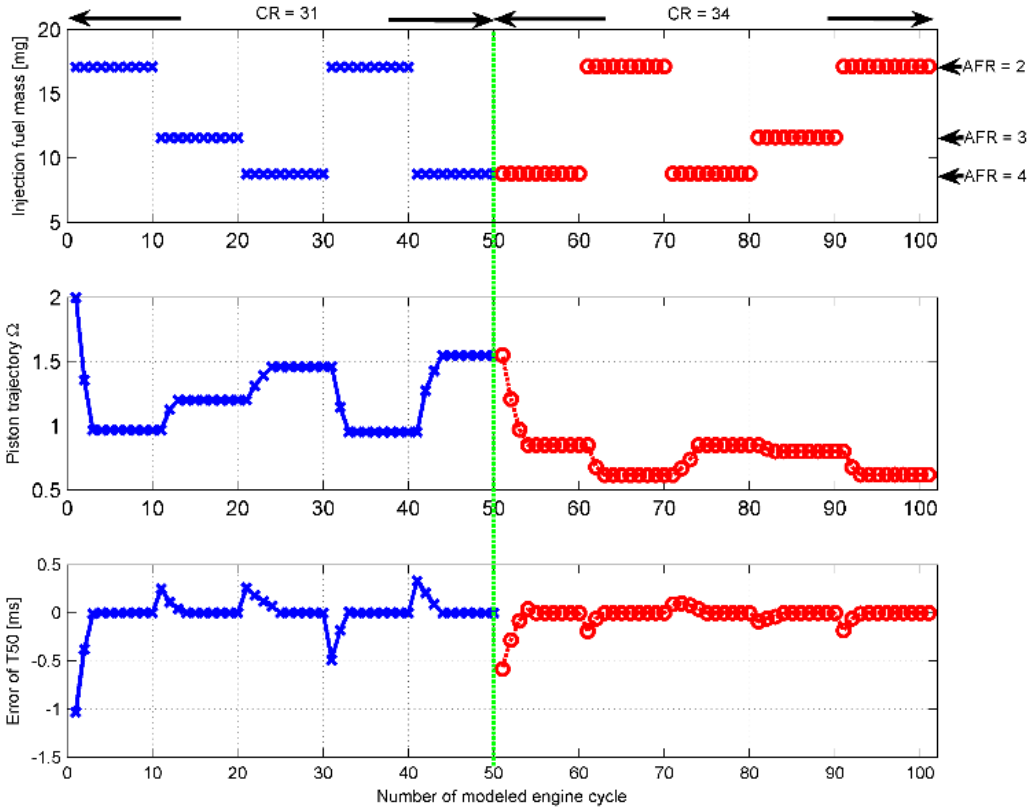

Figure 7.10 Searching process of the optimal piston trajectories during the variation of multiple working conditions (various CRs and AFRs)

7.3 Conclusion

In this chapter, the approach to optimizing piston trajectory for the trajectory-based HCCI combustion control is presented. As claimed by the concept of trajectory-based combustion control, the derived optimal piston trajectory is considered as the optimal control signal to the FPE, which provides ultimate engine performance, in terms of maximal engine thermal efficiency and minimal emissions production. Both offline and online optimization are presented.

Refer to the offline optimization, two approaches are proposed and implemented into the model: The first approach represents the piston trajectory as a function of parameter Ω and converts the original problem to a parameters optimization problem. Both optimal symmetric trajectories (represented as a function of single Ω) and asymmetric trajectories (represented as a function of two Ωs) are derived at given CR. The advantages of this optimization approach lie on its much lighter computational burden and easily implemented result; the second method transforms the trajectory optimization problem into a static constrained nonlinear programming and then solves it via the SQP algorithm. By removing the constraints placed by parameter functions, this approach enlarges the candidate pool of various piston trajectories. Hence, the derived optimal trajectory further increases the engine output work and sustains the NOx emissions at the same level.

For the online optimization, a searching process is developed with the assistance of the proposed control-oriented model. The main idea of this searching process is to utilize the result of the control-oriented model to adjust the implemented piston motion pattern in order to achieve the designed the combustion phasing control. The simulation results

clearly show that no matter what kinds of variation on the working conditions are employed, the designed piston motion pattern can always be derived within 0.4s, which proves the effectiveness of this approach as an online optimization control on the HCCI combustion phasing.

Chapter 8

Conclusions and Future Works

8.1 Conclusions

The objective of the proposed research is to develop dynamic models and design optimal controls for the trajectory-based HCCI combustion enabled by the FPE. With an FPE, the engine piston trajectory can be controlled in real-time to actively regulate the combustion chamber volume and therefore adjust the gas pressure-temperature history and species concentration prior, during, and after the combustion event. This extra degree of freedom enables the optimization of chemical reactivity and heat transfer processes of HCCI combustion. The research aims to characterize and optimize the dynamics of HCCI combustion with unconstrained gas pressure-temperature history enabled by the FPE, which essentially opens up a new framework for controlling advanced combustion in real time.

The first part of the research focuses on the modeling and analysis of the trajectory-based combustion control in the FPE. Through extensive simulation studies, it is clear that the FPE is able to adjust the entire combustion process by varying the volume of the combustion chamber and therefore altering the in-cylinder gas temperature and pressure traces to improve the indicated output work. Besides, the trajectory-based combustion control can also influence the chemical kinetics of the combustion via manipulating the in-cylinder temperature. Specifically, unique asymmetric trajectories are designed that decreases the amount of NOx emission and increases the engine thermal efficiency

simultaneously. At last, the analysis of the trajectory-based combustion control is also extended to various renewable fuels, e.g. hydrogen, biogas, syngas, ethanol, DME, biodiesel, and F-T fuels. It shows that an optimal asymmetric piston trajectory can be designed for each specific renewable fuel, which enables a significant reduction in the NOx emission and an improvement in the thermal efficiency simultaneously. In this way, the trajectory-based combustion control realizes the co-optimization of fuels and engine operation.

The second part of the research focuses on the development of a new control-oriented model aimed to realize the trajectory-based HCCI combustion control in real-time. In order to reduce the computational burden and keep sufficient chemical kinetics information for HCCI combustion, the engine cycle is separated into four phases and in each phase, a specific reaction mechanism with the minimal size is applied. With the unique phase separation method, the proposed control-oriented model not only shows a good agreement with the detailed physical-based model, in terms of in-cylinder gas temperature and NOx emissions but also reduces the computation time by 95%. In addition, such a good agreement is sustained at various working conditions, including different CRs, multiple AFRs and various piston motion patterns Ω.

The last part of the research discusses systematic approaches to optimizing piston trajectory for the trajectory-based HCCI combustion control. As claimed by the concept of trajectory-based combustion control, the derived optimal piston trajectory is considered as the optimal control signal to the FPE, which provides ultimate engine

performance, in terms of maximal engine thermal efficiency and minimal emissions production. In this part, both offline and online optimizations are investigated.

For the offline optimization, two approaches are proposed and implemented into the proposed control-oriented model: The first approach represents the piston trajectory as a function of parameter Ω and converts the original problem to a parameters optimization problem. Both optimal symmetric trajectories and asymmetric trajectories are derived at given CR. The advantages of this optimization approach lie on its much lighter computational burden; the second method transforms the trajectory optimization problem into a static constrained nonlinear programming and then solves it via the SQP algorithm. By removing the constraints placed by piston motion patterns, this approach enlarges the candidate pool of various piston trajectories. Hence, the derived optimal trajectory further increases the engine output work and sustains the NOx emissions at the same level. For the online optimization, a searching process aimed to determine the optimal piston motion pattern Ω according to variable working conditions is developed. By using the proposed control-oriented model, the designed piston trajectory can be achieved within 0.4s under different working conditions, which enables real time optimal control of HCCI combustion phasing.

8.2 Future Works

In the future, the investigation of the advantages of FPE as an energy source for diverse automobile applications will be continued. Meanwhile, the trajectory-based combustion control will be further refined, in order to realize the great potential of the FPE.

8.2.1 Experimental Study of the Trajectory-based HCCI Combustion Control

The most important future work related to the study is to demonstrate the effectiveness of the trajectory-based HCCI combustion control in practice. Previously, a rapid compression expansion machine (RCEM) with a unique capability of real time piston trajectory control has been designed and manufactured by our group [142], [143]. Attributed to its controllable piston trajectory, the RCEM provides a perfect platform to examine fundamental linkages between piston trajectory and combustion processes. Within the RCEM, a hydraulic actuation system is used instead of the conventional pneumatic actuation, which forms a sound foundation for the precise and fast piston motion control due to the high stiffness of the fluid. Besides, a fuel preparation and emission measurement systems are also integrated into the RCEM, which provides sufficient information on the fuel properties and the corresponding emissions. At last, an optical diagnostics system is also designed, which enables the optimal access of the inside of the combustion chamber and thus provides real-time temperature, pressure, and species concentration measurement during the test.

Currently, the motoring test of the RCEM has been conducted and the experimental results have shown its capability of tracking various piston trajectories, i.e. hold volume at high pressure and high temperature, same piston motion pattern with different compression ratios and same compression ratio with different piston motion pattern. The preparation of the firing tests along those different piston trajectories is undergoing and if successful, the valuable experimental result showing the effects of various piston

trajectories on the combustion performance, such as the temperature, pressure histories, and the generated emission, can be achieved eventually.

8.2.2 Investigating FPE on Diverse Automobile Applications

Typically, the FPE can be categorized into two groups: the hydraulic FPE and the electric FPE, or so-called free-piston linear generator. Obviously, the former one is ideal to power off-road heavy machinery and the latter one is a great fit for on-road vehicles. In addition, the FPE also provides other benefits compared to the conventional ICE: 1. it can be powered by a diversity of alternative fuels; 2. it works in a hybrid powertrain due to its non-mechanical output; 3. it is a modular power source due to its instant on/off capability.

In spite of its huge potential, there is still a lack of study on the dynamic behavior and performance of the FPE on these diverse automobile applications. The main reason is the technical challenge of the piston motion control in the FPE. By overcoming the barrier via the virtual crankshaft mechanism, we are currently in a good position to initiate the exploration of this field. The potential research topics include 1. How does the FPE match variable loading dynamics of different automobile applications in real-time? 2. How does the FPE performance change if using alternative fuels? 3. What is the optimal energy management strategy for the FPE working in a hybrid powertrain? 4. What is the optimal distribution of FPE modules in the powertrain system? 5. By knowing more road information through connected vehicles technology, does the FPE perform more efficiently due to its high flexibility and if so, how much improvement it can obtain?

Bibliography

[1] The U.S. Department of Energy, "Quadrennial Technology Review: an Assessment of Energy Technologies and Research Opportunities", *September 2015.*

[2] Bhutto, A. W., Qureshi, K., Abro, R., Harijan, K., Zhao, Z., Bazmi, A. A., Abbas, T. and Yu, G., "Progress in the Production of Biomass-to-liquid Biofuels to Decarbonize the Transport Sector – Prospects and Challenges", *Royal Society of Chemistry Advances, issue. 6, pp. 32140-32170. 2016.*

[3] International Energy Agency, "Energy Climate and Change: World Energy Outlook Special Report", *Paris, France, 2015.*

[4] Ribeiro, S. K., Kobayashi, S., Beuthe, M., Gasca, J., Greene, D., Lee, S. D., Muromachi, Y., Newton, P. J., Plotkin, S., Sperling, D., Wit, R. and Zhou, P. J. "Transport and its infrastructure", *Cambridge, United Kingdom and New York, NY, USA, 2007.*

[5] Guo, M., Song, W. and Buhain, J., "Bioenergy and Biofuels: History, Status, and Perspective", *Renewable and Sustainable Energy Reviews, vol. 42, pp. 712-725, 2015.*

[6] Sadeghiezhad, E., Kazi, S. N., Sadeghinejad, F., Badarudin, A., Mehrali, M., Sadri, R. and Safaei, M., "A Comprehensive Literature Review of Biofuel Performance in Internal Combustion Engine and Relevant Costs of Involvement", *Renewable and Sustainable Energy Reviews, vol. 30, pp. 29-44, 2014.*

[7] Bergthorson, J. M. and Thomson, M. J., "A Review of the Combustion and Emissions Properties of Advanced Transportation Biofuels and Their Impact on Existing and Future Engines", *Renewable and Sustainable Energy Reviews, vol. 42, pp. 1393-1417, 2015.*

[8] Sangeeta, S. M., Pande, M., Rani, M., Gakhar, R., Sharma, M., Rani, J. and Bhaskarwar, A. N., "Alternative fuels: an Overview of Current Trends and Scope for Future", *Renewable and Sustainable Energy Reviews, vol. 32, pp. 697-712, 2014.*

[9] Salvi, B. L., Subramanian, K. A. and Panwar, N. L., "Alternative Fuels for Transpiration Vehicles: a Technical Review", *Renewable and Sustainable Energy Reviews, vol. 25, pp. 404-419, 2013.*

[10] Agarwal, A. K., "Biofuel (Alcohols and Biodiesel) Applications as Fuels for Internal Combustion Engine", *Progress in Energy and Combustion Science, vol. 33, pp. 233-271, 2007.*

[11] Demirbas, A., "Progress and Recent Trends in Biofuels", *Progress in Energy and Combustion Science, vol. 33, pp. 1-8 2007.*

[12] Sanchez, O. and Cardona, C. A., "Trends in Biotechnological Production of Fuel Ethanol form Different Feedstock", *Bioresource Technology vol. 99 pp. 5270-5295 2008.*

[13] Kampa, M. and Castanas, E., "Human Health Effects of Air Pollution", *Environmental Pollution, Vol. 151, Issue. 2, pp. 362-367, Jan 2008.*

[14] Mauzerall, D. L., Sultan, B., Kim, N. and Bradford D. F. "NOx Emissions from Large Point Sources: Variability in Ozone Production, Resulting Health Damages and Economic Costs", *Atmospheric Environment, Vol. 39, Issue. 16, pp. 2851-2866, May 2005.*

[15] "Light-Duty Vehicles and Trucks and Motorcycles Emission Regulation" provided by the United States Environmental Protection Agency. http://www.epa.gov/otaq/standards/light-duty/index.htm

[16] "European Emission Standards" provided by the European Parliament, Council. http://en.wikipedia.org/wiki/European_emission_standards

[17] Cho, H.M. and He, B. Q., "Spark Ignition Natural Gas Engines – A Review", *Energy Conversion and Management, Vol. 48, Issue. 2, pp. 608-618, Feb. 2007.*

[18] Alasfour, F. N., "NOx Emission from a Spark Ignition Engine Using 30% Iso-butanol-gasoline Blend: Part 2—Ignition Timing", *Applied Thermal Engineering, Vol. 18, Issue. 8, pp. 609-618, Aug 1998.*

[19] Ma, F., Liu, H., Wang, Y., Li, Y., Wang, J. and Zhao, S., "Combustion and Emission Characteristics of a Port-injection HCNG Engine under Various Ignition Timings", *International Journal of Hydrogen Energy, Vol. 33, Issue. 2, pp. 816-*

822, Jan 2008.

[20] Pierpont, D., Montgomery, D. and Reitz, R., "Reducing Particulate and NOx Using Multiple Injections and EGR in a D.I. Diesel", *SAE Technical Paper 950217, Feb 1995.*

[21] Hountalas, D. T., Mavropoulos, G. C. and Binder, K. B., "Effect of Exhaust Gas Recirculation (EGR) Temperature for Various EGR Rates on Heavy Duty DI Diesel Engine Performance and Emission", *Energy, Vol. 33, Issue. 2, pp. 272-283, Feb 2008.*

[22] Maiboom, A., Tauzia, X. and Hetet, J., "Experimental Study of Various Effects of Exhaust Gas Recirculation (EGR) on Combustion and Emissions of an Automotive Direct Injection Diesel Engine", *Energy, Vol.33, Issue. 1, pp. 22-34, Jan 2008.*

[23] Gu, X., Huang, Z., Cai, J., Gong, J., Wu. X. and Lee, C., "Emission Characteristics of a Spark-ignition Engine Fuelled with Gasoline-n-butanol Blends in Combination with EGR", *Fuel, Vol. 93, pp. 611-617, Mar 2012.*

[24] Han, Z., Uludogan, A., Hampson, G. and Reitz, R., "Mechanism of Soot and NOx Emission Reduction Using Multiple-injection in a Diesel Engine", *SAE Technical Paper 960633, Feb 1996.*

[25] Tow. T., Pierpont, D. and Reitz, R. D., "Reducing Particulate and NOx Emissions by Using Multiple Injections in a Heavy Duty D.I. Diesel Engine", *SAE Technical Paper 940897, Mar 1994.*

[26] Choi, C. Y. and Reitz, R. D., "An Experimental Study on the Effects of Oxygenated Fuel Blends and Multiple Injection Strategies on DI Diesel Engine Emissions", *Fuel, Vol. 78, Issue. 11, pp. 1303-1317, Sep 1999.*

[27] Adi, G., Hall, C. M., Snyder, D. B., Belt, B. W. D. and Shaver, G. M, "Fuel-Flexible Engine Control of Biodiesel Blends During Mixing-Controlled Combustion", *Journal of Dynamics Systems, Measurement, and Control, Vol.135, Issue 7, 061017, Aug. 2013.*

[28] Stone, R., (1999). Introduction to Internal Combustion Engines, Basingstoke, UK.

[29] J. Heywood, (1988). Internal Combustion Engine Fundamentals, McGraw-Hill.

[30] Weilenmann, M., Favez, Y. and Alvarez, R., "Cold-start Emissions of Modern Passenger Cars at Different Low Ambient Temperatures and Their Evolution over Vehicle Legislation Categories", *Atmospheric Environment, Vol. 43, Issue. 15, pp. 2419-2429, May 2009.*

[31] Henein, N. A and Tagomori, M. K., "Cold-start Hydrocarbon Emissions in Port-injected Gasoline Engines", *Progress in Energy and Combustion Science, Vol. 25, Issue. 6, pp. 563-593, Dec. 1999.*

[32] Salehi, R., Shahbakhti, M. and Hedrick, J. K., "Real-time Hybrid Switching Control of Automotive Cold Start Hydrocarbon Emission", *Journal of Dynamics Systems, Measurement, and Control, Vol. 136, Issue. 4, 041002, Mar 2014.*

[33] Su, E. C. and Rothschild, W. G., "Dynamic Behavior of Three-way Catalysts", Journal of Catalysis, Vol. 99, Issue. 2, pp. 506-510, Jun. 1986,

[34] Jackson, R., Peyton Jones, J., Pan, J. and Roberts, J., "Chemical Aspects of the Dynamic Performance of a Three-Way Catalyst", *SAE Technical Paper 1999-01-0312, Mar 1999.*

[35] Russel, A. and Epling, W. S., "Diesel Oxidation Catalysts", *Catalysis Reviews: Science and Engineering, Vol. 53, Issue. 4, pp. 337-423, Oct 2011*.

[36] Stein, H. J, "Diesel Oxidation Catalysts for Commercial Vehicle Engines: Strategies on Their Application for Controlling Particulate Emissions," *Applied Catalysis B: Environmental, Vol. 10, Issue. 1-3, pp. 69-82, Sep 1996.*

[37] Neeft, J. P., Makkee, M., and Moulijn, J. A., "Diesel Particulate Emission Control", *Fuel processing technology, Vol. 47, Issue. 1, pp.1-69, Apr. 1996*.

[38] Van Setten, B. A., Makkee, M., and Moulijn, J. A., "Science and Technology of Catalytic Diesel Particulate Filters", *Catalysis Reviews, Vol. 43, Issue. 4, pp. 489-564, 2001*.

[39] Koebel, M., Elsener, M., and Kleemann, M., "Urea-SCR: a Promising Technique to Reduce NOx Emissions from Automotive Diesel Engines", *Catalysis Today, Vol. 59, Issue. 3-4, pp. 335-345, Jun. 2000.*

[40] Onishi, S., Han Jo, S., Shoda, K., Do Jo, P., and Kato, S. "Active Thermo-Atmosphere Combustion (ATAC): A New Combustion Process for Internal

Combustion Engine." *SAT Technical Paper Series, Paper NO. 790501. 1997.*

[41] Zhao, F., Asmus, T.W., Assanis, D.N., and Dec, J.E. "Homogeneous Charge Compression Ignitions (HCCI) Engines: Key Research and Development Issues," *SAE International, PT-94,* 2003.

[42] Christensen, M., Hultqvist, A. and Johansson, B., "Demonstrating the Multi-Fuel Capability of a Homogeneous Charge Compression Ignition Engine with Variable Compression Ratio," *SAE Technical paper 1999-01-3679, 1999.*

[43] Akinyemi, O.C, "A Flame Sheet Model of Combustion and NO Formation in Diesel Engines," *Ph.D. Thesis,* Massachusetts Institute of Technology, 1997.

[44] Zhao, H., Peng, Z., Williams, J., Ladommatos, N., "Understanding the Effects of Recycled Gases on the Controlled Autoignition (CAI) Combustion in Four-Stroke Gasoline Engines." *SAE Paper No.2001- 01-3607, 2001.*

[45] Ladommatos, N. Abdelhalim, S, and Zhao, H. "The Effects of Exhaust Gas Recirculation on Diesel Combustion and Emissions." *Int J Engine Res no.1, pp. 107–26, 2000*

[46] Dec, J. E. "A Computational Study of the Effects of Low Fuel Loading and EGR on Heat Release Rates and Combustion Limits in HCCI Engines." *SAE Paper NO. 2002-01-1309, 2002.*

[47] Caton, P. A., Songm H. H., Kaahaainam N.B. and Edwards, C.F. "Strategies for Achieving Residual-Affected Homogeneous Charge Compression Ignition using Variable Valve Actuation." *SAE Paper NO. 2005-01-0165, 2005*

[48] Marriott, C. D and Reitz, R. D. "Experimental Investigation of Direct Injection Gasoline for Premixed Compression Ignited Combustion Phasing Control." *SAE Paper NO. 2002-01-0418, 2002.*

[49] Sjoberg, M., Edling, L. O., Eliassen, T., Magnusson, L. and Angstrom, H. E., "GDI HCCI: Effects of Injection Timing and Air-Swirl on Fuel Stratification Combustion and Emissions Formation." *SAE Paper NO. 2002-01-0106, 2002.*

[50] Pescara, R. P., "Motor compressor apparatus," US Patent, 1,657,641, 1928

[51] Mikalsen, R. and Roskilly, A. P., "A review of free-piston engine history and applications," Applied Thermal Engineering, Vol. 27, Issue 14-15, pp. 2339-2352,

Oct 2007.

[52] London, A. L. and Oppenheim, A. K., "The free-piston engine development – Present status and design aspects," Transactions of the ASME, 1952:74(2):1349-1361

[53] Hibi, A. and Ito, T., "Fundamental test results of a hydraulic free piston internal combustion engine", Proc. Inst. Mech. Eng., 2004:218:1149-1157

[54] Somhorst, Joop H.E. and Achten, Peter A.J., "The combustion process in a DI Diesel hydraulic free piston engine," SAE Trans., Vol. 105, 1996

[55] Tikkanen, S. and Vilenius, M., "Control of dual hydraulic free piston engine," International journal of vehicle autonomous systems, Vol. 4, Issue 1, 2006, pp 3-23

[56] Goldsborough, S.S. and Blarigan, P.V., "A Numerical Study of a Free Piston IC Engine Operating on Homogeneous Charge Compression Ignition Combustion," SAE Trans., Vol. 108, 1999

[57] Flynn, G., "Observations on 25,000 hours of free-piston-engine operation," SAE Trans., Vol. 65, 1957, pp. 508-515

[58] Noren, O.B. and Erwin, R.L., "The future of the free-piston engine in commercial vehicles," SAE Trans., Vol. 66, 1958, pp. 305-314

[59] Kosaka, H., Akita, T., Moriya, K., Goto, S., Hotta, Y., Umeno, T. and Nakakita, K., "Development of Free Piston Engine Linear Generator System Part 1 - Investigation of Fundamental Characteristics", *SAE Technical Paper 2014-01-1203, Apr. 2014.*

[60] Goto, S., Moriya, K., Kosaka, H., Akita, T., Hotta, Y., Umeno, T. and Nakakita, K., "Development of Free Piston Engine Linear Generator System Part 2 – Investigation of Control System for Generator", *SAE Technical Paper 2014-01-1193, 2014.*

[61] Kock, F., Haag, J. and Friedrich, H., "The free piston linear generator – Development of an innovative, compact, highly efficient range-extender module," *SAE Technical Paper*, 2013-01-1727, 2013.

[62] Tanaka, Y., Hiyoshi, R., Takemura, S., Ikeda Y. et al., "A study of a Compression Ratio Control Mechanism for a Multiple-Link Variable Compression Ratio Engine," *SAE Technical Paper*, 2007-01-3547, 2007.

[63] Schwaderlapp, M., Habermann K. and Yapici, K., "Variable Compression Ratio – A Design Solution for Fuel Economy Concepts," *SAE Technical Paper*, 2002-01-1103, 2002.

[64] Rabhi, V., Beroff, J. and Dionnet, F., "Study of a Gear-Based Variable Compression Ratio Engine," *SAE Technical Paper*, 2004-01-2931, 2004.

[65] Van Blarigan, P., "Advanced Hydrogen Fueled Internal Combustion Engines," *Energy & Fuels*, vol. 12, no. 1, pp. 72-77, Jan. 1998.

[66] Li, K., Sadighi, A. and Sun, Z., "Active Motion Control of a Hydraulic Free Piston Engine", *IEEE/ASME Transaction. Mechatronics*, *Vol. 19, Issue. 4, pp. 1148-1159, Aug 2014.*

[67] Achten, P., Van Den Oever, I., Potma J. and Vael, G., "Horsepower with brains: The design of the CHIRON Free Piston Engine," *SAE Technical Paper*, 2000-01-2545, 2000.

[68] Hu, J., Wu, W., Yuan, S. and Jing, C., "On-off Motion of a Hydraulic Free-piston Engine," *Proceedings of the Institution of Mechanical Engineers, Part D: Journal of Automobile Engineering, vol. 227, issue.3, pp. 323-333. Aug. 2012.*

[69] Zhao, Z., Zhang, F., Huang, Y., Zhao, C. and Guo, F. "An Experimental Study of the Hydraulic Free Piston Engine", *Applied Energy*, volume (99), pp. 226-233,2012.

[70] Johansen, T., Egeland, O., Aa Johannessen, E. and Kvamsdal, R., "Free-piston diesel engine timing and control-toward electronic cam-and crankshaft," *IEEE Trans. Control syst. Technol*, vol. 10, no. 2, pp. 177-190, Mar. 2002.

[71] Mikalsen, R. and Roskilly, A., "The control of a free-piston engine generator. Part 2: Engine dynamics and piston motion control". *Applied Energy*, volume (87), pp. 1281-1287, 2010.

[72] Xu, Z. and Chang, S., "Prototype Testing and Analysis of a Novel Internal Combustion Linear Generator Integrated Power System," *Applied Energy,* vol.87, issue. 4, pp. 1342-1348, April 2010.

[73] Kock, F. and Ferrari, C., "Flatness-based high frequency control of a hydraulic actuator," *Journal of Dynamic Systems, Measurement, and Control*, vol. 134, 021003.

[74] Li, K., Zhang, C. and Sun, Z., "Precise Piston Trajectory Control for a Free Piston Engine," *Control Engineering Practice, vol. 34, pp. 30-38, 2015*.

[75] Li, K., Zhang, C and Sun, Z., "Transient Motion Control for a Free Piston Engine," *Proceedings of the IMechE, Part D, Journal of Automobile Engineering, 2017.*

[76] Tomizuka, M., Tsao, T.C. and Chew, K. K., "Analysis and Synthesis of Discrete-time Repetitive Controllers," *ASME Trans. J.Dyn. Syst., Meas. Control, Vol. 111, pp.353-358, 1989.*

[77] Tsao, T.C. and Tomizuka, M., "Robust Adaptive and Repetitive Digital Tracking Control and Application to a Hydraulic Servo for Noncircular Machining," *ASME Trans. J.Dyn. Syst., Meas. Control, Vol. 116, pp.24-32, 1994.*

[78] Sun, Z. and Kuo, T., "Transient Control of Electro-Hydraulic Fully Flexible Engine Valve Actuation System," *IEEE Trans. on control systems technology, Vol. 18, No.3, 2010.*

[79] Zhang, C., Li, K. and Sun, Z., "Modeling of Piston Trajectory-based HCCI Combustion Enabled by a Free Piston Engine", *Applied Energy, vol. 139, pp. 313-326, 2015*.

[80] Zhang, C. and Sun, Z., "Using Variable Piston Trajectory to Reduce Engine-out Emissions", *Applied Energy, vol.170, pp. 403-414, 2016.*

[81] Law, C. K., Combustion Physics, *Cambridge University Press, 2006*.

[82] Yan, F. and Wang, J., "Engine Cycle-by-Cycle Cylinder Wall Temperature Observed-based Estimation through Cylinder Pressure Signals," *ASMETrans., J. Dyn. Sys, Meas, Control.Vol.134, 061014, 2012.*

[83] Rakopoulos, C. D. and Glakoumis, E. G., "Study of the Short-term Cylinder Wall Temperature Oscillations during Transient Operation of a Turbo-charged Diesel Engine with Various Insulation Schemes," *Int. J. Engine Res. Vol.9, pp.177-193, 2008.*

[84] Chang, J., Guralp, O., Filipi, Z. Assanis, D., Kuo, T. W., Najt. P. and Rask, R., "New Heat Transfer Correlation for an HCCI Engine Derived from Measurements of Instantaneous Surface Heat Flux," *SAE Technical paper, 2004-01-2996, 2004.*

[85] Goodwin, D., Malaya N. and Speth. R., "Cantera: An Object-oriented Software for Chemical Kinetics, Thermodynamics and Transport Processes," available at https://code.google.com/p/cantera/.

[86] Li, K. and Sun, Z., "Modeling and Control of a Hydraulic Free Piston Engine with HCCI Combustion," *Proceedings of the 52nd National Conference on Fluid Power, 2011.*

[87] Li, K. and Sun, Z., "Stability Analysis of a Hydraulic Free Piston Engine with HCCI Combustion," *Proceeding of 2011 Dynamic Systems Control Conference, Arlington VA, 2011.*

[88] Shahbakhti, M. and Koch, C. R., "Control Oriented Modeling of Combustion Phasing for an HCCI Engine," *in Proc. Amer. Control Conf.* (*ACC*), *pp. 3694-3699, 2007.*

[89] "Chemical-Kinetic Mechanisms for Combustion Application," University of California at San Diego at http://combustion.ucsd.edu.

[90] Kadota, M., Ishikawa, S., Yamamoto, K., Kato, M. and Kawajiri, S., "Advanced Control System of Variable Compression Ratio Engine with Dual Piston Mechanism," *SAE Int. J. Engines, Vol. 2, No. 1, pp. 1009-1018, 2009.*

[91] Curran, H. J., Pitz, W. J., Westbrook, C. K., Dagaut, P., Boettner, J. C. and Cathonnet, M. A., "Wide Range Modeling Study of Dimethyl Ether Oxidation," *International Journal of Chemical Kinetics. Vol.30, No.3, pp.229-241. 1998.*

[92] Fisher, E. M., Pitz, W. J., Curran, H. J.and Westbrook, C. K., "Detailed Chemical Kinetic Mechanisms for Combustion of Oxygenated Fuels," *Proceedings of the combustion institute. Vol.28, No.2, pp.1579-1586, 2000.*

[93] Seiser, H., Pitsch, K. H., Pitz, W. J. and Curran, H. J., "Extinction and Autoignition of n-Heptane in Counterflow Configuration," *Proceedings of the Combustion Institute. **Vol. 28**, pp. 2029-2037, 2000.*

[94] Wang, H., Retiz, R. D., Yao, M., Yang, B., Jiao, Q. and Qiu, L., "Development of an n-Heptane-n-butanol-PAH mechanism and its application for combustion and soot prediction", *Combustion and Flame, Vol. 160, Issue. 3, pp504-419, Mar 2013*.

[95] Zeldovich, Y. B., Sadovnikov, P, Y. and Frank-kamenetskii, D. A., "Oxidation of Nitrogen in Combustion", *Academy of Sciences of USSR, Institute of Chemical Physics, Moscow-Leningrad, 1947*.

[96] Bowman, C. T. "Kinetic of Pollutant Formation and Destruction in Combustion", *Progress in Energy and Combustion Science, Vol. 1, pp. 33-45, 1975.*

[97] Aichlmayr, H. T., Kittelson, D. B. and Zachariah, M, R., "Miniature Free-piston Homogeneous Charge Compression Ignition Engine-compressor Concept—Part II: Modeling HCCI Combustion in Small Scales with Detailed Homogeneous Gas Phase Chemical Kinetics", *Chemical Engineering Science, Vol. 57, pp. 4173-4186, 2002.*

[98] Kalinci, Y., Hepbasli. A. and Dincer, I., "Biomass-based Hydrogen Production: A Review and Analysis," *International Journal of Hydrogen Energy, vol. 34, pp. 8799-8817, 2008.*

[99] Kirtay, E., "Recent Advances in Production of Hydrogen from Biomass", *Energy Conversion and Management, vol. 52, pp. 1778-1789, 2011*.

[100] Poschl, M., Ward, S. and Owende, P., "Evaluation of Energy Efficiency of Various Biogas Production and Utilization Pathways", *Applied Energy, vol. 87, pp. 3305-3321, 2010*.

[101] The U.S. Department of Energy, "What is Biogas", *April 2010.*

[102] European Biomass Association, "A Biogas Road Map for Europe", *Jun 2010.*

[103] German Biogas Association, "Biogas Segment Statistic 2014/2015", *Nov 2015.*

[104] International Energy Agency, "Biogas Upgrading to Vehicle Fuel Standards and Grid Injection", *Dec 2006.*

[105] Asadullah, M., "Barriers of Commercial Power Generation Using Biomass Gasification Gas: A Review", *Renewable and Sustainable Energy Reviews, vol. 29, pp. 201-215, 2014.*

[106] Martinez J. D., Mahkamov, K., Andrade, R. and Silva Lora, E. E., "Syngas Production in Downdraft Biomass Gasifiers and its Application using Internal Combustion Engine", *Renewable Energy, vol. 38, pp, 1-9, 2012.*

[107] Tinaut, F. V., Melgar, A., Horrillo, A. and de la Rose, A. D., "Method for Predicting the Performance of an Internal Combustion Engine Fuelled by Producer Gas and other Low Heating Value Gases", *Fuel Processing Technology, vol. 87, pp. 135-142, 2006.*

[108] Sridhar, G., Sridhar, H. V., Dasappa, S., Paul, P. J., Rajan, N. K. S. and Mukunda, H. S., "Development of Producer Gas Engine", *Proceeding of the Institution of Mechanical Engineers, Part D: Journal of Automobile Engineering, vol. 219, pp. 423-438, 2005*.

[109] Balat, M. and Balat, H., "Recent Trends in Global Production and Utilization of Bio-ethanol Fuel", *Applied Energy, vol. 86, pp. 2273-2282, 2009.*

[110] Hahn-Hagerdal, B., Galbe, M., Gorwa-Grauslund, M. F., Liden, G. and Zacchi, G., "Bio-ethanol – the Fuel of Tomorrow from the Residues of Today", *Trends in Biotechnology, vol. 24, issue. 12, pp. 549-556, 2006.*

[111] The U. S. Energy Information Administration, "Monthly Biodiesel Production Report", *2014.*

[112] Ma, F. and Hanna, M. A., "Biodiesel Production: A Review", Bioresource Technology, *vol. 70, pp. 1-15, 1999.*

[113] Sadeghinezhad, E., Kazi, S. N., Badarudin, A., Oon, C. S., Zubir, M. N. M. and Mehrali, M., "A Comprehensive Review of Bio-diesel as Alternative Fuel for Compression Ignition Engines", *Renewable and Sustainable Energy Reviews, vol. 28, pp. 410-424, 2013*.

[114] Lapuerta, M., Armas, O. and Rodriguez-Fernandez, J., "Effect of Biodiesel Fuels on Diesel Engine Emissions", *Progress in Energy and Combustion Science, vol. 34, pp. 198-223, 2008*.

[115] Schulz, H., "Short History and Present Trends of FT Synthesis", *Applied Catalysis A General, vol. 186, pp. 1-16, 1999.*

[116] Wilhelm, D. J., Simbeck, D. R., Karp, A. D. and Dickenson, R. L., "Syngas Production for Gas-to-liquids Applications: Technologies, Issues and Outlook", *Fuel Processing Technology, vol. 71, pp. 139-148, 2001*.

[117] Ozawa, G., "Variable Compression Ratio Engine", *U.S. Patent 5,682,854, 1997.*

[118] Puig-Arnavat, M., Bruno, J. C. and Coronas, A., "Review and Analysis of Biomass Gasification Models", *Renewable and Sustainable Energy Reviews, vol. 14, pp. 2841-2851, 2010.*

[119] ASTM international standard specification for dimethyl ether for fuel purpose ASTM D7901.

[120] Van Blarigan, P., Paradiso, N. and Goldsborough, S., "Homogeneous Charge Compression Ignition with a Free Piston: A New Approach to Ideal Otto Cycle Performance", *SAE Technic Paper 982484, Oct. 1998.*

[121] Komnions, N. P. and Rakopoulos, C. D., "Modeling HCCI Combustion of Biofuels: A Review", *Renewable and Sustainable Energy Reviews, vol. 16, pp. 1588-1610, 2012*.

[122] DieselNet Technology Guide, "What Are Diesel Emissions", available at https://www.dieselnet.com/tech/emi_gas.php.

[123] Zhang, C. and Sun, Z., 2016, "Optimization of Trajectory-based HCCI Combustion," Proceedings of Dynamic Systems Control Conference, Minneapolis MN, 2016

[124] Shaver, G. M., Gerdes, J, C., Roelle, M. J., Caton, P. A. and Edwards, C. F, 2005, "Dynamic Modeling of Residual-affected Homogeneous Charge Compression Ignition Engines with Variable Valve Actuation," *Journal of Dynamics Systems, Measurement and Control, 127, pp. 374-381*

[125] Zhang, S., Song, R. and Zhu, G. G., 2017, "Model-based Control for Model Transition Between Spark Ignition and HCCI Combustion," *Journal of Dynamics Systems, Measurement and Control, 139(4), 041004.*

[126] Yang, X. and Zhu, G. G., 2011, "a Two-zone Control Oriented SI-HCCI Hybrid Combustion Model for the HIL Engine Simulation," Proceedings of 2011 American Control Conference, San Francisco, CA, 2011.

[127] Shahbakhti, M. and Koch, C. R., 2010, "Physics Based Control Oriented Model for HCCCI Combustion Timing," *Journal of Dynamics Systems, Measurement and Control, 132(2), 021010.*

[128] Karagiorgis, S., Collings, N., Glover, K. and Petridis, T., 2006, "Dynamic Modeling of Combustion and Gas Exchange Processes for Controlled Auto-ignition Engines," Proceedings of 2006 American Control Conference, Minneapolis, MN, 2006.

[129] Zhang, C. and Sun, Z., 2017, "Trajectory-based Combustion Control for Renewable fuels in Free Piston Engines," Applied Energy, 187(1), pp. 72-83

[130] Jones, W. P. and Lindstedt, R. P., 1988, "Global Reaction Schemes for Hydrocarbon Combustion," Combustion and Flame, 73(3), pp. 233-249

[131] Westbrook, C. K. and Dryer, F. L., 1980, "Simplified Reaction Mechanisms for the Oxidation of Hydrocarbon Fuels in Flames," Combustion Science and Technology, 27(1-2), pp. 31-43

[132] Yamada, H., Sakanashi, H., Choi, N., and Tezaki, A., 2013, "Simplified Oxidation Mechanism of DME Applicable for Compression Ignition," SAE Technical Paper 2003-01-1819.

[133] Zeppieri, S. P., Klotz, S. D., and Dryer, F. L., 2000, "Modeling Concepts for Larger Carbon Number Alkanes: a Partially Reduced Skeletal Mechanism for N-decane Oxidation and Pyrolysis," *Proceedings of the Combustion Institute*, *28*(2), pp. 1587-1595.

[134] Wang, L., Liu, Z., Chen, S. and Zheng, C., 2012, "Comparison of Different Global Combustion Mechanisms under Hot and Diluted Oxidation Condition," Combust. Sci. Technol., 184(2), pp. 1-18, 2012.

[135] Smith, G. P., Golden, D. M., Frenklach, M., Moriarty, N. W., Eiteneer, B., Goldenberg, M., Bowman, C. T., Hanson, R. K., Song, S., Gardiner Jr, W. C., Lissianski, V. V. and Qin, Z., *http://www.me.berkeley. edu/gri_mech/*

[136] Zhang, C., Li, K. and Sun, Z., "A Control-oriented Model for Piston Trajectory-based HCCI Combustion Control Enabled by Free Piston Engines," *Proceeding of the American Control Conference, Chicago, IL 2015.*

[137] Pontryagin, L. S., "Mathematical Theory of Optimal Processes," *CRC Press, 1987.*

[138] Bellman, R. E. and Dreyfus, S. E., "Applied Dynamic Programming," *Princeton, NJ: Princeton Univ. Press, 1962.*

[139] Fletcher, R., "Practical Methods of Optimization," *John Wiley and Sons, 1987.*

[140] Gill, P.E., W. Murray, and Wright, M. H. "Numerical Linear Algebra and Optimization," *vol. 1, Addison Wesley, 1991.*

[141] Han, S. P., "A Globally Convergent Method for Nonlinear Programming," *J. Optimization Theory and Applications, vol. 22, pp. 297, 1977.*

[142] Tripathi, A., Li, K., Zhang, C. and Sun, Z., "Modeling and Control of Controlled Trajectory Rapid Compression Expansion Machine," *Proceeding of 2016 American Control Conference (ACC), Chicago, IL.*

[143] Tripathi, A. and Sun, Z., "Nonlinear Feedforward Control for Electrohydraulic Actuators with Asymmetric Piston Area," *Proceeding of 2016 Dynamic Systems and Control Conference, Minneapolis, MN.*